An Experimental Study of

Surface Forces

William A. Ducker

A thesis submitted for the degree of Doctor of Philosophy
at the Australian National University

Canberra 1991

Preface

This dissertation is an account of research at the Department of Applied Mathematics, Research School of Physical Sciences and Engineering, Australian National University, during the period August 1987 to June 1991.

Much of the work described in this thesis was carried out in collaboration with other workers. Measurements of the forces between mica in ammonium salt solutions (reported in Chapters 3 and 4) were performed in collaboration with Dr Richard Pashley. Measurements on the Force between Nickel and Mica (Chapter 5) were done at the IBM T.J Watson Research Center, Yorktown Heights, New York, with Dr Robert Cook and Dr David Clarke, and the forces on silica colloids (Chapter 6) were measured in collaboration with Tim Senden and Dr Richard Pashley.

None of the work described in this thesis has been submitted to any other institution for any degree.

William Ducker

Acknowledgements

The work described in this thesis was funded by the Australian Government through a Commonwealth Postgraduate Research Award and by grants to the Department of Applied Mathematics, and for 16 months, by International Business Machines.

I would like to thank Ric Pashley, my supervisor, for his constant guidance and valuable teaching, and for his friendship over the last five years. I am grateful to my co-workers, John Parker, Hugo Christenson, Patrick Kekicheff, Andrew Fogden and Callum Drummond for valuble discussions, and to Barry Ninham for his continuous support.

I was fortunate to share an office with Mark Rutland who prepared me for this work with a trip to Europe, started my write-up with assaults on the Castle, and provided hours of entertainment and "serious" discussion. Tim Senden helped to make working with the AFM fun, and enticed me down canyons and into caves.

David Clarke gave me the opportunity to work at IBM and provided me with a more broad perspective of science. With Robert Cook and Dave Abraham I had many enlightening discussions. Duane, Paul and John encouraged me in the distractions of New York's night-life and Janyce, Bill, Suzanne, John and Bev made New York home for a year.

I would like to thank my parents and grandmother for their love and care, and my grandmother for inspiring me to become a scientist. Katharina gave me her love, companionship and understanding.

Publications

The Flotation of Quartz using a double-chained Cationic Surfactant
W.A. Ducker, R. M. Pashley and B. W. Ninham
Journal of Colloid and Interface Science **128** 66 (1989)

The Forces between Mica Surfaces in Ammonium Chloride Solutions
W.A. Ducker and R.M. Pashley
Journal of Colloid and Interface Science **131** 433 (1989)

Force Measurement using an ac Atomic Force Microscope
William A. Ducker, Robert. F. Cook and David R. Clarke
Journal of Applied Physics **67** 4045 (1990)

Rapid Measurement of Static and Dynamic Surface Forces
William A. Ducker and Robert. F. Cook
Applied Physics Letters **56** 2408 (1990)

Multilayer Adsorption of Cytochrome C on Mica around the Isoelectric pH
P. Kekicheff, W.A. Ducker, B.W. Ninham and M.P. Pelini
Langmuir **6** 1704 (1990)

Forces Between mica surfaces in the presence of rod-shaped divalent counter-ions
W.A. Ducker and R.M. Pashley
Accepted by *Langmuir*

Direct Measurement of the Forces on a Colloid Particle using an Atomic Force Microscope
William A. Ducker, Tim J. Senden and Richard M. Pashley
Accepted by *Nature*

The Surface Roughness of Plasma Treated Mica
Tim J. Senden and William A. Ducker
Submitted to *Langmuir*

Abstract

This thesis describes surface force measurements using a Surface Force Apparatus and an Atomic Force Microscope. The surface Force Apparatus was used in the examination of two systems. In the first, the interaction between mica surfaces in ammonium chloride solutions was found to be well described by DLVO theory at low concentrations but additional hydration forces were observed in more concentrated solutions. The forces between mica sheets in aqueous solutions of a diammonium salt were also examined, and related to the stability of montmorillonite clay under similar conditions. A short-ranged attractive force was measured for mica surfaces under conditions where the clay dispersion was found to be unstable.

Two new techniques for surface force measurement using an Atomic Force Microscope are described. In the first, the interaction between a sharp tip and a flat surface was determined by measurement of the resonant properties of a cantilever. This technique was used to measure the interaction between a nickel tip and a mica sheet with high lateral resolution. In the second Force Microscope technique, an individual colloid particle was attached to a cantilever, and the force on the particle was measured directly from the deflection of the cantilever. This technique was used to measure the force on a silica particle as a function of NaCl concentration and pH. This new method has great potential for the study of particle interactions in a wide range colloid systems.

Chapter 5: Force measurement between a nickel probe and a mica surface using an ac atomic force microscope

Chapter 6: Measurement of the force between silica surfaces using a commercial dc force microscope

Chapter 7: Conclusions

Appendix: Force measurement using an atomic force microscope

Chapter 1

Summary

It has been postulated that there are four universal forces: gravitational, electromagnetic and the strong and weak nuclear forces. Because of differences in the rate at which these forces decay with distance, the interaction between two bodies is usually dominated by only one or two of these forces. While the motions of massive bodies are dictated by gravitational forces, the interactions within the nucleus are dominated by the strong and weak nuclear forces. Between these two extremes of scale, interatomic and intermolecular interactions are dominated by electromagnetic forces. These forces dominate over a range of roughly one-tenth of a nanometer to one micrometer, and are not only important in the interaction between individual molecules and atoms, but also in the short-range interaction between larger bodies. The latter are usually known as surface forces and are the subject of this thesis. Surface forces determine the wetting, adhesion and lubricant properties of materials, and dominate the interaction between objects whose size is close to the range of intermolecular forces. Particles of this size are known as colloid particles, and occur in such diverse systems as soils, paints, paper, foodstuffs, biological materials and other composites.

This thesis describes a collection of measurements of surface forces performed using two devices - a Surface Forces Apparatus[1] and an Atomic Force Microscope[2]. A classification of surface forces and a review of some of the methods used for surface force measurement are given in chapter 2. Chapters 3 and 4 describe measurements using the Surface Forces Apparatus. This device has been previously employed to measure a variety of surface interactions and here has been used to measure forces in two systems. The first is the interaction between mica surfaces in ammonium chloride solutions. The forces were found to be similar to those measured in alkali metal ion solutions, being well described by DLVO theory at low concentrations but exhibiting a

hydration force above a critical salt concentration. The second system investigated is the interaction between mica surfaces in aqueous solutions of a diammonium salt. This salt appears to bridge between the negatively charged mica sheets causing adhesion at a mica-mica separation equal to the length of the molecule.

Chapters 5 and 6 describe force measurements an Atomic Force Microscope. This very high resolution microscope was developed in 1986 and few researchers have used this device for surface force measurement. In Chapter 5 a technique is described in which the surface force is obtained from measurement of the change in resonant frequency of a probe (ac measurement), and the results of measurements of the force between a nickel probe and a mica surface are presented. Chapter 6 describes a technique for force measurement using an AFM in which the force is determined directly from the deflection of a cantilever (dc measurement). This method is used to measure the interaction between silica surfaces as a function of aqueous NaCl concentration and pH. These are the first measurements of the force on an individual colloid particle.

References

1. Israelachvili, J.N. & Adams, G. *J. Chem. Soc. Faraday Trans. I* **74**, 975 (1978).
2. Binnig, G., Quate, C. & Gerber, G. *Phys. Rev. Lett.* **56**, 930 (1986).

Chapter 2

Introduction to Surface Forces

During the second world war, Derjaguin and Landau[1], and Verwey and Overbeek[2] independently developed a quantitative theory (DLVO theory) to describe the interaction between colloid particles in aqueous solution. According to DLVO theory, colloid stability is dependent on the magnitude of two opposing forces: an attractive van der Waals force, and a repulsive electrostatic force known as a double-layer force. This theory successfully explained the stability of some colloids, but a significant number of anomalies suggested that other forces were also important. During recent years, theoretical and experimental advances have confirmed the general features of DLVO theory, and a more comprehensive understanding of surface forces has been developed. Additional forces have been proposed due to such effects as solvation, liquid structure and steric interactions, and the forces originally considered in DLVO theory have been refined.

2.1 Classification of Surface Forces

Van der Waals Forces

A van der Waals force is the name given to the force which arises between atoms or molecules because of the interaction between temporary or permanent dipoles. Because all atoms are polarizable, this force is ubiquitous. For two isolated atoms or molecules this force is always attractive, but the situation is more complicated for systems of many atoms. However, between bodies of the same material, the van der

Waals force is force is always attractive, so all colloids would be unstable if this were the only force operating.

Van der Waals[3] proposed a ubiquitous attractive force between gaseous molecules as a correction to the ideal gas law, although postulation of a universal attractive force dates to the time of the Ancient Greeks. In the 1930's a formal mathematical treatment by London[4] showed that the potential between two molecules was inversely dependent on the sixth power of their separation. Early theories of the van der Waals force between macroscopic bodies attributed to Hamaker[5] summed the interaction between two molecules over the volume of the two bodies, assuming the pairwise additivity of these forces. The distance dependence of this force is dependent on the shape of the object, and for two infinite half spaces is given by:

$$V = -A / 12 \pi L^2 \qquad (1)$$

where V is the interaction energy per unit area, L is the distance between the parallel surfaces, and A is the Hamaker constant. The value of A depends on the the composition of the two half spaces and the intervening medium. At larger separations (greater than about 5 nm), the correlation between dipoles is weaker so the distance dependence increases, and the force is said to be retarded.

Modern theories of Van der Waals forces, mainly due to Lifshitz[6, 7], treat the interacting bodies as continuous media (so do not suffer from the limitations of pairwise summation) and consistently include the effects of retardation. Calculation of the force requires knowledge of the dielectric response of the interacting materials over a wide range of frequency (typically from microwave to far UV) since this is related to the manner in which the material interacts with an oscillating electric field.

Electrical Double-layer Forces

There is usually some charge separation at the interface between phases. If we consider the interface between a solid and liquid, this charging can be due to either the unequal dissolution of differently charged groups from the solid, or to the selective adsorption of charged species from the surrounding liquid. This charging process is more favourable in a liquid of high dielectric constant and thus is of particular importance in water. The surface charge is responsible for an electrical potential, and a consequent distribution of ions in the liquid phase: the diffuse electrical double-layer. When two similarly charged surfaces approach there is an electrostatic force generated by the overlap of the diffuse layers.

Early models of the double-layer, developed by Gouy [8] and Chapman[9], were based on a mean field approximation. Their models were based on the assumption that the potential is uniform across the charged surface and in each plane parallel to the surface and that ions in the double-layer have no finite size. A relatively simple mathematical description of this interaction can be obtained if the interaction between flat surfaces is considered. From Maxwell's equation, we have the relationship between the electric field, $\tilde{E}$ and the charge density, ρ at a point, $\tilde{r}$:

$$\tilde{\nabla}.\tilde{E}(\tilde{r}) = -\rho(\tilde{r})/\varepsilon \qquad (1)$$

where ε is the permitivity of the region. For the one dimensional (flat surface) case:

$$d^2\psi(x)/dx^2 = \rho(x)/\varepsilon \qquad (2)$$

where $\Psi(x)$ is the electric potential. The charged particles are distributed according to the Boltzmann Equation:

$$n(x) = n(\infty)\exp(-Q\psi(x)/kT) \qquad (3)$$

where n (x) is the ion density at x, Q is the charge on the ion, k is the Boltzmann constant and T is the absolute temperature. For a Z:Z electrolyte:

$$\rho(x) = qZ\Sigma_i n_i(x) = -2Zqn(\infty)\cosh[Zq\psi(x)/kT] \qquad (4)$$

where q is the magnitude of the charge on an electron.

Combining equations 2 and 4 yields the Poisson-Boltzmann Equation for symmetrical electrolytes:

$$d^2\psi(x) / dx^2 = \frac{-2Zqn(\infty)}{\varepsilon} \sinh (Zq\psi(x) / kT) \qquad (5)$$

At equilibrium the pressure throughout the film must be uniform, so it is only necessary to calculate the pressure in one plane. There is no net electrostatic field at the midplane between two similarly charged surfaces, so here the pressure, π, between the surfaces depends only on the osmotic pressure due to the difference in solute concentration at the midplane and in bulk solution:

$$\pi = kT \Sigma [n_i(m)-n_i(\infty)] \qquad (6)$$

If $\psi(x)$ can be obtained, the ion density profile can be calculated from the Boltzmann distribution equation. A procedure for obtaining exact numerical solutions to the Poisson-Boltzmann equation has been derived by Chan *et al*[10], and thus the double-layer force can be simply calculated. However, the solution of (4) depends on the choice of boundary conditions. As the two surfaces approach, each surface may influence the charge on the other[11]. The highest energy interaction occurs when the charge on each surface remains constant, but surface adsorption or desorption may cause a reduction in charge. The interaction of lowest energy occurs when the electrostatic potential on the surface remains constant.

An example of a measured surface force is shown in figure 2.1. The points are measurements made by Pashley in 1981[12] and the solid lines were calculated using DLVO theory at the limits of constant charge and potential. The force is dominated by repulsive double-layer forces at large distance, and is dominated by attractive van der Waals forces in the last few nm.

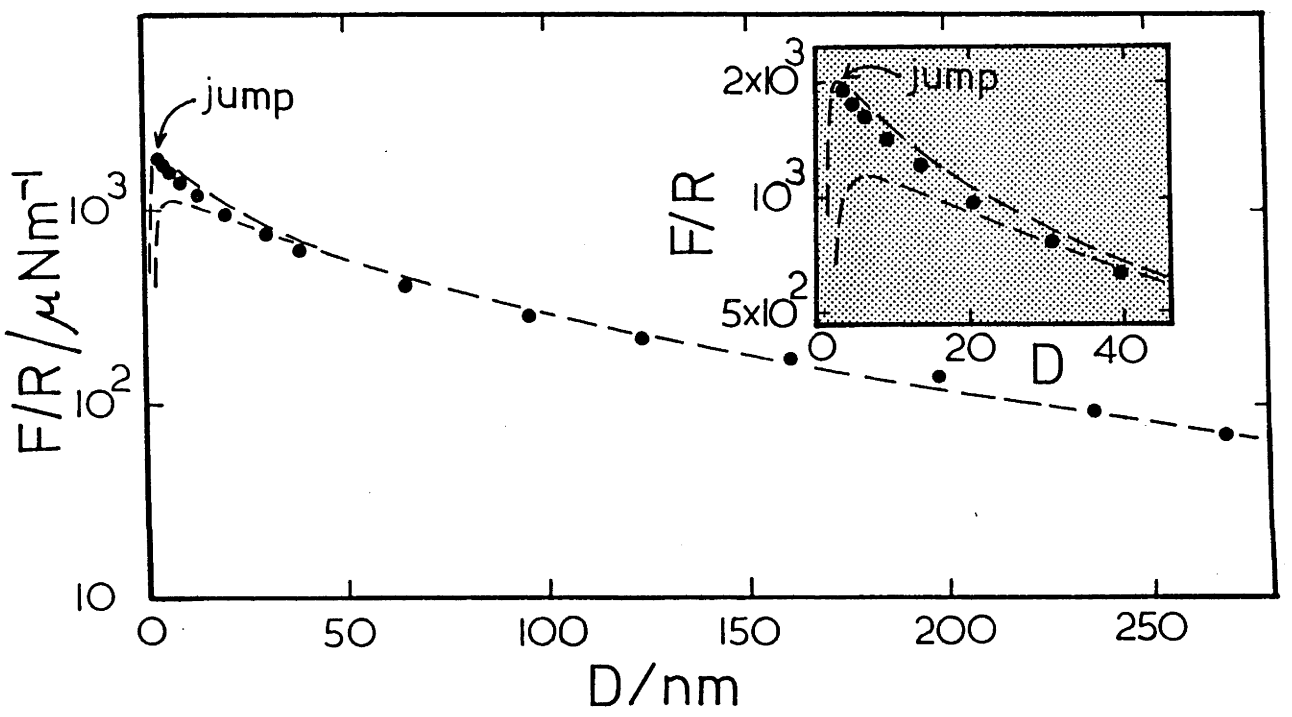

Figure 2.1: An example of double-layer and van der Waals forces: The force between two mica sheets in water measured by Pashley using the Surface Forces Apparatus[12].

The original DLVO theory considered a van der Waals force together with a double layer force calculated with the above Gouy-Chapman assumptions of uniform potentials and point ions. It is with these assumptions that calculations are made in this thesis. However, in recent years several improvements have been made to double-layer theory. Attard, Mitchell and Ninham[13], noting the inconsistency of including molecule-molecule interactions in Van der Waals theory but not in double-layer theory have included ion-ion correlations in their theory, as well as the effect of image charges. The same authors have investigated the contribution of large surface dipoles to the van der Waals interaction[14]. When the zero frequency correlations between dipoles were added to the Lifshitz result, good agreement was obtained with force measurements on lipid bilayers[15] and adsorbed proteins[16]. Mitchell and Ninham have also shown that solutions to the Poisson-Boltzmann equation overestimate the decay-length of double-layer forces, particularly for asymmetric electrolytes[17]. Recent measurements of the forces between mica surfaces in solutions of cytochrome C (a 12:1 electrolyte) are in agreement with their findings[18]. Kjellander and Marcelja[19] have also developed a more sophisticated double-layer model using Hypernetted Chain (HNC) Theory. Poisson-Boltzmann theory agrees well with their results at large separations and low electrolyte concentrations, but poorly in concentrated solutions, particularly in those containing multivalent ions. Experimental measurements of forces between sheet silicates in concentrated Ca^{2+} are consistent with calculations using HNC theory[20].

Structural forces

Both the Lifshitz theory of van der Waals forces and the Gouy-Chapman theory of the double-layer treat all media as continuous. However, it is not surprising when a liquid is in a film which is only a few times the diameter of the constituent molecules there may be effects due to molecular granularity. Computer simulations[21] and theoretical studies[22, 23] of the structure of liquids near smooth, hard walls show that the liquid packs in layers parallel to the surface. The density of liquid molecules alternates between maxima and minima, each separated by a distance close to the diameter of the liquid molecule. The magnitude of the maxima and minima decreases with distance from the wall until the constant bulk density occurs at a distance of about 6-7 molecular diameters from the surface. Since the pressure depends on the momentum transfered to the wall by the particles, it was expected that the force should exhibit the same oscillatory distance dependence. In 1981, Horn and Israelachvili measured the forces between smooth, hard mica sheets immersed in a liquid composed of large, rigid, approximately spherical molecules (octamethylcyclotetrasiloxane) and found that the force as a function of distance was oscillatory, with the magnitude of the maxima and minima decaying roughly exponentially from the surface[24]. Similar results were found by Pashley and Israelachvili in aqueous KCl solutions[25] (as shown in figure 2.2), by McGuiggan and Pashley in concentrated NaCl solutions[117] and by Christenson in a variety of liquids[26, 27]. These forces have also been observed when only one of the surfaces is smooth, but not when both surfaces are rough[28] or when the surfaces are fluid[29].

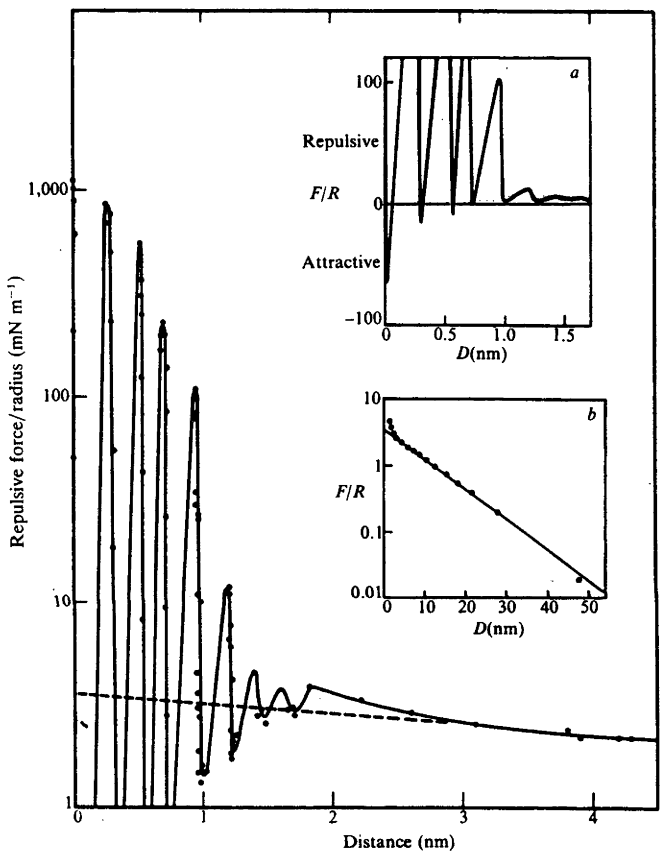

Figure 2.2: The force between two mica sheets immersed in 10^{-3} M KCl measured by Israelachvili and Pashley[25].

Solvation Forces

DLVO theory also neglects the influence of specific interactions between the solvent and the surface. For most liquids, no specific interaction has yet been measured, but for water, there are phenomena which cannot be explained by DLVO forces alone. These forces are usually known as hydration forces if the interaction is repulsive and hydrophobic forces if the interaction is attractive.

Solvation forces were postulated in the early 1930's by Langmuir[30] to explain the stabilization of colloids. Subsequently, detailed force measurements on a variety of systems have revealed repulsive forces in addition to those predicted by DLVO theory. Lyklema and Mysels[31] and Clunie *et al* [32] performed measurements on soap bubbles, the latter finding a monotonic increasing force in addition to DLVO forces at film thicknesses less than 2.5 nm. Similar forces were measured by Parsegian, Rand and others[29, 33, 34] in lamellar systems, by Peschel *et al* [35], Rabinovich *et al* [36]and Horn *et al*[28] between silica surfaces, by Horn[28], and Marra and Israelachvili[37] between lipids adsorbed to mica, by Viani[38] in clays and by Pashley, Israelachvili and others[39, 40] between mica surfaces. In the latter case, the force was attributed to hydration of adsorbed ions. Forces were found to decay exponentially with a decay length of about 0.6-1 nm between solid surfaces, and 0.2 -0.4 nm between fluid surfaces, and to extend to about 1-2 nm per surface.

The question of whether a hydration-like force occurs in liquids other than water is unresolved. Because most force measurements have been performed between smooth mica surfaces, and there are almost always oscillatory structural forces present in these measurements, it is difficult to determine whether solvation forces occur, or even whether it is sensible to make a distinction between solvation and structural forces. Christenson found no need to invoke an additional force to explain the interaction between mica surfaces in acetone(which has a large dipole moment) or in

methanol(which is hydrogen bonding)[41]. Likewise, no additional repulsive force was observed in measurements in ethan-1,2-diol (glycol)[26] although analysis was complicated by the presence of repulsive double-layer forces. Other workers have measured solvation forces between lecithin molecules in glycol[42].

Theoretical modeling of these interactions is difficult because of the complexity of the water-water interactions: the water molecule is asymmetric and because the dipole moment for water varies according to the size of the water cluster, pairwise summations offer poor approximations[43]. However, a simple mechanism for hydration forces is that the force is due to the ordering of water molecules near polar groups or surface adsorbed charges. As a second surface approaches, there are increasing demands for the orientation of the water molecules resulting in a loss of entropy and breakage of hydrogen bonds, and thus a repulsive force[40, 44].

An example of measurement of this "additional" repulsive force is the measurement of the force between mica surfaces in 10^{-2} M NaCl shown in figure 2.3

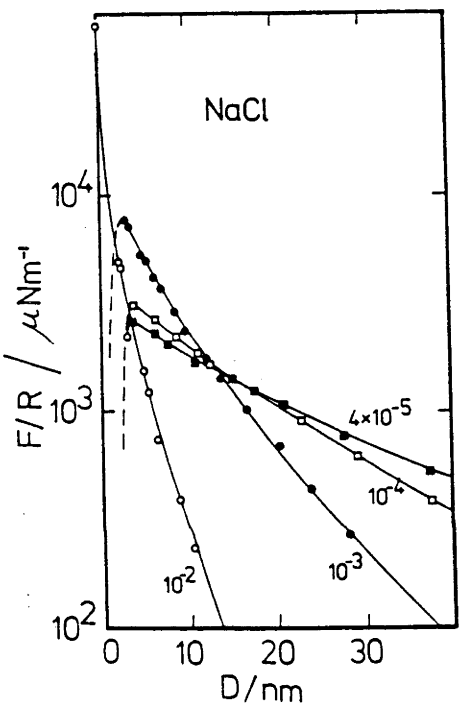

Figure 2.3: An example of double-layer, Van der Waals and hydration forces: The force between two mica sheets in NaCl solutions measured by Pashley using the Surface Forces Apparatus[40]. Note that at the highest concentration, (10^{-2} M) the van der Waals force does not dominate at small separation. This has been attributed to hydration forces.

Current understanding of hydrophobic forces is far less advanced than for hydrophilic forces. Although the hydrophobic effect has been studied for some years[45, 46], most investigations have focussed on the interaction between small non-polar molecules and water, not measurement of the force law between hydrophobic surfaces. When these non-polar molecules dissolve in water, the local structure of the water is modified, presumably to form clathrate-like, but dynamic structures. Structures of this nature have been produced in computer simulations [47]. Although their formation may be accompanied by an increase in hydrogen-bonding, the structures are more ordered than bulk water and the decrease in entropy more than compensates for the enthalpic change. Clustering of hydrophobic molecules minimizes the free energy gain, so the interaction between hydrophobic molecules is attractive. This has been confirmed by simulations[47] and theory[48] and is suggested by the existence of structures in water consisting of aggregated amphiphiles (*e.g.* micelles).

The nature of the force between hydrophobic surfaces is less well understood. Currently there is no theory which can predict either the distance dependence or the magnitude of the force, and experiments reveal a complicated picture . Experiments by Pashley, Israelachvili, Christenson, Claesson and others [50-57] show that the forces are of much longer range than hydration forces, extending to surface separations of 100 nm and sometimes even to 200 nm[57, 58]. The force law is roughly exponential, but in some cases exhibits two regimes, with decay lengths of about 1 nm and 5 nm. The enormous range of this force suggests that there may be an electrostatic contribution, particularly in the long-range component, but forces measured in solutions of varying screening length (ionic strength) do not support this hypothesis[59].

Steric Forces

When two polymer-coated surfaces approach in solution, a repulsive force can arise if solvated polymer chains are confined to a smaller volume. This is analogous to the double-layer force, where the repulsion is due to the confinement of the diffuse layer of ions. This steric repulsion helps in the stabilization of a wide range of colloidal systems including paints, glues, ink and foodstuffs. Stabilization can be achieved by adsorption of a block copolymer to the colloid. If the solution is a bad solvent for one section of the polymer, attachment to the colloid is ensured, and if the solution is a good solvent for the other section of the polymer these sections will be repelled by similar sections attached to another particle, preventing coagulation by van der Waals forces. Obviously, if there is a net attraction between the polymer segments there will be an attractive force between the particles leading to flocculation.

Recent measurements of forces between surfaces in polymer solutions have largely confirmed these traditional theories of colloid stabilization. Typically, measured forces are monotonically repulsive over a distance (per surface) at least equal to the radius of gyration of the polymer [60, 61, 62]. The range of the force increases when the medium is a better solvent for the polymer[63].

Undulation Forces

In some lamellar systems, the equilibrium spacing of the bilayers exceeds the range of conventional surface forces[64]. Helfrich has proposed that these phases are stabilized by a long-range force due to steric interactions caused by thermal fluctuation of the bilayers[65, 66].

2.2 Techniques for the measurement of surface forces

This section contains a review of force measuring techniques. More detailed descriptions of a Surface Forces Apparatus and an Atomic Force Microscope are given in sections 2.3 and 2.4 since both of these have been used for measurements described in this thesis.

Measurement of thin wetting films on glass

In 1938 Langmuir[30] used measurements of the liquid levels in thin capillaries to estimate surface forces. The extent to which a water capillary rises in a wetting glass tube depends on the effective diameter of the tube, and thus on the thickness of any thin liquid film on the glass. By calculating the thickness of the film for a variety of ionic concentrations, he was able to obtain reasonable agreement with estimates of double-layer forces.

The following year, Derjaguin and Kussakov[67] published results of measurements of the force between an air-bubble and a flat glass plate separated by a thin liquid film. The dimensions of the film were measured by an interference technique, and the film pressure was calculated from the radius of the bubble using the Laplace Equation. The pressure was then changed by applying a hydrostatic pressure to the inside of the bubble. Measurements using this technique show general agreement with double-layer theory in the region 30-130 nm[68-70].

Soap Film Measurements.

Force distance relationships have been measured on thin (5-100 nm) soap films drawn from a reservoir on a wire support[31, 32]. The thickness of the films was controlled by competition between forces tending to thin the film: van der Waals and hydrostatic forces, and forces preventing thinning: double-layer and hydration forces. The equilibrium thickness of the soap layer were measured as a function of either the height above the bulk liquid (hydrostatic pressure) or the relative vapour pressure (chemical potential of the liquid). The thickness of the film was usually determined from the reflectivity of the film and these values are dependent on modelling of the film layer. This leaves an uncertainty of about 1-2 nm in the determination of film thicknesses. In a later version of this technique the film pressure was determined directly from light scattering measurements[71]. Experiments using soap films provided general verification of DLVO theory, and provided some of the first experimental evidence of hydration forces.

In analagous studies of surface films, the thickness has been measured more accurately by ellipsometry[72-74].

Osmotic Stress Measurements

Parsegian, Rand and LeNeveu[29] have developed a technique for measuring the surface pressure between amphiphile layers in lamellae and this has been applied to a variety of lipids. In their method, the pressure in the lamellae is set, and the corresponding thickness of the water film between the lipid bilayers is determined using X-ray scattering. The repeat unit of solutions of known lipid volume fraction are measured to determine the relationship between repeat unit and interlipid spacing, then, in the experiment, the repeat unit is measured as a function of pressure by applying an osmotic stress in one of three ways:

1)The lipid lamellae are placed in equilibrium with a solution of dextran of known osmotic strength.

2)A pressure is applied to the lamellae via a piston, and water is removed though a semi-permeable membrane.

3)The lipid lamellae are placed in equilibrium with a range of saturated salt solutions via the vapour phase.

Capacitance measurements

Starting in the 1950's, Sparnaay and Overbeek developed a technique for the direct measurement of surface forces and have used this for the measurement of van der Waals forces between glass, quartz or silica plates[75-78]. A capacitance gauge was used to determine the deflection of a spring attached to one of two substrates interacting across air or vacuum and the interaction force was calculated using the spring constant. The distance between the plates was determined by noting the change in colour of the light reflected from an interferometer formed by the plates. This estimation of colour was made by eye. At small separations (<100 nm), the distance was estimated from the ratio of intensity of incident and reflected light. Changes in separation were achieved using micrometers and mechanical pressure transducers.

Recently, Tonck, Georges and Loubet [79] have measured the forces between aluminium oxide surfaces using a device in which capacitance gauges measure both the deflection of a spring and the surface separation. In their device, the distance between the surfaces is altered by controlling the temperature of the metallic section of the mechanical linkage between the surfaces.

The Force Balance

Derjaguin, Rabinovich, and Churaev[80] have developed force measuring instruments which are distinguished from the other devices discussed here in that the separation between the surfaces is controlled, rather than allowed to come to an equilibrium separation determined by the forces. In the devices developed by Israelachvili[81] and Overbeek[75], the displacement of one surface relative to another is altered by changing the displacement of one surface relative to the undeflected end of a spring. The surface at the free end then moves until equilibrium is achieved between the surface force and the spring force. In the devices of Derjaguin *et al*, the distance between the surfaces is set by the experimenter, and a feed-back loop produces the force necessary to maintain that position (i.e. equal and opposite to the surface force). The force is measured between two fibres oriented perpendicular to each other (numbered 1 and 3 in figure 2.4), one of which is fixed, and the other is attached to a pivot arm. At one end of this arm is a coil in a magnetic field (3), and at the other end, a mirror (4). By reflecting a beam of light from the mirror on to two photoresisters (L_1 and L_2), the angle of the pivot arm is measured, and thus the distance between the surfaces known. Once an inter-fibre distance is selected, a feed-back loop produces a current in the coil which interacts with a magnetic field to produce the force necessary to maintain the position. The surface force is then calculated from the current through the loop.

The advantage of this technique over conventional measurements of the deflection of a spring is that with a feed-back loop of sufficient speed, the force can be measured at any distance because it is not subject to the mechanical instability of a spring. This device has thus been particularly successful for the measurement of attractive van der Waals forces but has also been used for measurements to determine the nature of double-layer forces. The chief disadvantage of this device is that because the distance between the surfaces is not measured explicitly, errors can be introduced by the bending of the fibres and deformations in the contact zone.

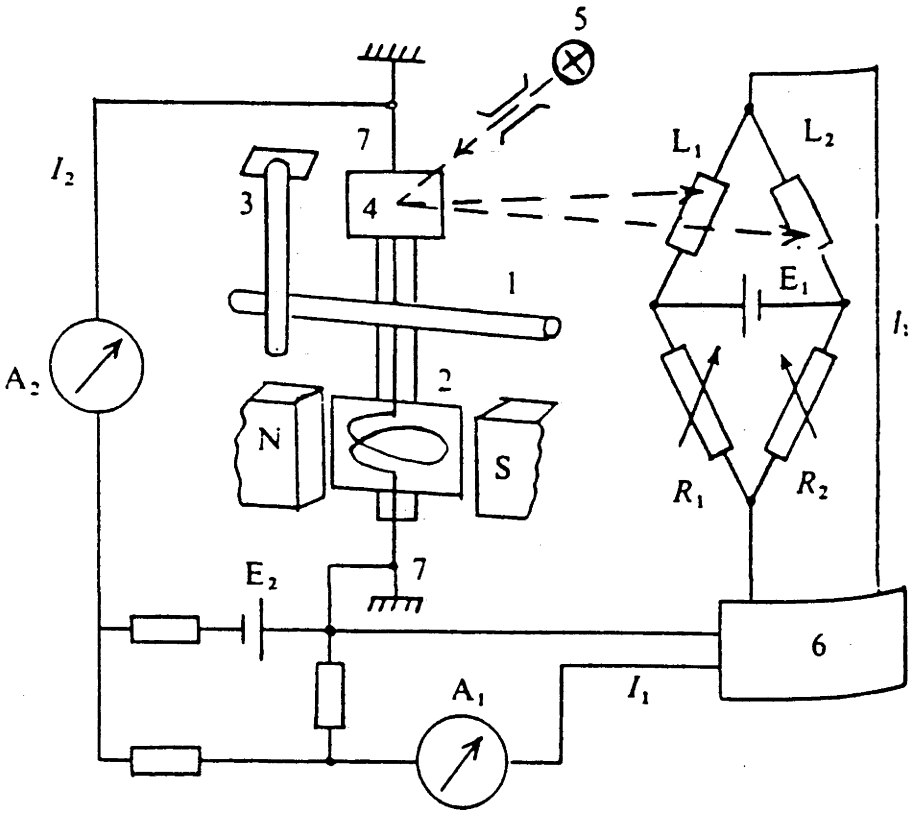

Figure 2.4: Schematic diagram illustrating the force balance. The crossed fibres are labelled 1 and 3. Figure reproduced from reference[80]

The Surface Forces Apparatus

One of the most popular methods for the measurement of surface forces uses an apparatus which has been developed over a number of years by Tabor and Winterton[82], Israelachvili and Tabor[83], Israelachvili and Adams[81], Israelachvili,[84] and Parker, Christenson and Ninham[85], commonly known as the Surface Forces Apparatus (SFA). In this device, the distance between two thin mica sheets is measured explicitly by interferometry and the separation is altered either by mechanical means or by the use of piezo-electric devices. One of the surfaces is attached to a spring and the force is calculated from the deflection of the spring. Parker has developed a modification of this technique in which the force is measured using a piezoelectric bimorph[86]. Because the SFA was used for some of the measurements reported in this thesis, its operation will be considered in some detail in the next section.

2.3 The Surface Forces Apparatus.

Introduction

The Surface Forces Apparatus (SFA) has been developed over a number of years, and both the versions of Israelachvili and Adams[81], and Parker *et al* [85] were used for measurements reported in this thesis. However, because measurement using the two devices is fundamentally the same, only the latter will be described here. Both dynamic measurements[87, 88], and measurements between other surfaces have been performed[28, 89] using these devices. However because only static forces between mica surfaces in water are reported here, only the technique for such measurements will be described. Figure 2.5 shows a cross-section view of the apparatus which will be described below in terms of distance measurement, control of surface separation, force measurement, and preparation of samples and solutions.

Measurement of surface separation with the SFA

Surface separation is determined interferometrically by analysis of Fringes of Equal Chromatic Order (FECO fringes)[90, 91]. White light is passed through a five-layer cavity consisting of silver-mica-fluid-mica-silver which allows the transmission of wavelengths which are an integral fraction of the optical distance between the silver surfaces. The wavelengths of transmitted light are measured using a spectrometer and appear as a series of bright fringes on a dark background. Measurements using the interferometer depend on the thickness of the mica sheets and the optical distance between them, but for the pressure ranges applied in these experiments, the thickness of the mica is effectively constant. This is thus a very direct method for determining surface separations and unlike some other measurement techniques, drifts in measured distances are insignificantly small.

At the beginning of an experiment the thickness of the mica is calculated from measurement of the wavelength when there is no gap between the surfaces:

$$Y = n\,\lambda_n / 4\,\mu_m \quad , \quad n=1,2....$$

where Y is the thickness of each mica sheet, n is the order of the fringe, and μ_m is the refractive index of the mica. When there is a thin film between the mica sheets, each fringe moves to a longer wavelength, which is given by:

$$\tan(2\pi\mu_w T / \lambda_n^T) = \frac{2\bar{\mu}\sin\{\pi\,[1-(\lambda_n^0/\lambda_n^T)]\,/\,[(1-(\lambda_n^0/\lambda_{n-1}^0)]\}}{(1+\bar{\mu}^2)\cos\{\pi\,[1-(\lambda_n^0/\lambda_n^T)]\,/[\,1-(\lambda_n^0/\lambda_{n-1}^0)]\} \pm (\bar{\mu}^2-1)}$$

where: λ_n^T is the wavelength of the nth fringe with a film of thickness, T, between the mica sheets,

μ_w is the refractive index of water at that frequency,

$\bar{\mu} = \mu_m / \mu_w$

λ_n^0 and λ_{n-1}^0 are the wavelengths of the nth and (n-1)th order fringes when there is no gap between the mica sheets, and

+ refers to n odd, and - to n even.

When the silver layers are far apart (2Y+T is large), there is a smaller wavelength difference between adjacent fringes and a lower resolution of surface separation. Thus for high resolution it is important to obtain mica sheets which are quite thin - in practice, about 1-5 μm in thickness. Measurement of separation also becomes less accurate as the surfaces are moved further apart. In adhesion measurements, the surfaces can separate to distances of the order of micrometers, and here the distance is often calculated in a different manner. Each time the mica sheets are moved so that a fringe passes through the wavelength equal to λ_n^0, the surfaces move exactly $\lambda_n^0 / 2\mu_m$, so large changes in surface separation can be measured simply by counting the fringes as they pass λ_n^0.

A big advantage of the interferometric technique is that the above equations hold for each point in the interferometer cavity and thus the fringes reveal the geometry of the contact zone. The mica sheets are usually in the shape of half cylinders mounted with their axes perpendicular, so when viewed in section appear as a semicircle against a flat. Because of different magnifications parallel and perpendicular to the optical path, the fringes appear as portions of an ellipse, and a radius, R, of the surface can be calculated from the dimensions of this ellipse. A point on the ellipse is chosen and the difference in separation between the surfaces at that point on the fringe and at the surface, x, is measured using the above equation. The width of the fringe at that point is measured using a graticule, and the other dimension, y, is calculated using the magnification of the optical path. The radius is then determined using simple geometry:

$$R = \frac{y^2}{8x}$$

A perpendicular radius is also measured, and the two radii characterize the geometry of the contact zone.

Because the geometry of the surfaces is revealed in the shape of the fringes it is possible to see whether the surface separation (and thus the force) is constant over areas greater than the wavelength of light, and thus to detect local inhomogeneities such as particles or other phases. It is also possible to see deformations caused by large loads, and to measure the refractive index of the film in the contact zone.

Changing the surface separation in the SFA

In the Surface Forces Apparatus, the lower surface is connected to the upper surface via a spring, some structural components, and the devices for altering surface separation (see figure 2.5). To change the surface separation, the distance between point A and B (the distance Z in figure 2.6) is changed, causing the spring to deflect until equilibrium is reached between the surface force and the force exerted by the spring. The distance Z is changed by one of three methods. The most coarse level of control is achieved using a translation stage. With a DC motor attached to this stage via reduction gearing, the distance can be controlled to within 10 nm. The next stage of operation uses a similar translation stage, but it is connected to the apparatus via a weak spring which pushes on a flexure hinge, reducing movement by a factor of about 1000. The final stage of control is achieved by changing the length of a piezoelectric crystal by application of a potential across its wall. Recently, Stewart and Christenson have developed a technique where the surface attached to the spring may be moved by application of a magnetic force[92]. However, this method has not been used in measurements described in this thesis.

Measurement of Surface Forces with the SFA

The first stage in force measurement is to determine a region of zero surface force, which by definition occurs at large surface separation (*e.g.* at separations greater than 800 nm). When using a piezoelectric crystal, the voltage across the crystal is increased, the corresponding reduction in surface separation is measured, and thus the calibration of distance moved per volt applied can be obtained. At large separation this value is constant, indicating zero force. As the surfaces move closer together, the change in surface separation per volt changes, indicating that the spring has deflected.

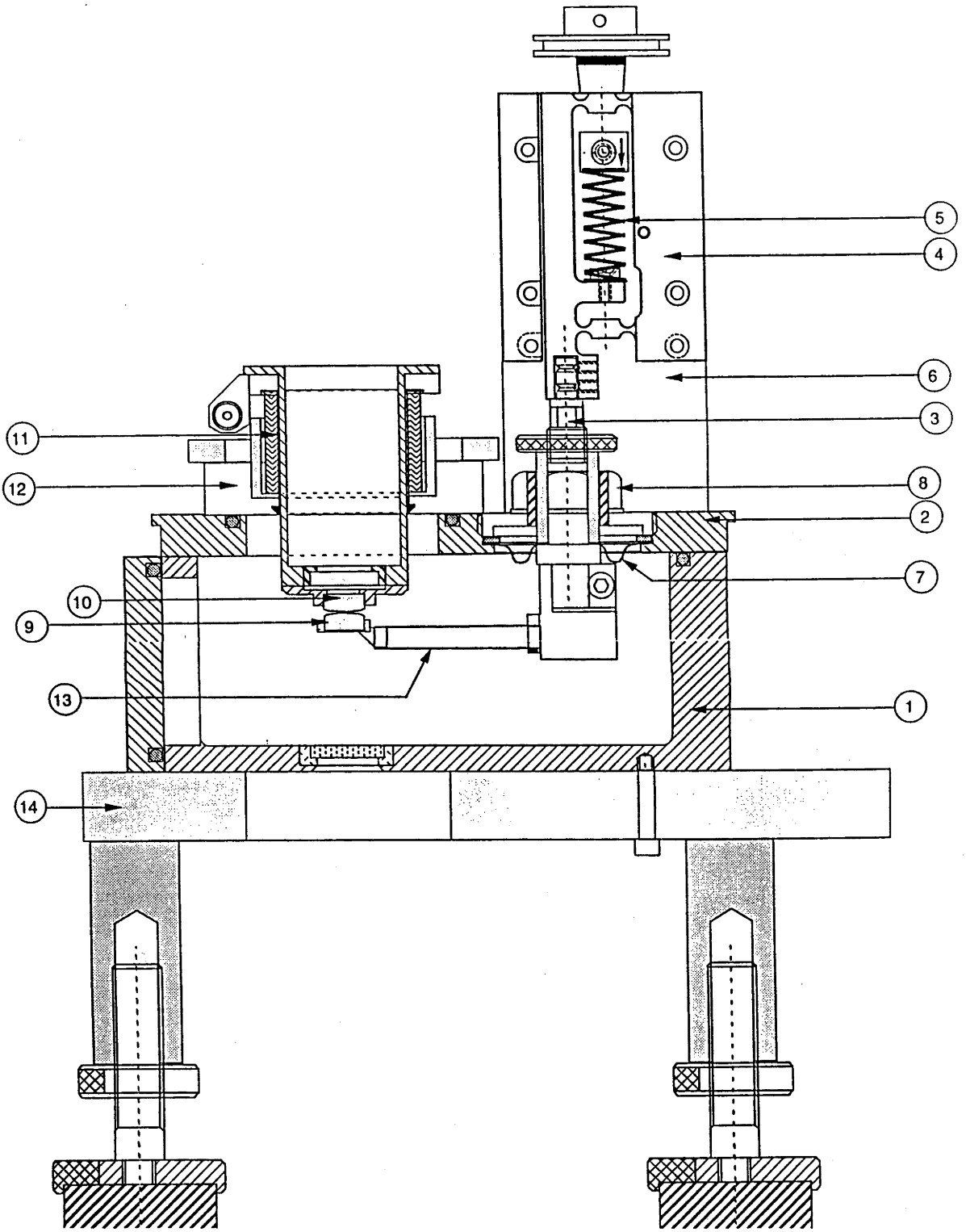

Figure 2.5: Drawing of the surface forces apparatus mark IV

The amount of spring deflection can then be calculated by subtracting the change in surface separation ($S-S_0$) from the expansion of the crystal($Z-Z_0$). Similarly, if a micrometer stage is used to change the separation, the distance can be calibrated if the rotation of the micrometer shaft is monitored with a potentiometer. It is important to ensure that the micrometer stage or piezo movement is linear. Calculation of the force from the spring deflection requires only the value of the spring constant, and this is measured at the end of an experiment by loading the spring with a known mass and measuring the deflection with a travelling microscope. The double spring used in the apparatus confines motion of the lower surface to vertical translation, rather than allowing it to roll, as with a single spring.

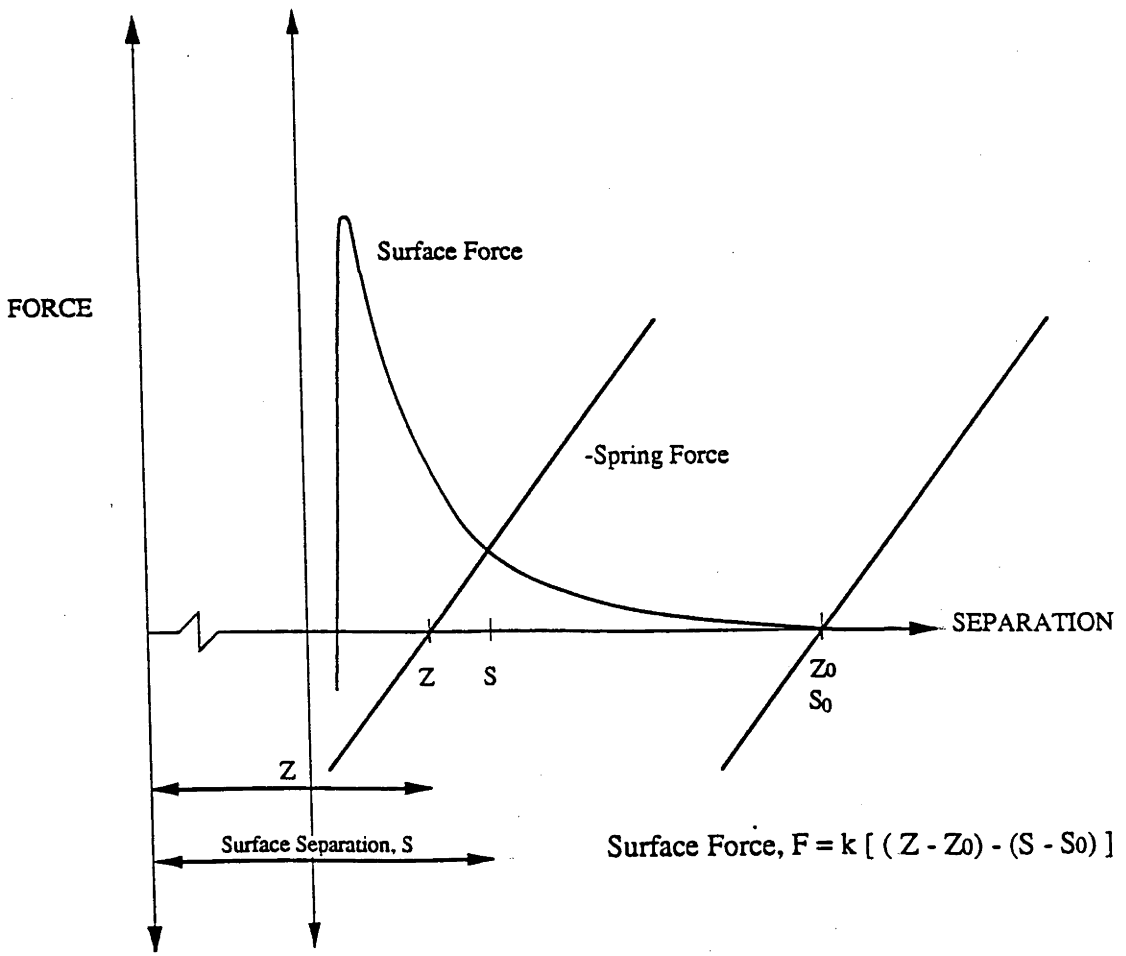

Figure 2.6: See text for explanation.

Preparation of substrates and solutions for the SFA

The mica used in all SFA experiments is prepared in a laminar flow cabinet in the following manner. Large sheets of muscovite mica (mica supplies, Christchurch UK) are cleaved until interference colours and the flexibility of the sheets indicate that the thickness is in the range of 1-5 μm. These sheets are cut into rectangles of about 1 cm^2 using a red hot platinum wire, and made to adhere to a large freshly cleaved mica sheet for clean storage and to facilitate handling. A 530 Å layer of silver is then evaporated onto the cut pieces (for use in the interferometer). At the beginning of an experiment, two mica pieces are removed from the backing sheet and glued, silver side down, to silica supports. Two pieces of equal thickness are chosen to simplify interferometric calculations. The cleaved mica is very flexible and adopts the cylindrical geometry of the silica supports, although under high loads in an experiment the mica and glue in the contact zone will deform to produce a flattened region.

In these experiments it is important to use purified reagents, as only a small amount of surface active impurity can drastically alter surface forces. The water used in all SFA experiments described in this thesis was purified by passage through ion-exchange and charcoal columns, filtration through a 0.2 μm filter then distillation in a glass still. Water was always freshly distilled the day before commencement of an experiment, and stored in a laminar flow clean air cabinet. To prevent the formation of bubbles on the mica surfaces and springs, the water was de-aerated with a water pump for about 30 minutes immediately prior to an experiment. Because of equilibration with atmospheric CO_2 during an experiment the water had a pH of about 5.7 and a conductivity of 1 μScm^{-1}.

The measurement geometry in surface force measurements

Measurements using the Surface Forces Apparatus utilize mica sheets of cylindrical geometry with the axes oriented perpendicular to each other and in a plane perpendicular to the direction of applied force. The advantage of this geometry is twofold. Firstly, it facilitates alignment of the surfaces. The crossed cylinder interaction is still maintained if either surface is translated in any of the three dimensions, or if either cylinder is rotated about its axis. If the angle between the axes of the cylinders is not exactly 90°, the effective radii of curvature of the interaction region are altered, but these can be measured interferometrically. The only alignment which must be done is to ensure that the plane of contact is perpendicular to the loading direction, otherwise a shearing force, rather than a normal force will be applied. The second advantage of cross-cylinders is that a line of contact zones on each surfaces is accessible because the geometry is unaltered by translation along the axis of either cylinder. This is important because it allows the experimenter to avoid particles and chemical contaminants. In an interaction between a sphere and a flat sheet (chapter 6), alignment is very easy because the geometry is unchanged by any translation or rotation (although there is the same loading requirement as for the crossed cylinders), but only one position on the sphere is accessible. For a sphere-sphere interaction, two degrees of translational freedom are constrained, because the interaction changes if the spheres are not body-centered. In addition, only one position on each of the surfaces is accessible. For the flat-flat geometry, translational movement does not alter the geometry, but rotation in two dimensions for each surface critically alters the geometry: the two surfaces must be made very parallel. In addition, there is only one position which is accessible, and it includes all of both surfaces.

The most convenient geometry to model theoretically is usually the interaction between two flat surfaces. Derjaguin[93] has derived a simple equation relating the force, F, between a sphere of radius, R, and a half-space to the energy per unit area, E, between

equivalent flat surfaces which is valid when the range of the force is much smaller than the radius of the particle[93]:

$$F/R = 2\pi E$$

For crossed cylinders, R in the above equation is replaced by the geometric mean of the radii of the two cylinders.

2.4 The Atomic Force Microscope

One of the reasons why surface forces are of interest is their importance in the interaction between colloid particles so it would be useful to be able to measure these forces directly. Until recently this has not been possible because of the difficulty in manipulating microscopic objects and in measuring the minute forces involved. Since the magnitude of surface forces depends on the radius of curvature of the substrate, the normalized surface force could be measured more accurately between surfaces with large radius. For example, in the SFA technique, the radius of substrates is about 2 cm, and this requires a resolution of about 1 μN for typical double-layer experiments. For analogous measurements on a 2 μm particle a resolution of about 0.1 nN is required. However, the development of the Scanning Tunneling Microscope (STM) by Binnig and Rohrer in 1982[94] and its spectacular success in microscopic measurement have changed the scale on which scientists contemplate measurement. One implication of these developments for surface force measurement is that the technology now exists for measurement of forces on colloid-sized objects. Measurements of this kind are described in Chapters 5 and 6. This section contains a brief description of the STM and the derivative Atomic Force Microscope (AFM) which have enabled these measurements.

A STM measures surface topography by scanning a fine metallic tip over a conducting surface. The tip and surface are positioned only a few Å apart, so when an electrical potential is applied between them, a tunneling current flows across the gap. The tip is raster scanned across the surface, and in the most common mode of operation, the current is held constant by forcing the tip to maintain a constant displacement from the surface. This is achieved with by feedback of the (amplified) tunneling current to a piezoelectric crystal on which the tip is mounted. A record of the vertical movement of the piezoelectric translator then corresponds to a topographical map of the surface. Because the tunneling current varies exponentially with tip-sample displacement, and

the decay length is very short (~1 Å), the resolution in distance perpendicular to the surface is very high. If the tip is made very sharp relative to the surface, the short range of tunneling also allows high horizontal resolution to be obtained. STM's have now been used to image the surfaces of a variety of metals and semiconductors with atomic resolution, as well as to image surface adsorbates and larger scale features[95]. In addition, by measuring the tunneling current as a function of applied voltage, electronic structure can be investigated (I-V spectroscopy).

The limitation of atomic scale microscopy to conducting substrates was removed in 1986 when Binnig, Gerber and Quate developed the Atomic Force Microscope (AFM)[96]. An AFM uses the same control mechanisms as a STM, but instead of detecting distance by measuring a tunneling current, an AFM detects distance by measuring the force between the tip and sample. The tip is situated at the end of a cantilever beam and the force is measured by recording the deflection of the cantilever. To date, this deflection has been measured with STMs[96], capacitance gauges[97], a laser deflection scheme(similar to the force balance described in section 2.2)[98], a diode-laser feedback scheme[99] and heterodyne [100], differential[101], Michelson[102] and fibre optic[103] interferometers. Since surface forces are ubiquitous, force microscopy can be used on any condensed material. In addition, because some surface forces decay rapidly with distance, the lateral and vertical resolution can be high. For sharp tips which image using the Born repulsion force, individual atoms can be resolved in some cases[104]. The microscope has also been used to image in regimes where van der Waals forces, magnetic or electrostatic forces dominate[95], although the lateral resolution in these measurements is usually lower because the forces have greater range, and because the tip is usually held further from the surface.

When the tip is not in contact with the surface, it is usually more susceptible to vibration, and the surface force is often smaller. For these measurements the signal to noise ratio may be increased by employing modulation of the tip signal (ac

microscopy)[100]. Usually the vertical displacement of the tip relative to the sample is modulated using a piezoelectric crystal. If the end of the cantilever away from the tip is vibrated, the amplitude of vibration of the tip will depend on the gradient of the forces experienced by the tip (from the cantilever and external forces) and the mass distribution of the cantilever. Changes in amplitude as a function of changes in force gradient will be most pronounced just off the resonance of the cantilever, so the highest sensitivity is obtained by modulation at this frequency.

Most work using Force Microscopes has focused on imaging surfaces, and the forces experienced by the tip have usually been investigated only in so far as they influence imaging. However, the force microscope is also a useful tool with which to examine surface forces. Durig *et al* have measured the forces between tungsten and silver[105] and between iridium surfaces[106] in UHV. They measured attractive forces which were attributed to van der Waals forces and metallic adhesion. The interaction force became repulsive after the iridium was coated in aluminium and then oxidized. Martin *et al* [100] measured an attractive force between a tungsten tip and silicon, and Yamada *et al*[107] have measured forces between a tungsten tip and graphite. In the latter case, both attractive forces (at separations up to 20 nm) and repulsive forces (ascribed to surface deformations) were measured. AFMs have also been used to measure forces in the plane of the surface. Erlandsson *et al* [108] and Cohen *et al* [109] have measured the frictional forces on a tip as it is scanned across mica, and Taubenblatt[110] has measured similar forces on graphite .

In later developments, Bryant *et al*[111] have developed a AFM where attractive forces can be measured in a feed-back system and Miller *et al* [112] and Joyce and Housten[113] have developed an AFM force balance. In this technique a surface separation can be maintained even if the force gradient exceeds the cantilever constant by feeding back on the tip-sample separation. Burnham *et al*[114, 115] have measured van der Waals

forces for surfaces with and without low surface energy coatings. Weisenhorn *et al* have measured the force between a Si_3N_4 cantilever and mica in air and water[116].

2.5 Conclusions

Whilst the forces incorporated into the DLVO theory have been thoroughly investigated by a number of techniques, other forces remain less well understood. Examination of solvation forces has been limited to a restricted number of solvents and substrates, and understanding of hydrophobic forces is very incomplete. One reason for this is that attractive forces are difficult to measure, and further investigation awaits the use of force balances. The recent development of these for both AFM and SFA applications will allow new measurements and perhaps greater insight into attractive forces.

Experimentation has also been restricted to a limited choice of substrates - principally clay minerals and silica. Examination of a variety of metals, metal oxides, and ionic and covalent solids should be possible with new measuring devices. Direct measurement of surface forces has also been restricted to studies of macroscopic substrates.

2.6 References for chapter 2

1. Derjaguin, B. & Landau, L. *Acta Physiochem.* **14**, 633 (1941).
2. Verwey, E.G.W. & Overbeek, J.T.G. *Theory of the Stability of Lyophobic Colloids*, Elsever, Amsterdam (1948).
3. van der Waals,. *PhD Thesis,* University of Leiden. (1873).
4. London, F. *Z. Phys.* **63**, 245 (1930).
5. Hamaker, C.C. *Physics* **4**, 1058 (1937).
6. Lifshitz, E.M. *Sov. Phys. JETP* **2**, 73 (1956).
7. Dzyaloshinski, I.E. & Lifshitz, E.M. *Adv. Phys.* **10**, 165 (1961).
8. Gouy, G. *J. Phys. Radium* **9**, 457 (1910).
9. Chapman, D.L. *Phil. Mag.* **25**, 475 (1913).
10. Chan, D.Y.C., Pashley, R.M. & White, L.R. *J.Col.Int.Sci.* **77**, 283 (1980).
11. Ninham, B.W. & Parsegian, V.A. *J. Theor. Biol.* **31**, 405 (1971).
12. Pashley, R.M. *J. Coll. Int. Sci* **80**, 153 (1980).
13. Attard, P., Mitchel, D.J. & Ninham, B.W. *J. Chem. Phys.* **88**, 4987 (1988).
14. Attard, P., Mitchell, D.J. & Ninham, B.W. *Biophs. J.* **53**, 457 (1988).
15. Marra, J. *J. Col. Int. Sci.* **109**, 11 (1985).
16. Kekicheff, P. & Ninham, B.W. *in preparation*
17. Mitchell, D.J. & Ninham, B.W. *Chem. Phys. Lett.* **53**, 397 (1978).
18. Kekicheff, P. & Ninham, B.W. *Europhysics Letters* **12**, 471 (1990).
19. Kjellander, R. & .Marcelja, S. *Chem. Phys. Lett.* **142**, 485 (1987).
20. Kjellander, R., Marcelja, S., Pashley, R.M. & Quirk, J.P. *J. Chem. Phys.* **92**, 4399 (1990).
21. Lane, J.E. & Spurling, T.H. *Chem. Phys. Lett.* **33**, 231 (1980).
22. Mitchell, D.J., Ninham, B.W. & Pailthorpe, B.A. *Chem. Phys. Lett.* **51**, 257 (1977).
23. Kjellander, R. & Sarman, S. *Faraday Transactions* (in press).
24. Horn, R.G. & Israelachvili, J.N. *Chem. Phys. Letts.* **71**, 192 (1980).

25. Israelachvili, J.N. & Pashley, R.M. **306**, 249 (1983).

26. Christenson, H.K. *J. Chem. Phys.* **78**, 6906 (1983).

27. Christenson, H.K. & Horn, R.G. *Chemica Scripta* **25**, 37 (1985).

28. Horn, R.G., Smith, D.T. & Haller, W. *Chemical Physics Letters* **162**, 404 (1989).

29. LeNeveu, D.M., Rand, R.P. & Parsegan, V.A. *Nature* **259**, 601 (1976).

30. Langmuir, I. *J. Chem. Phys.* **6**, 837 (1938).

31. Lyklema, J. & Mysels, K.J. *J. Am Chem. Soc.* **87**, 2539 (1965).

32. Clunie, J.S., Goodman, J.F. & Symons, P.C. *Nature* **216**, 1203 (1967).

33. Lis, L.J., McAlister, M., Fuller, M., Rand, R.P. & Parsegan, V.A. *Biophys. J.* **37**, 657 (1982).

34. Parsegian, V.A., Fuller, N. & Rand, R.P. *Proc. Acad. Nat. Sci. USA* **76**, 2750 (1979).

35. Peschel, G., Belouschek, P., Muller, M.M., Muller, M.R. & Konig, R. *Colloid and Polymer Science* **260**, 444 (1982).

36. Rabinovich, Y.I., Derjaguin, B.V. & Churaev, N. *Adv. Coll. Interface Sci.* **16**, 63 (1982).

37. Marra, J. & Israelachvili, J.N. *Biochemistry* **24**, 4608 (1985).

38. Viani, B.E., Low, P.F. & Roth, C.B. *J. Coll. Int. Sci.* **96**, 229 (1983).

39. Pashley, R.M. & Israelachvili, J.N. *J.Col.Int.Sci.* **97**, 446 (1984).

40. Pashley, R.M. *J.Coll. Int. Sci.* **83**, 531 (1981).

41. Christenson, H.K. *J. CHem. Soc. Faraday Trans. I* **80**, 1933 (1983).

42. Persson, P.K.T. & Bergenstahl, B.A. *J. Biophys.* **47**, 743 (1985).

43. Marcelja, S. in *Liquids at Interfaces* (eds. Charvolin, J., Joanny, J.F. & Zinn-Justin, J.) (Elsevier, 1990).

44. Attard, P. & Batchelor, M.T. *Chem. Phys. Lett.* **149**, 206 (1988).

45. Franks, F. in *Water: A Comprehensive Treatise Vol 1* (Ed. Franks) (Plenum Press, New York, 1975).

46. Tanford, C. *The Hydrophobic Effect* (Wiley, New York, 1980).

47. Zichi, D.A. *J. Chem. Phys.* **83**, 797 (1985).

48. Pratt, L.R. & Chandler, D. *J. Chem. Phys.* **67**, 3683 (1977).

50. Pashley, R.M. & Israelachvili, J.N. *Col. and Surf.* **2**, 169 (1981).

51. Israelachvili, J.N. & Pashley, R.M. *Nature* **300**, 341 (1982).

52. Israelachvili, J.N. & Pashley, R.M. *J. Coll. Int. Sci.* **98**, 500 (1984).

53. Pashley, R.M., McGuiggan, P.M., Ninham, B.W. & Evans, D.F. *Science* **229**, 1088 (1985).

54. Claesson, P.M., Blom, C.E., Herder, P.C. & Ninham, B.W. *J. Coll. Int. Sci.* **114**, 234 (1986).

55. Claesson, P.M. & Christenson, H.K. *J. Phys. Chem.* **92**, 1650 (1988).

56. Christenson, H.K. & Claesson, P.M. *Science* **239**, 390 (1988).

57. Christenson, H.K., Claesson, P.M., Berg, J. & Herder, P.C. *J. Phys. Chem.* **93**, 1472 (1989).

58. Kurihara, K., Kato, S. & Kunitake, T. *Chem. Lett* 155 (1990).

59. Christenson, H.K., Fang, J., Ninham, B.W. & Parker, J.L. *J. Phys. Chem.* **94**, 8004 (1990).

60. Israelachvili, J.N., Tandon, R.K. & White, L.R. *J. Col. Int. Sci.* **78**, 430 (1980).

61. Klein, J. *J. Chem. Soc. Faraday Trans.* **79**, 99 (1983).

62. Gotze, T. & Sonntag, H. *Colloids and Surfaces* **31**, 181 (1988).

63. Hadziiounnau, G., patel, S., Granick, S. & Tirrell, M. *J. Amer. Chem. Soc.* **108**, 1868 (1986).

64. Basswereau, P., Marignan, J. & Porte, G. *J. Physique.* **48**, 673 (1987).

65. Helfrich. *Naturforsch* **33a**, 305 (1978).

66. Helfrich, W.Z. *Naturforsch* **28c**, 693 (1973).

67. Derjaguin, B.V. & Kussakov, M. *Acta Physiochim* **10**, 25 (1939).

68. Derjaguin, B.V., Titijevskaia, A.S., Abricossova, I.I. & Malinka, A.D. *Disc. Faraday. Soc.* **18**, 24 (1954).

69. Schofield, R.K. *Trans Faraday Soc.* **42**, 219 (1946).

70. Read, A.D. & Kitchener, J.A. *J. Colloid and Int. SCi.* **30**, 391 (1969).

71. Donners, W.A.B., Rijnbout, J.B. & Vrij, A. *J. Col. Int. Sci.* **61**, 249 (1976).

72. Pashley, R.M. & Kitchener, J.A. *J. Col. Int. Sci.* **71**, 491 (1979).

73. Gee, M.L., Healy, T.W. & White, L.R. *J. Col. Int. Sci.* **131**, 18 (1989).

74. Beaglehole, D., Radlinska, E.Z., Ninham, B.W. & Christenson, H.K. *Phys Rev Lett* **66**, 2084 (1991).

75. van Blockland, P.H.G.M. & Overbeek, J.T.G. *J. Col. Int. Sci.* **68**, 96 (1979).

76. Black, W., De Jongh, J.G.V., Overbeek, T.H.G. & Sparnaay, M.J. *Trans. Faraday Soc.* **56**, 1597 (1960).

77. Overbeek, J.T.G. & Sparnaay, M.P. *Disc. Faraday. Soc.* **18**, 12 (1954).

78. Overbeek, J.T.G. & Sparnay, M.J. *J. Col. Int. Sci.* **7**, 343 (1952).

79. Tonck, A., Georges, J.M. & Loubet, J.L. *J. Col. Int. Sci.* **126**, 150 (1988).

80. Derjaguin, B.V., Rabinovich, Y.I. & Churaev, N.V.*Nature* **272**, 313 (1978).

81. Israelachvili, J.N. & Adams, G. *J. Chem. Soc. Faraday Trans. I* **74**, 975 (1978).

82. Tabor, D. & Winterton, R.H.S. *Proc. Roy. Soc.* **A312**, 435 (1969).

83. Israelachvili, J.N. & Tabor, D. *Proc. R. Soc. Lond.* A **331**, 19 (1972).

84. Israelachvili, J.N. & McGuiggan, P.M. *J. Mater. Res.* **5**, 1 (1990).

85. Parker, J.L., Christenson, H.K. & Ninham, B.W. *Rev. Sci. Instrum.* **60**, 3135 (1989).

86. Parker, J.L. *Langmuir* (Submitted).

87. Chan, D.Y.C. & Horn, R.G. *J. Chem. Phys.* **83**, 5311 (1985).

88. Israelachvili, J.N. *J. Col. Int. Sci.* **110**, 163 (1986).

89. Horn, R.G., Clarke, D.R. & Clarkson, M.T. *J. Mater. Res.* **3**, 413 (1988).

90. Tolansky, S. *Multiple-Beam Interferometry of Surfaces and Films* (Oxford University Press, London, 1948).

91. Israelachvili, J.N. *J. Col. Int. Sci.* **44**, 259 (1973).

92. Stewart, A.M. & Christenson, H.K. *Meas. Sci. Technol.* **1**, 1301 (1990).

93. Derjaguin, B. *Kholloid Zh.* **69**, 155 (1934).

94. Binnig, G. & Rohrer, H. *Helv. Phys. Acta.* **55**, 726 (1982).

95. Wickramasinghe, H.K. *Scientific American* **October**, 74 (1989).

96. Binnig, G., Quate, C. & Gerber, G. *Phys. Rev. Lett.* **56**, 930 (1986).

97. Neubauer, G., Cohen, S.R., McClelland, G.M., Horne, D. & Mate, C.M. *Rev. Sci. Inst.* **61**, 2296 (1990).

98. Meyer, G. & Amer, N.M. *Appl. Phys. Lett.* **53**, 1045 (1988).

99. Sarid, d., Iams, D.A., Ingle, J.T. & Weissenberger, V. *J. Vac. Sci. Technol.* **A8**, 378 (1990).

100. Martin, Y., Williams, C. & Wickramasinghe, H. *J. Appl. Phys.* **61**, 4723 (1987).

101. Schoenenberger, C. & Alvardo, S.F. *Rev. Sci. Instrum.* **60**, 3131 (1989).

102. den Boef, A.J. *Appl. Phys. Lett* **55**, 439 (1989).

103. Rugar, D., Mamin, H.J., Erlandson, R., Stern, J.E. & Terris, B.D. *Rev. Sci Instrum.* **59**, 2337 (1988).

104. Meyer, G. & Amer, N.M. *App. Phs. Lett.* **56**, 2100 (1990).

105. Durig, U., Gimzewski, J.K. & Pohl, D.W. *Phys. Rev. Lett.* **57**, 2403 (1986).

106. Durig, U., Zuger, O. & Pohl, D.W. *J.Microsc.* **152**, 259 (1988).

107. Yamada, H., Fujii, T. & Nakayama, K. *J. Vac. Sci. Technol.* **A6**, 293 (1988).

108. Erlandsson, R., Hadziioannou, G., Mate, C.M., McClelland, G.M. & Chiange, S. *J. Phys. Chem.* **89**, 5190 (1988).

109. Cohen, S.R., Neubauer, G. & McClelland, G.M. *J. Vac. Sci Technol.* **A8**, 3449 (1990).

110. Taubenblatt, M.A. *Appl. Phys. Lett.* **54**, 801 (1989).

111. Bryant, P.J., Kim, H.S., Deeken, R.H. & Cheng, Y.C. *J. Vac. Sci. Technol.* **A8**, 3502 (1990).

112. Miller, G.L., Griffith, J.E., Wagner, E.R. & Grigg, D.A. *Rev. Sci. Instrum.* **62**, 705 (1991).

113. Joyce, S.A. & Housten, J.E. *Rev. Sci. Intrum.* **62**, 710 (1991).

114. Burnham, N.A. & Colton, R.J. *J. Vac. Sci. Technol.* **A7**, 2906 (1989).

115. Burnham, N.A., Dominguez, D.D., Mowery, R.L. & Colton, R.J. *Phys. rev. Lett.* **64**, 1931 (1990).

116. Weisenhorn, A.L., Hansma, P.K., Albrecht, T.R. & Quate, C.F. *Appl. Phys. Lett.* **54**, 2651 (1989).

117. McGuiggan, P.M. & Pashley, R.M. *J. Phys. Chem.* **92**, 1235 (1988)

Chapter 3

The forces between mica surfaces in ammonium chloride solutions

3.1 Introduction

This chapter examines the forces between sheets of mica immersed in ammonium chloride solutions. Because cations from aqueous solution can be exchanged for the original potassium ions on the surface of mica, measurement of surface forces provides an understanding of the ion-exchange properties of mica and the hydration of the surface induced by the adsorbed ions.

In a large reservoir of pure water, the surface potassium ions are almost completely exchanged for protons. In this case there is a small negative charge on the mica due to the desorption of about one proton every 10 nm^2 but when electrolyte is added other cations may adsorb at the surface altering the surface charge and other surface properties. The ion-exchange behaviour of mica in the presence of alkali and alkali-earth metal ions has been studied in some detail[1, 2]. If the size of the ion is included, then a simple ion-exchange model allowing competitive adsorption of metal ions and proton can account for the surface dissociation and charging properties.

The hydration of the mica surface in the presence of adsorbing alkali and alkali-earth metal ions has also been studied. Short range repulsive forces in addition to those predicted by DLVO theory have been observed, and have been attributed to water structure[1, 3]. However, when protons adsorb to the same surface no hydration force is measured, probably because some unique chemical bonding of the proton at or beneath the mica surface prevents the proton from perturbing the water structure. (A possible site for the binding of protons is to the hydroxide groups below the basal

plane oxygen atoms.) This observation, together with the fact that the onset of hydration forces occurs over a narrow concentration range, led Pashley[1] to propose that for mica, the hydration force is determined by the exchange of hydrated cations for protons as mica sheets are pushed together. This exchange is in turn dependent on the relative concentrations of protons and other cations in the bulk phase, as well as the binding constants[4]. The extent of proton binding and its exchange are thus important in determining both the charge and the hydration properties of the surface.

The adsorption of acidic cations is therefore of interest because there is the possibility of the dissociation of the acid on the surface to leave a bound proton and a neutral group in solution. This allows the possibility of ion exchange simply by the transfer of a neutral molecule from the surface to solution. There is also the possibility of direct hydrogen-bonding between water molecules and NH_4^+ ions. This chapter reports an investigation of the hydration and ion-exchange properties of the acidic cation, NH_4^+.

As described in the introduction to this thesis, previous experiments have shown that the hydration force can be a complicated function of distance. When monatomic cations remain adsorbed to the surface of mica in water, the resultant repulsive force is an oscillatory function of distance (thought to be a result of packing of the water molecules between the flat surfaces) superimposed on a large repulsive force due to the work required to dehydrate the ions adsorbed to the surface. No oscillatory forces are measured between lipid bilayers when adsorbed to mica[5] or in lamellar phase[6], presumably because the surface is sufficiently rough for the oscillatory structure to be averaged out. The forces between surfaces containing adsorbed ammonium ions is thus of interest both because the ion is polyatomic, and because the ion can hydrogen bond with the solvent.

3.2 Materials and Methods

The experiments reported in Chapters 3 and 4 of this thesis involve measurements of forces measured between surfaces of muscovite mica. Muscovite mica is a convenient substrate for surface force measurements because it may be cleaved to form pieces which are smooth to within 2 Å over regions centimeters square. Mica is a sheet silicate which is related to pyrophyllite by substitution of aluminium for one quarter of the tetrahedral silicon atoms. The discrepancy in charge is satisfied by the addition of potassium ions between the layers of aluminosilicate, yielding an overall chemical composition of $KAl_2(AlSi_3)O_{10}(OH)_2$ [7] and the structure shown in figure 3.1. The surface of the sheet structure consists of rings of 12 covalently bonded atoms, 6 of which are oxygen and on average 4.5 silicon and 1.5 aluminium. The potassium ions lie between the silicate sheets and are located where the aluminium atoms occur, on average one every second ring. Since each ring occupies an area of 0.24 nm^2, the area per aluminiun/potassium site is 0.48 nm^2. When sheets of mica are cleaved along a basal plane, the potassium ions are distributed evenly between the two new surfaces. Situated between the surface rings is a layer of aluminium-oxygen and hydroxide groups. The oxygen of the hydroxide is about 0.4 nm from the plane of the potassium ions[8].

A force microscope image of the surface of mica is shown in figure 3.2. The operation of a force microscope is explained in section 2.4. Note that the image shows a rectangular lattice with a periodicity of 0.52 nm, indicating that in this case the microscope resolves only pairs of silicate tetrahedra.

Forces were measured using the Surface Forces Apparatus as described in the introduction.

Analytical grade ammonium chloride from AJAX chemicals was used without further purification

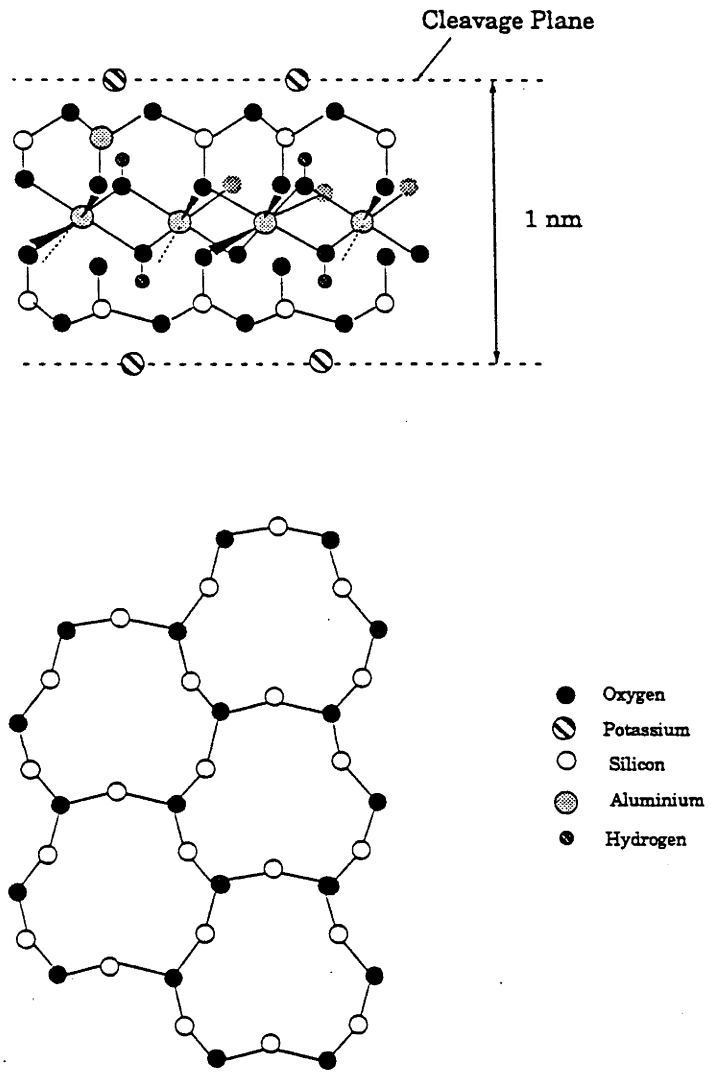

Figure 3.1: The structure of muscovite mica. The top figure shows the lattice viewed along the basal plane, and the bottom figure shows the structure in a perpendicular view. (This figure has been copied with permission from John Parker's PhD thesis, ANU,1989)

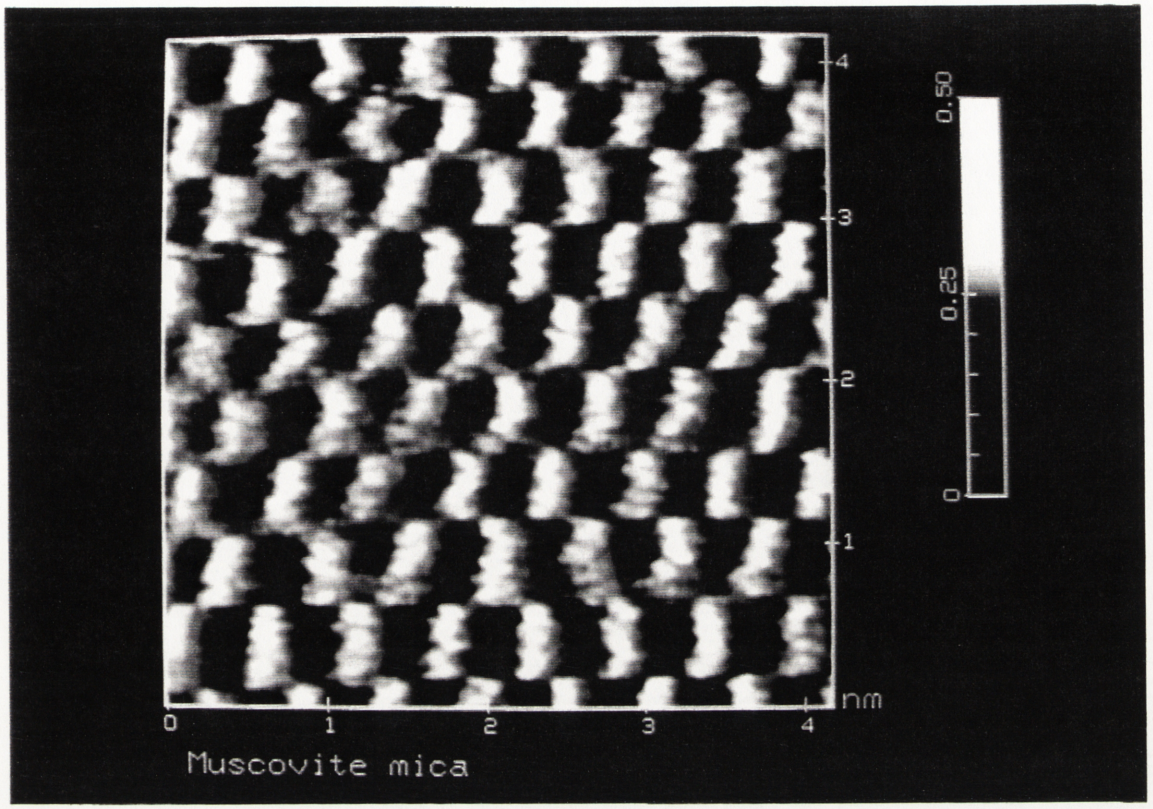

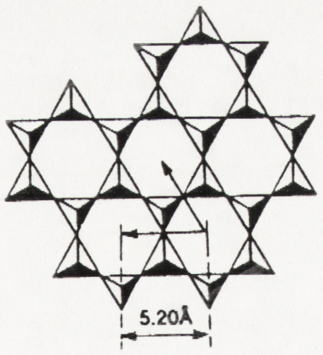

Figure 3.2: a)Atomic Force Microscope image of the surface of muscovite mica. b)Tetrahedral structure of the basal plane. Note that two tetrahedra.are related to one high (white) region of (a).

3.3 Results and Discussion

Force measurements in a range of NH_4Cl solutions

The forces between two mica surfaces immersed in a range of NH_4Cl solutions at 21°C are shown in figures 3.3 to 3.6. Because the range of the interaction is much less than the radius of the substrates (about 2 cm) the Derjaguin approximation (see section 2.4) may be used so the forces have been plotted scaled by the radius of the mica substrates. In each figure the solid line is the best fit of the experimental data by DLVO theory calculated using an exact numerical solution of the Poisson-Boltzmann equation[9] and a non-retarded Hamaker attraction. A Hamaker constant of 2.2×10^{-20} J has been used for the mica/water/mica system[10], and the origin for the plane of charge has been set at the position of closest approach of the mica. The magnitude of the fitted double-layer repulsion is a function of the surface potential and the decay (the debye-length) is determined by the solvent concentration. The double-layer equation can be solved for various boundary conditions, with all cases lying between the upper limit of constant surface charge and the lower limit of constant surface potential[11]. In this experiment, each set of measured points lies close to the constant charge case so only this limit has been shown.

Figure 3.3 shows the interaction in 10^{-5} M and 1.1×10^{-4} M NH_4Cl solutions. For the 10^{-5} M solution, the theoretical curve was calculated with a surface potential of -100 mV, a surface charge of -0.0013 Cm^{-2} and a Debye-length of 96 nm (as expected at this concentration). In the 1.1×10^{-4} M solution, the DLVO curve was calculated using a surface potential of -90 mV, a surface charge of -0.0038 Cm^{-2} and a Debye-length of 26 nm (compared to the value of 29 nm expected for this concentration). In both cases, the forces could not be measured beyond the force maximum because of the nature of the measurement technique. When the slope of the attractive force

becomes greater than the spring constant, the system is unstable so the surfaces jump to the next stable position (in this case primary minimum contact at D=0). For the relatively weak spring used in this experiment (spring constant = 148 Nm^{-1}), the jump starts roughly at the position of maximum force. In the 10^{-5} M solution, the last measurement before the jump was at 4.2 nm separation, which is close to the predicted jump distance of 3.7 nm, and in the 1.1 x 10^{-4} M solution, where the surfaces should jump from 2.2 nm apart, the last measurement was made at 3.3 nm. The interfacial energy for the mica/ammonium solution was also measured at these two concentrations, and was found to be close to that measured for mica in water

At $1.1x10^{-3}$ M NH_4Cl (figure 3.4), the measured forces agreed well with those predicted by DLVO theory for a surface potential, Ψ_0 of -82 mV, a surface charge, σ_0 of -9.3x 10^{-3} Cm^{-2} and a Debye-length, κ^{-1} of 8.7 nm (calculated 9.2 nm) at distances greater than about 1.5 nm separation. Below this distance the measured force was greater than that predicted by DLVO theory indicating an additional repulsive force. This force was large enough to prevent the surfaces from being brought into contact because the spring used for the measurement was too weak. This type of force has previously been identified as a hydration force or more precisely, a secondary hydration force[12]. When the applied force was reduced, the surfaces jumped apart only a small distance (about 10 nm) which, together with the fact that the surfaces were not in contact indicated the presence of a weak hydration minimum[1]. This region of the force curve is discussed in more detail later.

When the concentration was increased to $3x10^{-3}$ M (figure 3.5), the measured forces still agreed well with DLVO theory (Ψ_0 = -82 mV, σ_0 = -0.015 Cm^{-2}, κ^{-1} = 5.5 nm (κ^{-1} calculated = 5.6 nm)) up to about 1 nm separation, after which the additional hydration force again prevented the surfaces from coming into adhesive contact. However, despite the three-fold increase in concentration from the previous measurement, the fitted potential did not decrease. The significance of this will be

discussed in the next section. Figure 3.6 shows the results for 1.2×10^{-2} M NH_4Cl, where once again the forces agree well with DLVO theory (Ψ_0 = -65 mV, σ_0 =- 0.022 Cm^{-2}, κ^{-1} = 2.7 nm, κ^{-1} calculated = 2.8 nm) until the hydration force becomes significant.

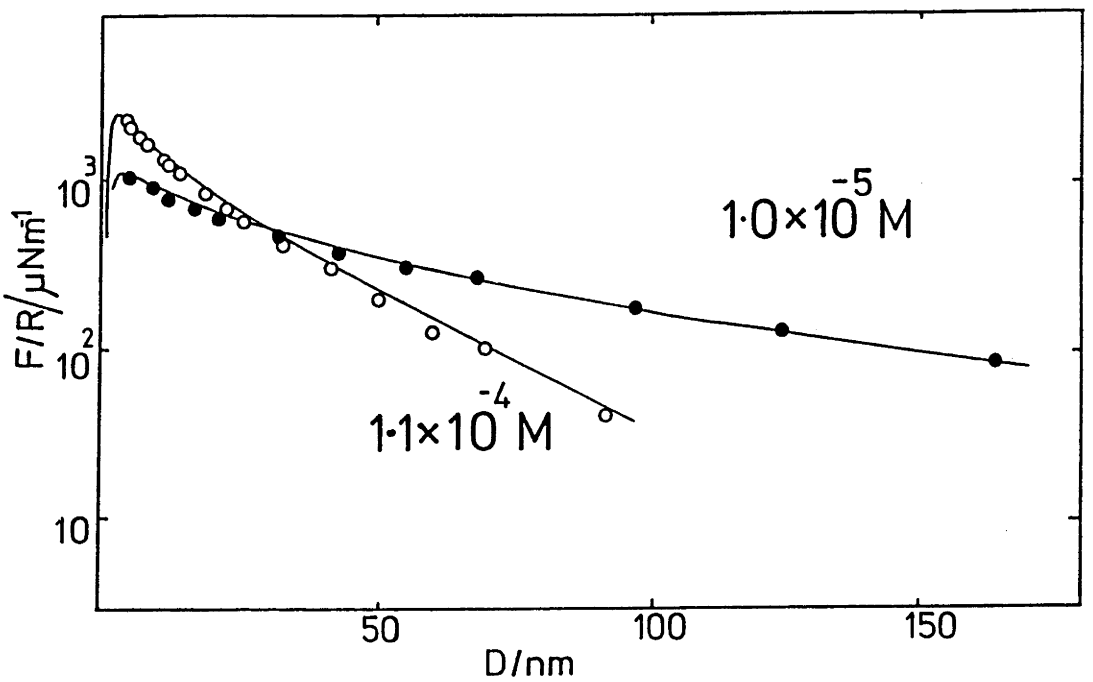

Figure 3.3: Forces between mica surfaces in dilute NH_4Cl solutions. Note that the forces have been scaled by the radius of curvature of the surfaces so are proportional to the energy/unit area between equivalent flat surfaces. The filled circles represent measurements at 1.0×10^{-5} M and the open circles measurements at 1.1×10^{-4} M. The solid lines are the best fits to DLVO theory using an exact numerical solutions of the Poisson-Boltzmann equation at constant charge and a non-retarded Van der Waals with a Hamaker constant of 2.2×10^{-20} J. This fit suggests that that the surfaces interact almost at constant charge. At 1.1×10^{-4} M the surfaces interact with a surface potential at infinite separation of -90 mV, a surface charge of -0.0038 Cm^{-2} and a Debye-length of 26 nm. At 10^{-5} M the corresponding values are -100 mV, -0.0013 Cm^{-2} and 96 nm.

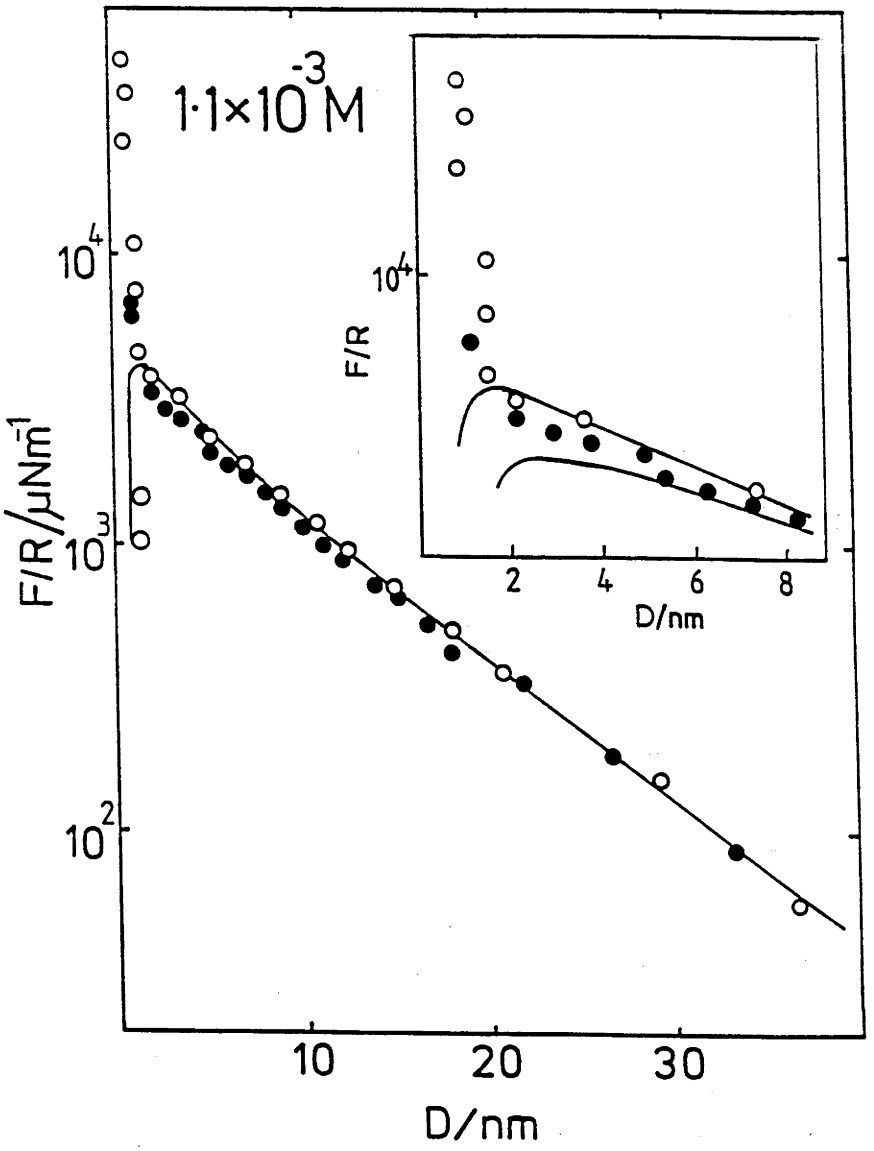

Figure 3.4 Forces between micas surfaces in 1.1×10^{-3} M NH_4Cl solution. The open and filled circles represent repeat measurements. The solid line represents the best fit to DLVO theory with the constant charge boundary condition with a surface potential of -80 mV, a surface charge of -0.0093 Cm^{-2} and a Debye-length of 8.7 nm. At separations less than about 2 nm the force is greater than the DLVO limit at constant charge indicating the presence of a hydration force. This can be seen in the inset where the constant charge and constant potential interactions (together with a Van der Waals contribution) are shown by the upper and lower lines respectively. The two points at 1.5 nm and 10^3, 1.5×10^3 μNm^{-1} indicate the presence of a secondary minimum.

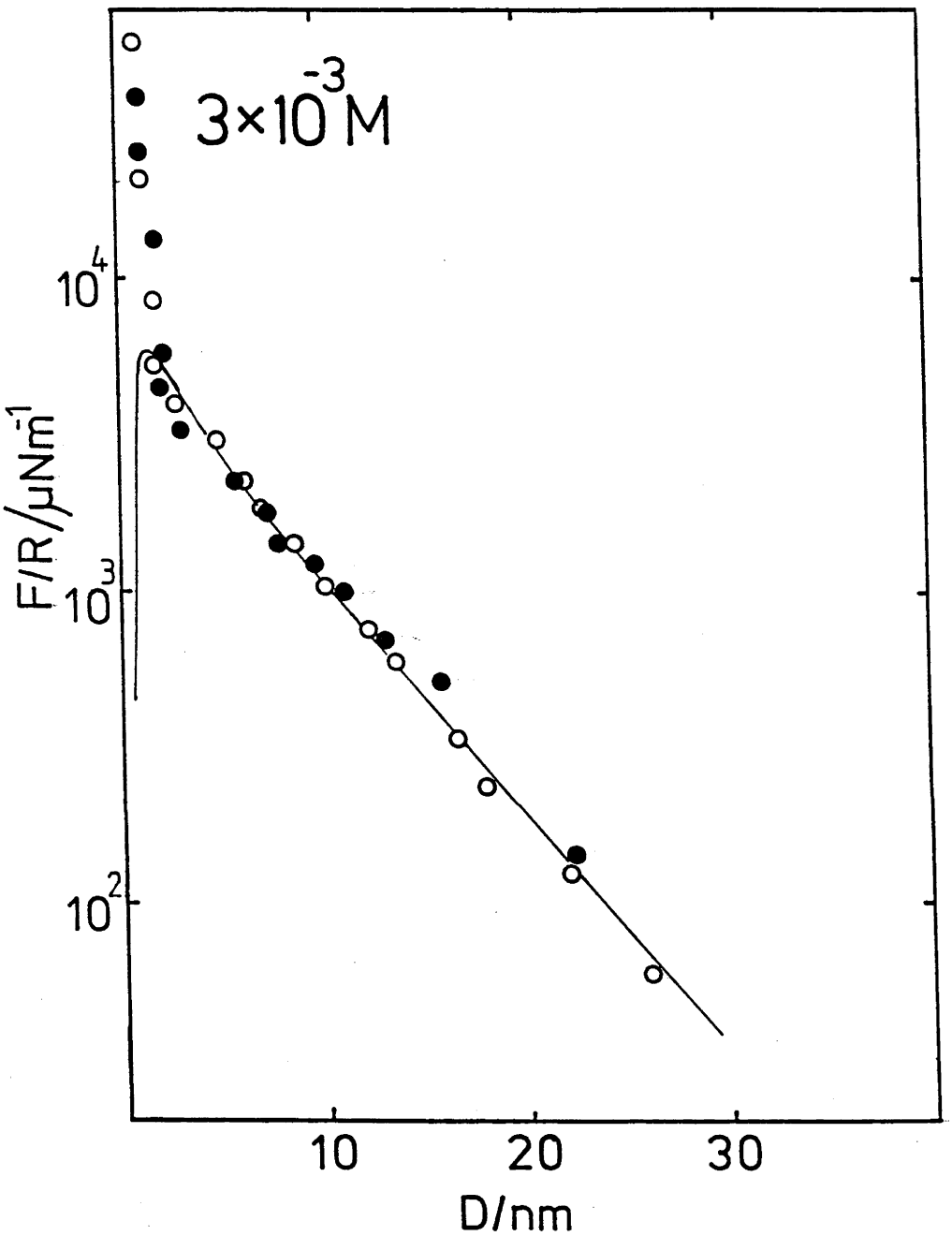

Figure 3.5 Forces between mica surfaces in $3x10^{-3}$ M NH_4Cl solutions. The open and filled circles represent repeat measurements. The solid line is the best fit as explained in the caption to figure 3.3, with a surface potential of -82 mV, a surface charge of -0.015 Cm^{-2} and a Debye-length of 5.5 nm.

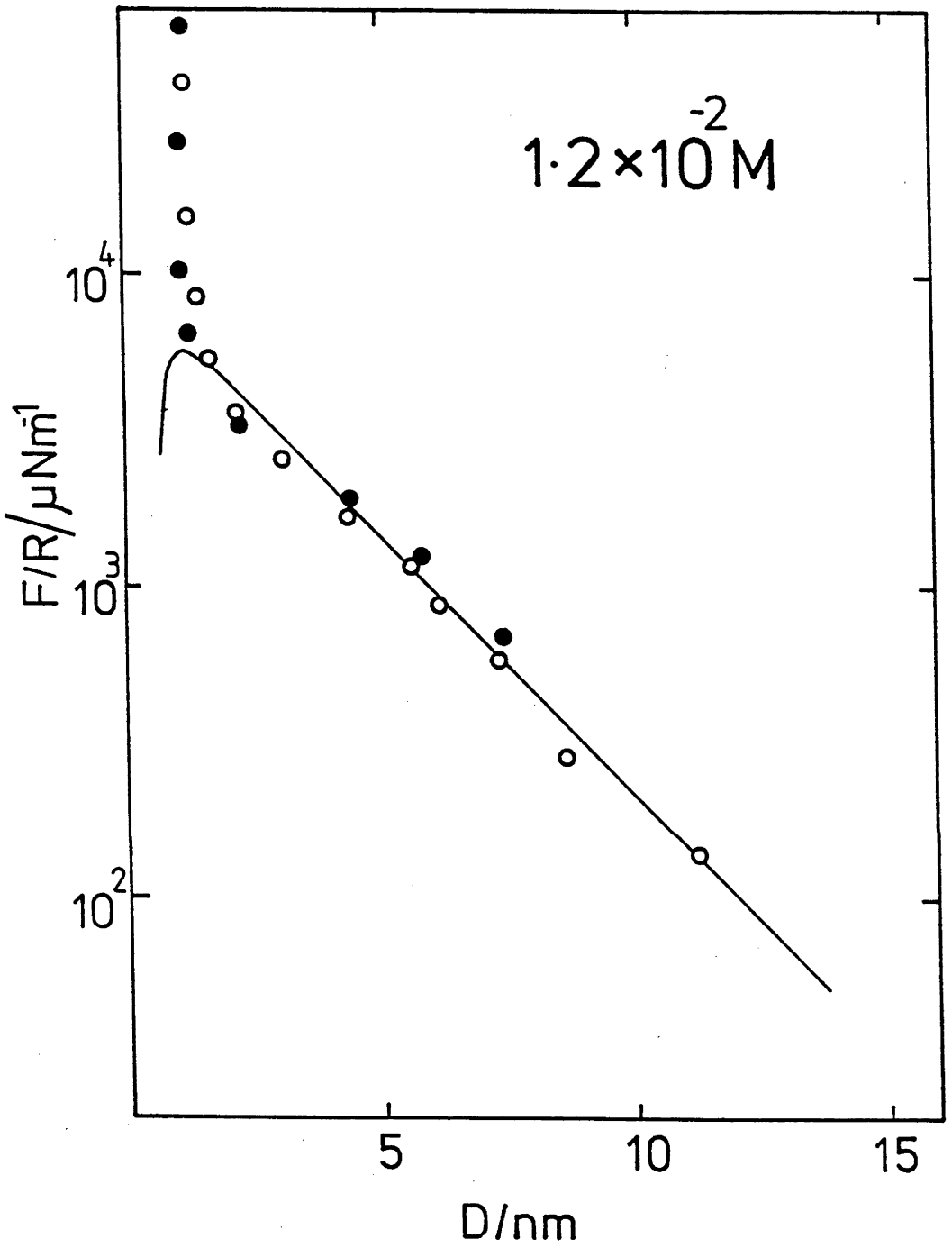

Figure 3.6: Forces between mica surfaces in 1.2×10^{-2} M NH_4Cl solutions. The open and filled circles represent repeat measurements. The solid line is the best fit as explained in the caption to figure 3.3, with a surface potential of -65 mV, a surface charge of -0.022 cm^{-2} and a Debye-length of 2.7 nm.

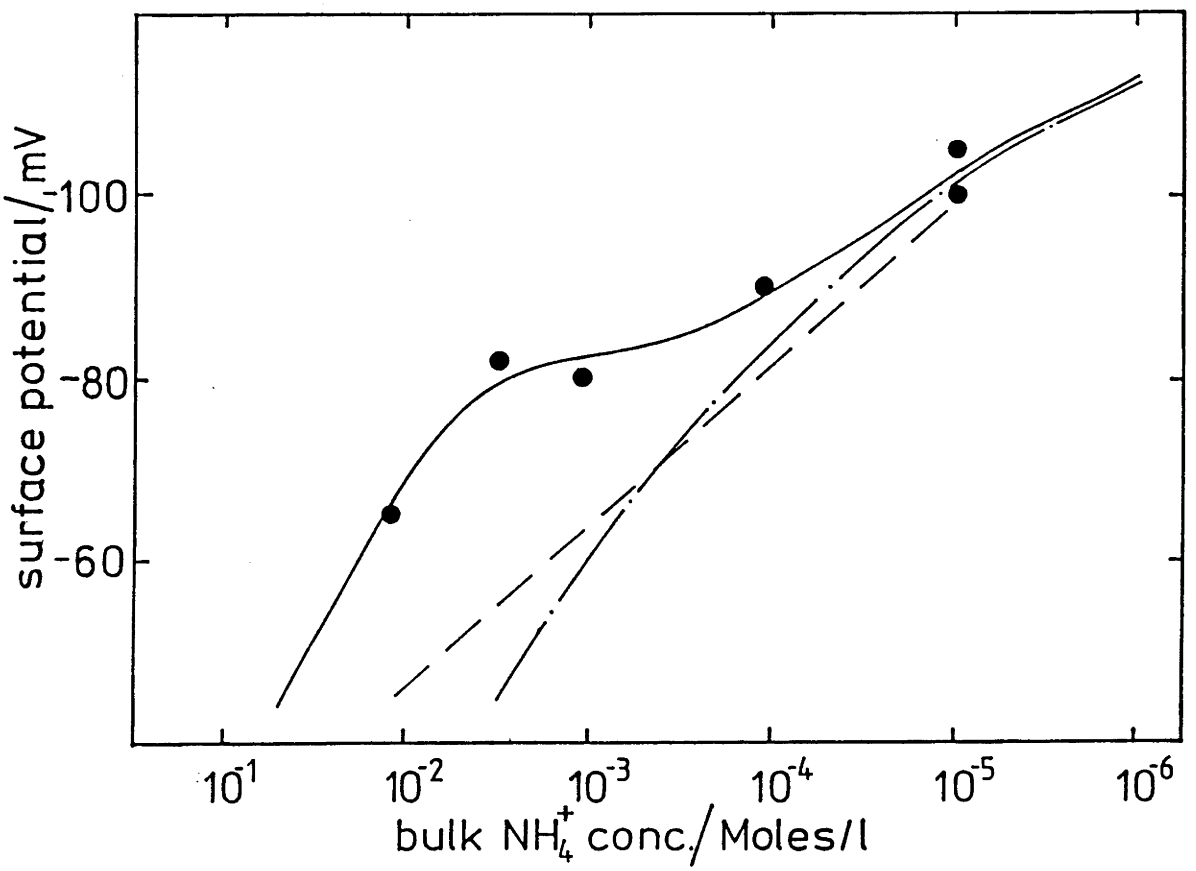

Figure 3.7 The surface potentials obtained in figures 3.3 to 3.4 are plotted here as a function of concentration. The solid line was calculated using the model described in the text with the following parameters: $A_N = 0.52$ nm^2 ; $A_H = 0.48$ nm^2; $pK_N = 3.12$ and pH = 5.4 and the dashed/dotted line with the same binding constant, but with $A_N = A_H = 0.48$ nm^2. The dashed line was calculated by assuming there is no binding of NH_4^+(K_N infinite), only electrolyte screening.

Mass action model of ion-binding

The surface potential values obtained from the theoretical fits in figures 3.3 to 3.6 are summarized in figure 3.7. It should be noted that the systematic error in the force measurements of about 10% due to determination of the spring constant and radius translates to an error of only a few mV at low potentials (<50 mV) but causes a large error at high potentials. Three theoretical curves are also shown in this figure. These are based on models developed by Pashley[1]. The dashed curve was calculated from a model in which the only potential determining ion is the proton, and thus the ammonium ion only influences the system by screening the electrical interaction. When this model was extended to allow the ammonium ion to bind to the mica surface in competition with the proton, the fit to the experimental points was also poor (dotted and dashed line). However, as observed previously for Li^+, $Na^+$and K^+, a good fit to the experimentally measured potentials can be derived from an ion-exchange model in which the adsorbing ion occupies a larger area than the mica binding site (the full line in figure 3.7). A statistical mechanical treatment of this model by Miklavic and Ninham[13] shows that the simple treatment by Pashley works well if the area occupied by the ion is similar to the area of the binding site.

This model considers surface dissociation reactions represented by the following equations:

$$SNH_4 \Leftrightarrow S^- + NH_4^+ \qquad (1)$$

$$SH \Leftrightarrow S^- + H^+ \qquad (2)$$

where S^-, SNH_4 and SH represent an unoccupied negative site, a site bound to an ammonium ion, and a site bound to an adsorbed proton, respectively. The corresponding mass action equations for these equilibria are:

$$K_N = \frac{[S^-][NH_4^+]_{surface}}{[SNH_4]} \quad (3)$$

$$K_H = \frac{[S^-][H^+]_{surface}}{[SH]} \quad (4)$$

where the surface concentrations of the adsorbing ions are related to the bulk terms by the Boltzmann equation:

$$[cation]_{surface} = [cation]_{bulk} \exp\left(\frac{-q\psi_0}{kT}\right) \quad (5)$$

where ψ_0 is the surface potential. The number of vacant sites per unit area on the mica surface, V is given by :

$$V = S\,(1 - n_N A_N - n_H A_H) \quad (6)$$

where S is the number of lattice sites per unit area on the mica surface; n is the number of ions adsorbed per unit area; A is the effective area occupied by an adsorbed ion and the subscripts N and H refer to the ammonium ion and proton, respectively. Values of $pK_H = 6.0$ and $A_H = 1/N_S = 0.48\ nm^2$ were obtained from previous work[2]. *

The surface charge density, σ_0 is related to the surface potential by the Gouy-Chapman equation:

$$\sigma_0 = \{8\varepsilon_0 DkT([H^+]_{bulk} + [NH_4^+]_{bulk})\}^{1/2} \sinh\left(\frac{q\psi_0}{2kT}\right) \quad (7)$$

(where ε_0 is the permittivity of free space and D is the dielectric constant of water) and also to the surface density of adsorbed ions by the following equation:

$$\sigma_0 = -q\,(S - n_N - n_H) \quad (8)$$

These equations can be solved numerically for given values of A_N and K_N to give ψ_0 as a function of concentration. Because A_H and A_N are set either equal to or greater than $0.48\ nm^2$ the surface is not allowed to change sign. The curve which best fits the experimental data (see figure 3.7) was calculated with an effective surface area for the NH_4^+ ion, A_N of $0.52\ nm^2$ (c.f. K^+ : $0.53\ nm^2$, Cs^+ : $0.51\ nm^2$) [1] and a K_N of 1260 ($pK_N = 3.1$) at pH 5.4.

Details of the hydration force

Measurements given in the previous section indicated that the hydration force arose at an NH_4Cl concentration of between $1.1x10^{-4}$ M and $1.1x10^{-3}$ M. Further experiments showed that this force was absent up to $8x10^{-4}$ M and that as in previous experiments with K^+ ions [10] there was fine structure in the force distance relationship (see figure 3.8). Much thinner mica was used to enable greater accuracy in distance measurement, and a stiffer spring (constant = 1600 Nm^{-1}) was used to achieve the high pressures necessary to obtain small mica separations. This precluded accurate measurements at larger distances where the forces were relatively weak. A pressure of about 17 atmospheres was applied to bring the surfaces into primary minimum and the highest pressure applied in contact was about 28 atmospheres. Because the glue used to attach the thin mica sheets to the silica support discs was relatively elastic, these high applied pressures caused flattening of the surfaces. (In this experiment the maximum flattening occurred over an area of about 1300 μm^2.) The forces plotted in figure 3.8 are scaled by the undeformed radius, R^*, measured at large separation so F/R^* provides an overestimate for $2\pi E$ at small separations. The results shows one hydration minimum at a separation of about 0.4 nm. The dashed lines show regions where the force could not be measured because the gradient exceeded the spring constant. The jump inwards at point J was most likely due to the effect of attractive van der Waals forces.

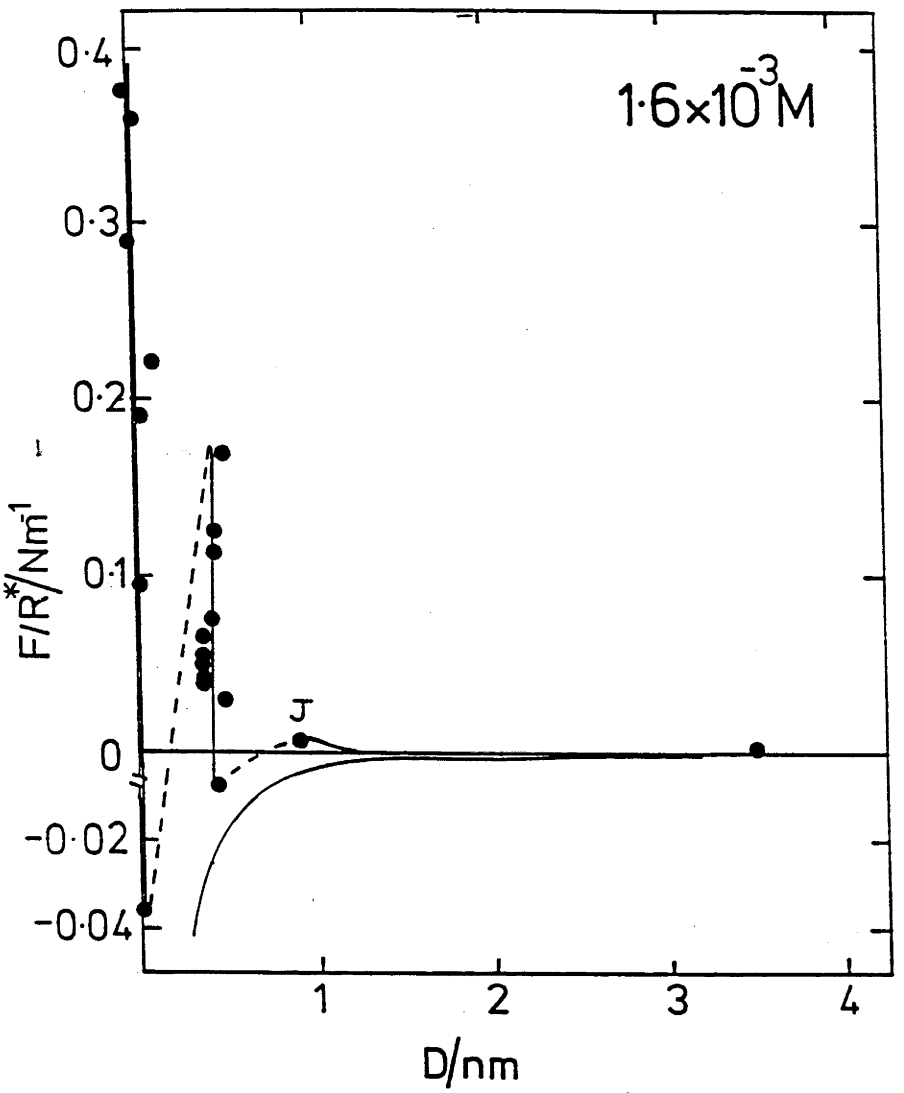

Figure 3.8: The forces between mica surfaces in 1.6 x 10^{-3} M NH_4Cl at 24 °C. The forces shown in this figure are scaled by the radius at large separations, R^*, not the actual radius of curvature since this is continually changing when the surfaces deform under the large forces applied. Note also that the scale on the force axis is linear, there is a different scale for positive (repulsive) and negative (attractive) forces, and that F/R^* is presented in N, not μN. The lower line is the theoretical Van der Waals force between the surfaces. On this scale the double-layer force lies close to the zero force line. The surfaces jump in from about 0.9 nm (point J) to where they are held in a metastable hydration minimum at D=0.4 nm.

At higher concentrations of ammonium chloride (figures 3.5 and 3.6), the measured hydration force was monotonic, and no outward jumps were recorded. This does not indicate that there is no liquid structure at these concentrations since the magnitude of the force (most likely due to hydration) is much greater than when structural forces were observed. At these higher concentrations the hydrated ammonium ions must remain between the surfaces on compression, whereas at lower concentrations they can be forced out to be replaced by protons (1,4), which has the effect of reducing the hydration force.

Oscillatory hydration forces have previously been measured when K^+ [14] or Ca^{++} [15] ions are adsorbed to the surface of mica. The forces shown here for NH_4^+ are somewhat different in that the distance between consecutive force maxima is about 0.4 nm rather than the 0.3 nm measured for the other ions. However, the method used for distance measurement in this experiment was slightly different to that used previously. With the interferometric technique used, the separation can be measured using either an odd or an even order fringe[10]. This is significant because only even order fringes are dependent on the refractive index of the medium between the surfaces. The data given in figure 3.8 was obtained from measurement of an even order fringe, and calculated using a pure water refractive index (1.333). In order to account for the discepency in the period of oscillation an index of about 1.45 is required, but this figure is unreasonably large since the model predicts that the concentration of NH_4^+ on each surface is only about 2.8 M at infinite separation, and decreases as the surfaces approach contact. The fact that such a variety of ions cause the same type of oscillatory force lends further support to the idea that the force is caused by the layering of water molecules in thin films held between molecularly smooth rigid surfaces, however, it is possible that some specific ion-water interaction can vary the periodicity of these oscillations.

Comparison of NH_4^+ to other cations

Table 1 shows a comparison of the ion-exchange and hydration properties of K^+, Cs^+ and NH_4^+ ions. From this it is clear that the properties of NH_4^+ closely resemble those of both $K^+$and Cs^+. The dissociation constant for NH_4^+ on mica is the same as that for $Cs^+$and the onset of hydration forces for NH_4^+ lies in the range measured for both $K^+$and Cs^+. In another study, K^+ and NH_4^+ have been found to have similar ion-adsorption constants on a variety of other surfaces, including layered aluminosilicates[16]. Finally, the area over which the hydrated NH_4^+ ion excludes other ions on the surface of mica was found to be intermediate between the values found for $K^+$and Cs^+, which is consistent with measurements of hydrated ion sizes obtained from conductivity measurements[17].

TABLE 1

	NH_4^+	K^+	Cs^+
pK_{diss} (mica) ✳	3.1	3.5	3.1
Onset of hydration force (x 10^{-4} M)	8-11	0.4-3.0	1-10
Exclusion area of hydrated ion on mica	0.52 nm^2	0.53 nm^2	0.51 nm^2

(The results shown for $K^+$and Cs^+ were measured in previous work by Pashley[1])

3.4 Conclusions

(1)The measured forces between mica surfaces in aqueous NH_4Cl solutions agree well with those predicted by classical DLVO theory at concentrations up to about $8x10^{-4}$ M. At higher concentrations, an additional short range repulsive force prevents the surfaces from reaching a primary minimum. This force is similar to forces previously observed for a range of other cations on mica surfaces. These forces were attributed to hydration of adsorbed cations.

(2)A detailed study at a concentration close to where the adsorption of NH_4^+ ions give rise to this repulsion indicates that the force is oscillatory and has a periodicity approximately equal to the diameter of a water molecule. This structure appears to be caused by the layering of water molecules in the thin film.

(3)The ion-exchange and hydration properties of NH_4^+ on mica were found to be similar to the alkali metal ions even though this ion is polyatomic, can hydrogen-bond to the solvent and may be able dissociate at the mica surface

3.5 References for chapter 3

1. Pashley, R.M. *J.Col.Int.Sci.* **83**, 531 (1981).
2. Pashley, R.M. & Israelachvili, J.N. *J.Col.Int.Sci.* **97**, 446 (1984).
3. Attard, P. & Batchelor, M.T. *Chem. Phys. Lett.* **149**, 206 (1988).
4. Claesson, P.M., Herder, P., Stenius, P., Erikson, J.C. and Pashley, R.M. *J.Col.Int.Sci.* **109**, 31 (1986).
5. Horn, R.G. *Biochim. Biophys. Acta* **778**, 224 (1984).
6. Lis, L.J., McAlister, M., Fuller, M., Rand, R.P. and Parsegian, V.A. *Biochem.* **17**, 3163 (1978).
7. Hunter, R.J. *Foundations of Colloid Science Volume 1* (Oxford University Press, New York 1987) Page 28.
8. Guven, N. *Zeitschrift Krystallographie* **134**, 196 (1971).
9. Chan, D.Y.C., Pashley, R.M. & White, L.R. *J.Col.Int.Sci.* **77**, 283 (1980).
10. Israelachvili, J.N. & Adams, G. *J. Chem. Soc. Faraday Trans. I* **74**, 975 (1978).
11. Chan, D.Y.C. & Mitchell, D.J. *J.Col.Int.Sci.* **95**, 193 (1983).
12. England, D. *In: Water, A Comprehensive Treatise* 1-47 (Plenum, New York, 1975).
13. Miklavic, S.J. & Ninham, B.W. *J. Col. Int. Sci.* **134**, 305 (1990).
14. Israelachvili, J.N. & Pashley, R.M. *Nature* **306**, 249 (1983).
15. Kjellander, R., Marcelja, S., Pashley, R.M. & Quirk, J.P. *J. Chem. Phys.* **92**, 4399 (1990).
16. Krishnamoorthy, C. & Overtreet, R. *Soil Sci.* **69**, 41 (1950).
17. Nightingale, J., E.R. *J. Phys. Chem.* **69**, 1381 (1959).

Chapter 4

The forces between mica surfaces in the presence of rod-shaped divalent ions

4.1 Introduction

In the previous section it was shown that the forces between mica surfaces immersed in solutions containing the polyatomic ammonium ion are similar to those measured in the presence of the alkali metal ions, K^+ and Cs^+. At concentrations below 10^{-4} M NH_4Cl, the measured forces agree well with classical double-layer theory using a fitted potential. At concentrations above 10^{-3} M, the forces still agree well with classical double-layer theory at separations beyond 2 nm, but at smaller separations, an additional force was measured, and attributed to the work required to dehydrate the surface adsorbed NH_4^+ ions. Similar forces have been measured in solutions which contain a divalent counter-ion, Ca^{2+}[1]. However, at high concentrations, additional effects occur because of the divalent ion [2]. This chapter describes experiments in which the forces in solutions of a divalent diamine salt were measured and comparison is made to the forces previously measured in Ca^{2+} solutions. Because these systems are important in the understanding of clay swelling , a brief description of this will be given.

In an earlier study [3], it was demonstrated that when the native K^+ ions of mica are replaced by Na^+ by immersion in NaCl solutions, , the forces between mica surfaces were similar to those observed in the swelling of Na-montmorillonite[4]. More recently, the short-range (< 1.5 nm) oscillatory forces observed between mica surfaces immersed in water (see figure 1.2.2) have been related to the stepped or 'crystalline' swelling of clays. This periodicity in the force curve was predicted from molecular simulations of fluids trapped between two hard walls [6] and have now been observed

for many liquids [7]. They arise because of the packing constraints on the fluid molecules which favour layering and are analogous to the oscillatory correlation function observed for bulk fluids.

In previous measurements it was also shown that a short-ranged repulsive force arises when the concentration of metal ions at a given pH is above some particular value, the critical hydration concentration, chc [8]. This force has been attributed to the removal of the water of hydration from the adsorbed ions and has been shown to be dependent on ion exchange of metal ions for H^+ at the mica surface. When two mica sheets are forced together in a solution below the chc, adsorbed hydrated metal ions are exchanged for H^+ ions, which seem to be able to bind to the aluminosilicate surface of mica with no residual hydration[9]. Desorption of the Na^+ ions under pressure can be prevented by either increasing the bulk Na^+ ion concentration or by raising the pH of the solution. This dehydrated form of H^+ adsorption does not appear to occur for clays other than mica and this has been discussed by Quirk and Pashley[9]. Prevention of ion-exchange therefore leads to forces which can be compared directly with those generated in clay swelling. A range of cations have been studied on the mica surface [10] and each gives rise to a short-range repulsive force the magnitude of which is related to the degree of hydration of the ion.

In any comparison between the force measurements on mica, and aqueous clay systems it is necessary to consider the difference in reservoirs in the two cases. Thus, for example, a high surface area Na^+ or Ca^+ clay cannot exchange with cations in the bulk solution without affecting the concentration of the latter. By comparison, in surface force measurements, the mica surface is immersed in an effectively infinite reservoir, so that ion-exchange at the surface does not affect the concentration of the reservoir.

In a recent series of theoretical and experimental studies[2, 11] the outstanding problem in soil management of the prevention of clay swelling by Ca^{2+} ions has been addressed in some detail. The results of this study indicate that there is an ion-ion correlation effect which gives rise to a strong adhesive force acting over a narrow distance range (~ 0.6 - 1.2 nm) for divalent ions. Such a force has been observed for mica surfaces in $CaCl_2$ solutions [2]. This ion correlation force is not included in the smeared-out charge model of Gouy-Chapman and could be considered to be a type of van der Waals force. In this chapter the forces between mica surfaces in the presence of a rod-shaped divalent cation are described and compared to the results obtained from a sedimentation study of Na^{+}-montmorillonite in the presence of Ca^{2+} and the rod-shaped ion.

4.2 Methods and Materials

Forces were measured using the Surface Forces Apparatus as described in the introduction. In all experiments approximately 2 cm^2 area of mica crystal were immersed in about 0.35 dm^3 of aqueous solution. Analytical grade NaCl and 1,3-propyldiamine were used to prepare the solutions. The divalent cation, 1,3-propyldiammonium chloride was prepared by titrating the diamine with HCl acid to give a 0.1 M solution at pH = 6.8. All force measurements were carried out at about 21-22°C.

Na-Montmorillonite clay samples were kindly provided by Professor P.F. Low.

4.3 Results and Analysis

In an earlier study[8] it was reported that repulsive hydration forces were only observed for mica surfaces in NaCl solutions above a critical concentration somewhere between 10^{-3} and 10^{-2} M. At lower concentrations the forces were reasonably well described by DLVO theory and the surfaces came into adhesive primary minimum contact, similar to that observed in distilled water. (In distilled water the mica is completely protonated).*

In this work the concentration of NaCl in the force measuring apparatus was increased more gradually. At a concentration of 5 x 10^{-3} M no repulsive solvation forces were observed and the surfaces came into primary minimum contact once a repulsive double-layer barrier was overcome. By comparison, at the slightly higher concentration of 7 x10^{-3} M NaCl a strong, short-range repulsive force was observed in addition to a diffuse double-layer force. The measured forces are given in Figure 4.1.

At separations greater than about 1.5 nm the forces are accurately described by the diffuse electrical double-layer theory of Gouy-Chapman calculated using an exact numerical solution [12] to the Poisson-Boltzmann equation assuming constant surface potential. The Debye-length used to fit the measured curve was 3.6 nm, as expected for this concentration of NaCl.

The surface potential of -130 mV is in reasonable agreement with values obtained in an earlier study[8], but the error is fitting potentials is very large at this high potential. This study shows that there is only a slight difference in adsorption density between the concentrations of 5x10^{-3} M and 7x10^{-3} M. It was for this reason that the large difference in short-range forces could not be explained by changes in adsorption density but can be explained in terms of proton exchange under pressure [13].

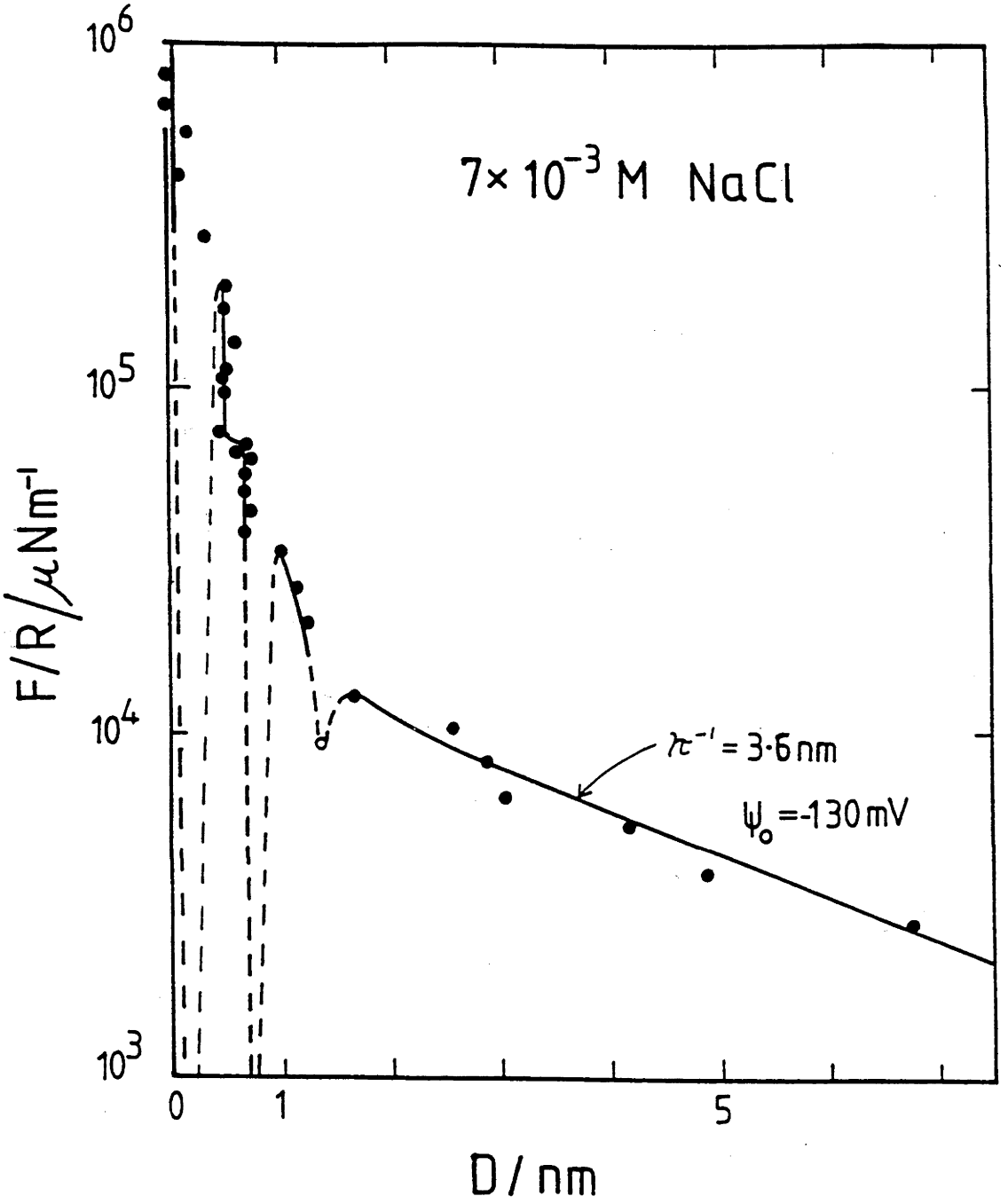

Figure 4.1: Forces measured between mica surfaces immersed in 7×10^{-3} M NaCl. At separations greater than about 1.5 nm the forces were well described by Gouy-Chapman theory. Oscillatory forces were observed at smaller separations. These have a periodicity close to the size of the water molecule. Minima were observed at 0.8 nm (-1.8×10^4 μNm^{-1}) and at 0.2 nm (-5.4×10^4 μNm^{-1}).

At separations less than 1.5 nm the forces are clearly complex. Although the short range forces are overall repulsive, they have a strong oscillatory component which produces both a stepped repulsion and several adhesive minima (see Figure 4.1).* On forcing the surfaces together as $D \rightarrow 0$ a primary minimum contact is obtained with a similar adhesive strength to that measured in distilled water. This result suggests that under pressure the adsorbed Na^+ ions can be forced out from between the surfaces and replaced by protons.

At the higher concentration of 1.4×10^{-2} M NaCl, shown in Figure 4.2, the Debye-length fell to 2.4 nm and the surface potential to -80 mV. Although the range of the solvation forces is similar to that measured in 7×10^{-3} M, the magnitude is greater and it was not possible to apply a large enough force to push the mica surfaces into contact with the cantilever used here (k= 2600 Nm^{-1}). In addition, at this concentration the minimum at a separation of about 0.85 nm was no longer adhesive.

To this solution, 3 mM of the divalent salt 1,3-propyl diamine dihydrochloride was added. The longer range forces observed are shown in figure 4.3.* These demonstrate that the diffuse double-layer force was almost completely removed and essentially only an attractive van der Waals force was measured at separations greater than about 2 nm. A steep repulsive force was measured at smaller separations and details of these forces are given in figure 4.4. The overall repulsive strength of the short-range, stepped forces was found to be unchanged, but, the minimum around 0.8-0.9 nm was altered from repulsive to strongly adhesive. When the pH was raised and the diamine neutralized by addition of 6 mM NaOH, double-layer forces were again observed and the minimum at 0.8 nm was removed.*

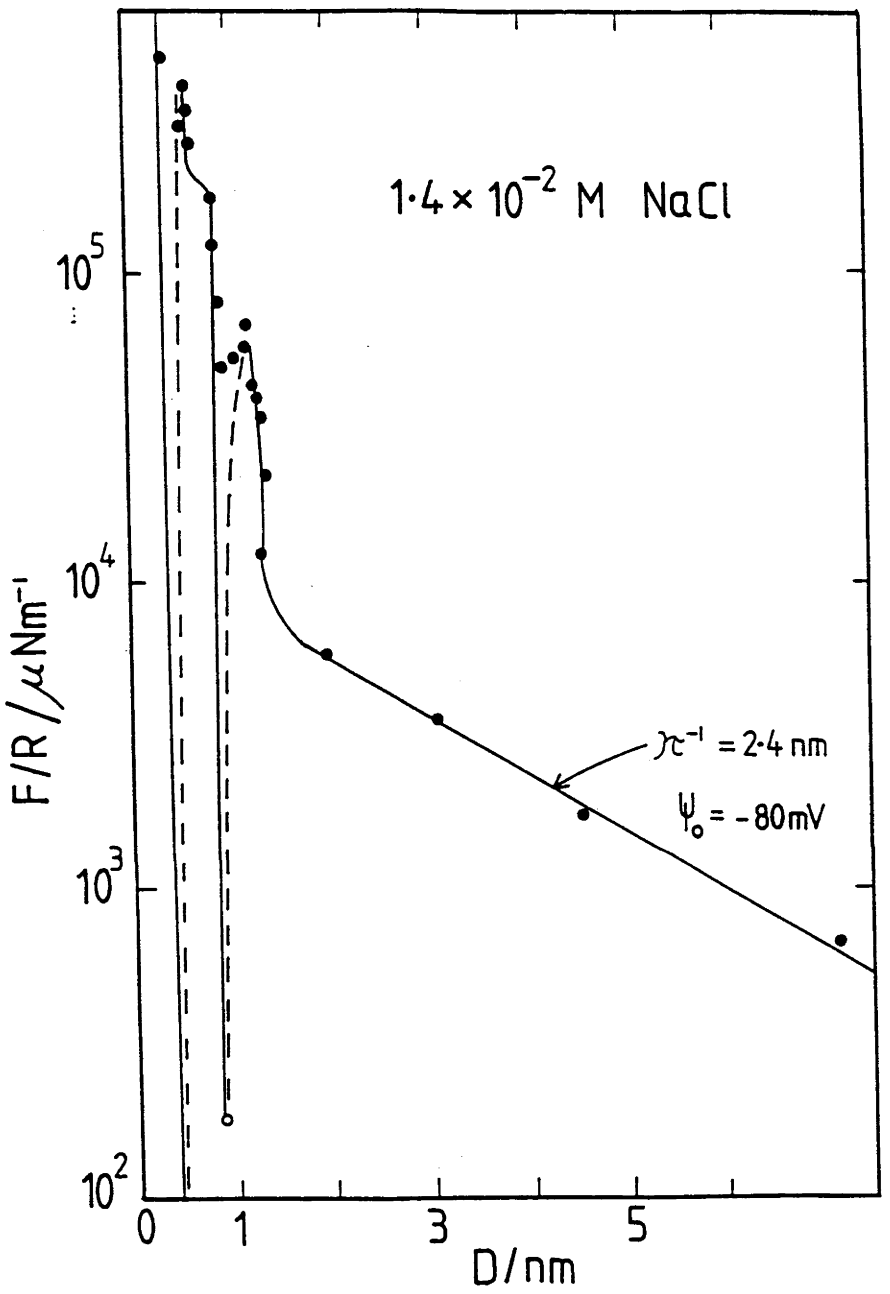

Figure 4.2: Forces measured between mica surfaces in 1.4×10^{-2}M NaCl. At separations greater than about 1.5 nm the forces can be explained by Gouy-Chapman theory. The oscillatory forces at smaller separations exhibited a repulsive minimum at about 0.85 nm and an adhesive minimum at 0.45 nm (-8.6×10^3 μNm^{-1}).

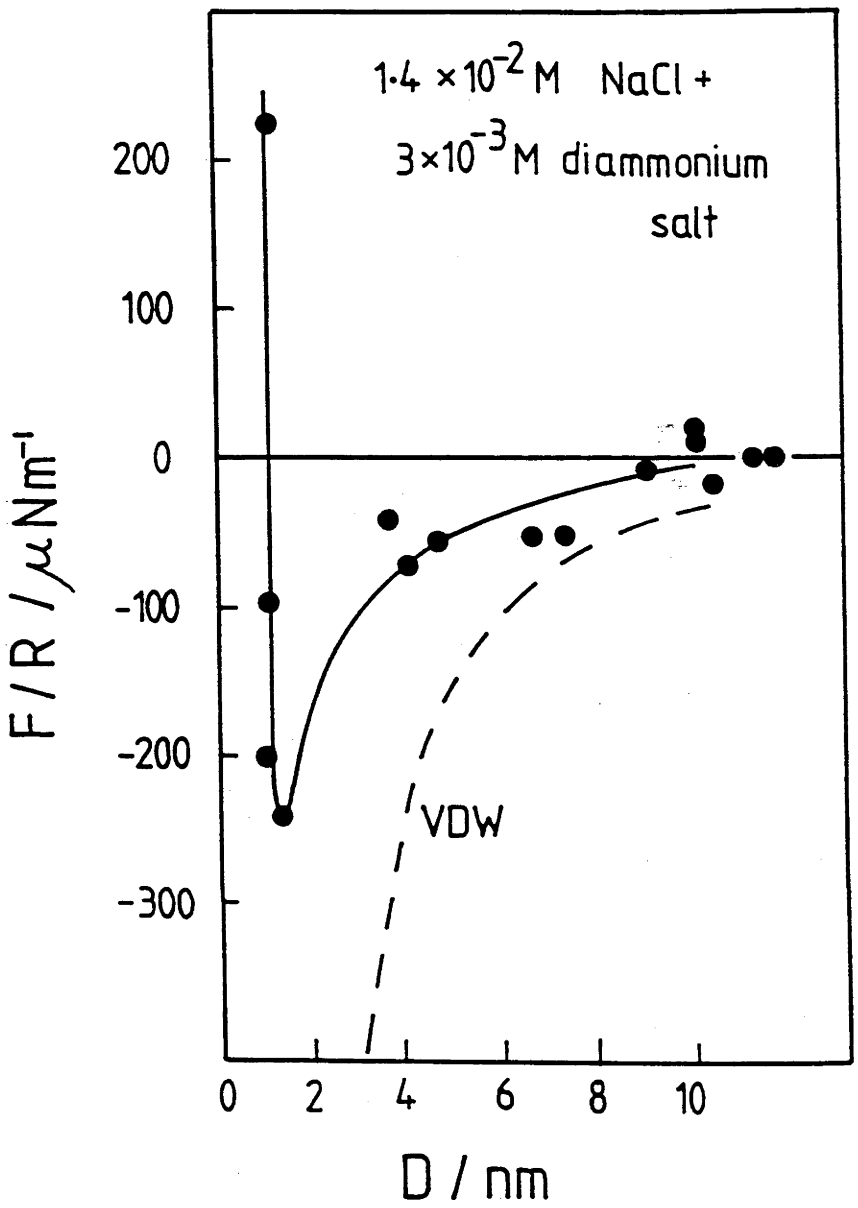

Figure 4.3: Forces measured between mica surfaces in 1.4×10^{-2} M NaCl and 3×10^{-3} M diammonium salt. Addition of the divalent salt almost completely removes the double-layer force and the forces approach those expected for a van der Waals force (using a Hamaker constant of 2.2×10^{-20} J). At small separations, repulsive structural forces were still present. Detailed measurements at these distances are shown in Figure 4.4.

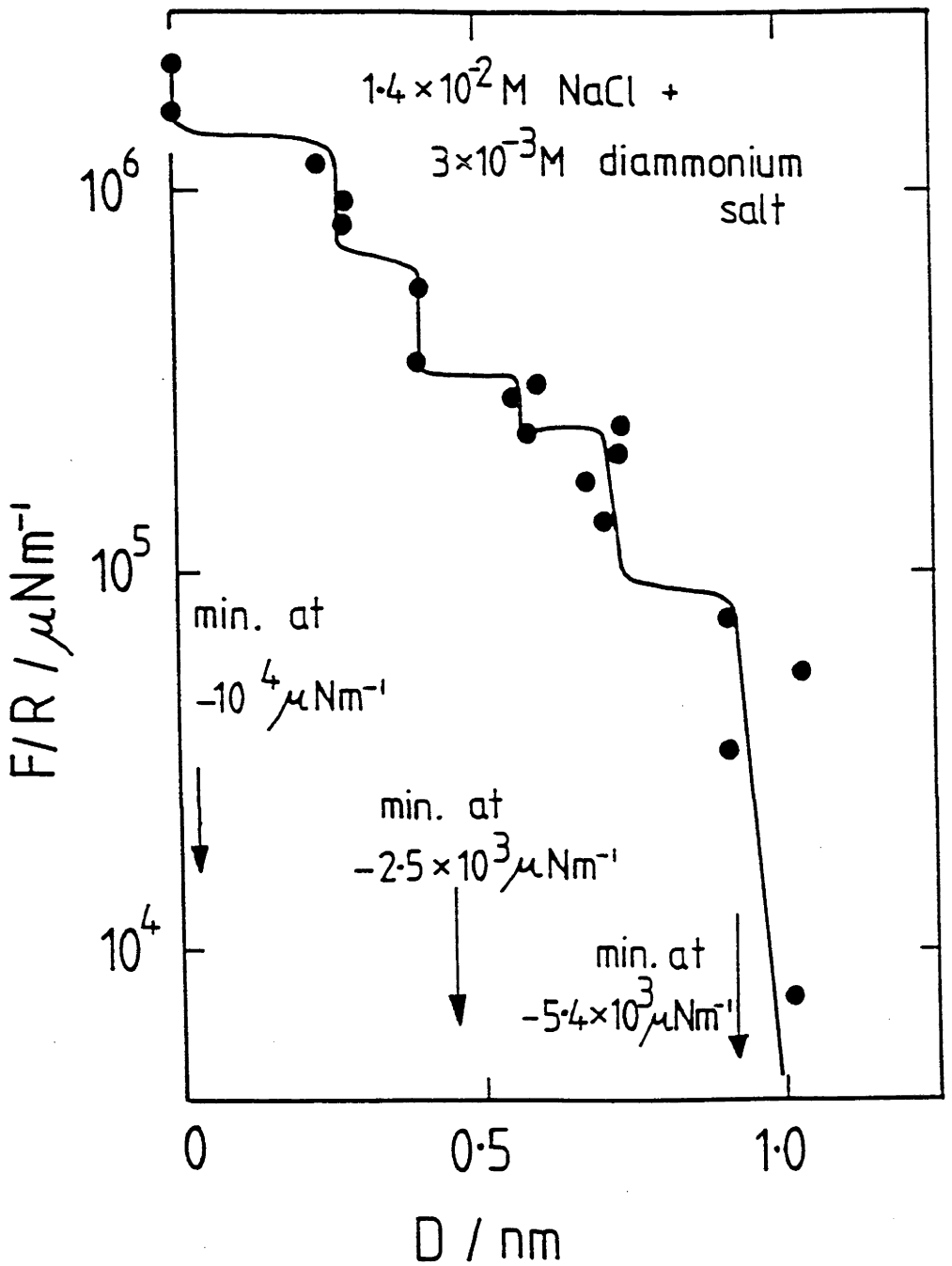

Figure 4.4: Short-range structural forces measured in 1.4 x 10^{-2} M NaCl and 3 x 10^{-3} M diammonium salt. The stepped (oscillatory) repulsive forces are of a similar magnitude to those measured in NaCl solution alone but the minimum at about 0.9 nm has become strongly attractive.

The effects of the diamine and Ca^{2+} ions on an aqueous dispersion of Na-montmorillonite was also investigated. A 0.6% dispersion of this clay in water produced a uniform, opaque solution of the 0.2 μm clay platelets, which remained stable and fully dispersed after 24 hours immersion in water. Dispersion in 3 mM $CaCl_2$ produced some immediate precipitation but a large proportion remained dispersed for a few hours. By comparison, the 3 mM diamine had a rapid and marked effect on de-stabilizing the clay dispersion. Large clay clumps were produced and these caused complete settling of the clay within about 10 mins. The photographs in figure 4.5 demonstrate these effects. A dispersion of clay was equilibrated for 24 hours, shaken, then photographed immediately and after 10 minutes. Clearly the diamine binds the clay platelets very effectively to induce rapid coagulation.

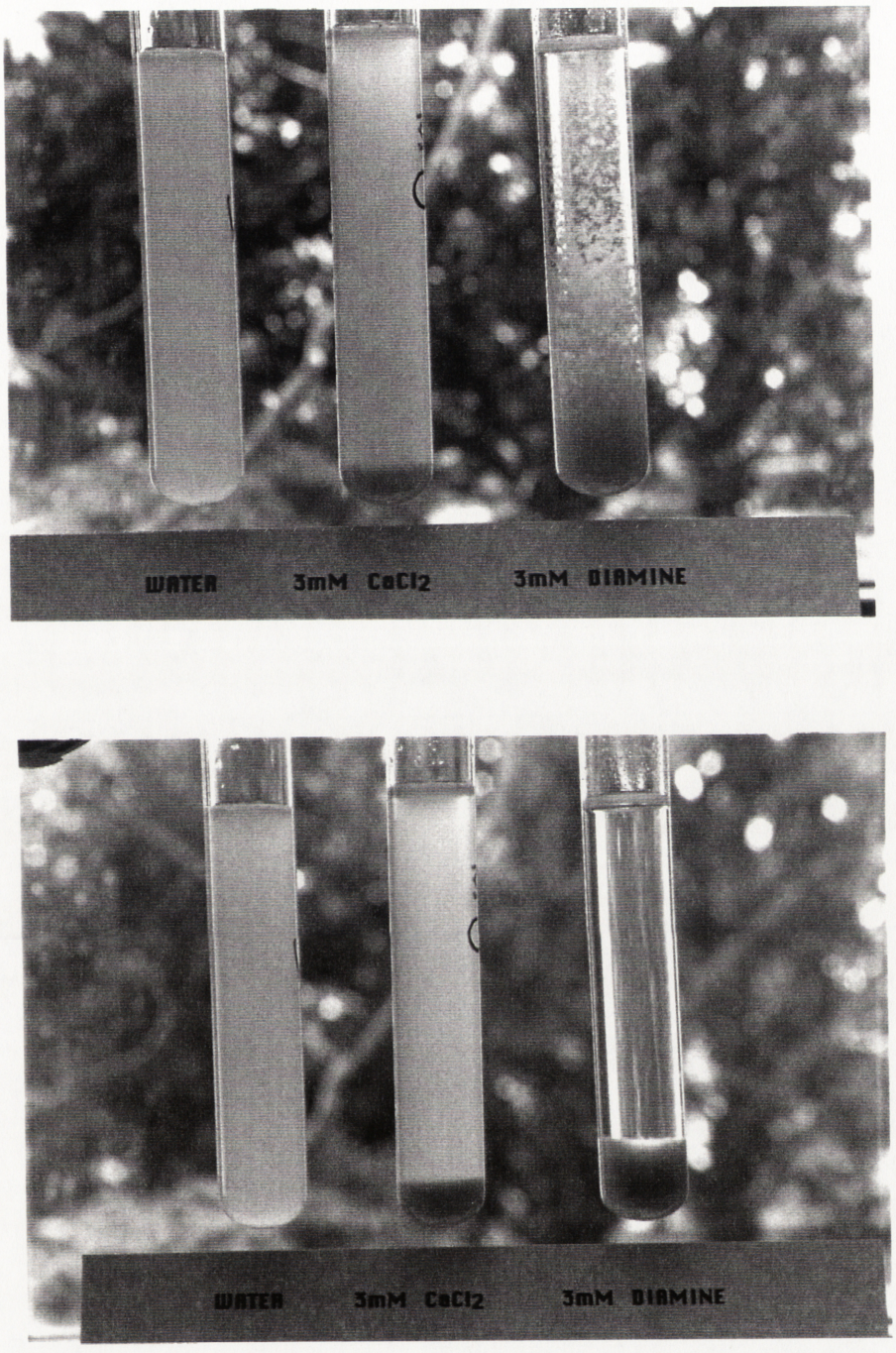

Figure 4.5: Dispersions of Na-montmorillonite (0.6%). In both photographs, the tube on the left contains water, the tube in the center, 2 mM $CaCl_2$, and the tube on the left, 3 mM diammonium salt. The dispersions were pre-equilibrated in these solutions for 24 hours before re-shaking. The upper photograph was taken a few seconds after re-shaking, and the lower photograph was taken 10 minutes after re-shaking.

4.4 Conclusions

The results presented here demonstrate that at 3 mM the divalent diamine is sufficiently strongly adsorbed at the mica surface to almost completely neutralize the surface charge. A comparison with mica in $CaCl_2$ under similar solution conditions [14] (i.e. 2 mM $CaCl_2$ in 8×10^{-4} M NaCl) shows that the Ca^{2+} ion does not bind as strongly and a moderately strong double-layer force was observed. In fact, Ca^{2+} is known to be only weakly adsorbed at the mica surface [15]. In addition, the short-range ion correlation effect for Ca^{2+} only becomes significant concentrations of at least 100 mM[2, 11]. On both counts then the diamine has a much stronger effect at lower concentrations on the swelling forces between mica crystals. These results suggest that more effective agents can be produced to prevent clay swelling. In fact, some patented drilling mud additives (used to control clay swelling) already appear to have incorporated the diamine moiety[16]. The powerful effect of the diamine ion is apparently due to a combination of strong adsorption and direct bridging between facing aluminosilicate surfaces.

4.5 References for chapter 4

1. Pashley, R.M. & Israelachvili, J.N. *J.Col.Int.Sci.* **97**, 446 (1984).
2. Kjellander, R., Marcelja, S., Pashley, R.M. & Quirk, J.P. *J. Chem. Phys.* **92**, 4399 (1990).
3. Pashley, R.M. & Quirk, J.P. *Colloids and Surfaces* **9**, 1 (1984).
4. Viani, B.E., Low, P.F. & Roth, C.B. *J. Coll. Int. Sci.* **96**, 229 (1983).
6. Jonsson, B. *Chem. Phys. Lett.* **82**, 520 (1981).
7. Israelachvili, J.N. *Acc. Chem. Res* **20**, 415 (1987).
8. Pashley, R.M. *J.Col.Int.Sci.* **83**, 531 (1981).
9. Pashley, R.M. & Quirk, J.P. *Soil Sci. Soc. Am. J.* **53**, 1660 (1989).
10. Pashley, R.M. *Chemica Scripta* **25**, 22 (1985).
11. Kjellander, R., Marcelja, S., Pashley, R.M. & Quirk, J.P. *J. Phys. Chem.* **92**, 6489 (1988).
12. Chan, D.Y.C., Pashley, R.M. & White, L.R. *J. Col. Int. Sci.* **77**, 283 (1980).
13. Claesson, P.M., Herder, P. & Pashley, R.M. *J. Col. Int. Sci.* **107**, 31 (1986).
14. Marra, J. & Hair, M.L. *J. Col. Int. Sci.* **128**, 511 (1989).
15. Goulding, K.W.T. & Talibudeen, O. *J. Col. Int. Sci.* **78**, 15 (1980).
16. Lipowski, S.A., Miskel, J.J.J. & Schick, M.J. *US PAtent US 45050833* (1985).

Chapter 5

Force measurement between a nickel probe and a mica surface using an ac atomic force microscope

5.1 Introduction

This chapter presents a force microscope technique in which both the static and dynamic components of surface forces can be determined simultaneously. This technique uses an atomic force microscope based on a laser deflection scheme (optical lever)[1] built by the author. The force between a nickel probe and mica in air and water has been measured using this method. Two different forces are measured in air, demonstrating the high lateral resolution of this device. An exponentially decaying force is measured in water.

5.2 A method for the measurement of static and dynamic surface forces

In the resonance method, a microscopic lever is driven at constant amplitude, A, and frequency, $\omega/2\pi$, and changes in surface force are sensed via changes in the amplitude of vibration, , of the free end of a cantilever. For a probe with effective mass m, and spring constant, k, subject to velocity-dependent force, $m\gamma\dot{z}$, and surface separation dependent force, F, the equation of motion for small amplitudes and low velocities of vibration is

$$m\ddot{z} + m\gamma(Z)\dot{z} + [k - F'(Z)]z = kA\cos(\omega t) + B \qquad (1)$$

where z is the displacement of the tip of the probe from the surface, Z is the equilibrium value of z and $\dot{}$ and ' represent differentiation with respect to time and displacement, respectively. It is assumed that $F'' = 0$ and $\gamma' = 0$ over the range of

vibration and thus F', γ, and B are constants for given values of Z. Previous ac force-measurement techniques have made the additional assumption that γ is constant[2], but this assumption has been found to be false. Appendix A describes measurements demonstrating this, as well as some preliminary force measurements. Here it has been assumed that γ is a function of Z, so γ will be allowed to vary over displacements larger than the amplitude of tip vibration. Solving equation (1), the motion of the lever is given by[3]

$$z = R \cos(\omega t + \theta) + Z, \tag{2}$$

where the amplitude, R, and the phase relative to the driving force, θ, are given by

$$R(Z) = \frac{kA}{m}\left[\omega^2\gamma(Z)^2 + \left(\frac{k - F'(Z)}{m} - \omega^2\right)^2\right]^{-1/2} \tag{3a}$$

$$\theta(Z) = \tan^{-1}\left(\frac{\omega\gamma(Z)}{\frac{k - F'(Z)}{m} - \omega^2}\right). \tag{3b}$$

The coefficient of velocity-dependent force, γ and the surface force gradient F' are thus given by

$$\gamma(Z) = \left(\frac{(\omega_0^{\infty})^2}{\omega}\right)\left(\frac{A}{R(Z)}\right)\sin\theta(Z), \tag{4a}$$

$$F'(Z) = k\left[1 - \left(\frac{\omega}{\omega_0^{\infty}}\right)^2 - \left(\frac{A}{R(Z)}\right)\cos\theta(Z)\right] \tag{4b}$$

where $\omega_0^{\infty} = \sqrt{k/m}$ is the resonant frequency of the probe in the absence of the surface force (i.e., at large Z) and a dissipative medium, and $\theta(Z = \infty) = -\pi/2$ by definition. Once ω_0^{∞} has been determined, A and ω are chosen and F' and γ can then be obtained simply from measurements of R(Z) and θ(Z). Hence, by measuring both R(Z) and θ(Z), we obtain F'(Z) without the incorrect assumption that $d\gamma/\delta Z = 0$, and γ(Z) is also measured. Note that γ could also be obtained from Fourier analysis of signal decay.

One advantage of this technique over any dc deflection measurement is that both static and velocity-dependent forces are measured. In contrast, a dc measurement convolutes the two together. In addition, resolution is not as strongly dependent on the spring constant as in a dc measurement (this is desirable because the spring constant also determines access to different surface separations) and, as with all ac techniques, the signal-to-noise ratio is improved by measurement at high frequency.

5.3 Description of the ac force microscope

Figure 5.1 shows a schematic diagram of the microscope built for these experiments. Tip-sample separation was controlled in three stages, all by movement of the sample. The first two stages utilized micrometers, the more coarse allowing control to within about 2 μm and the more fine, at a mechanical disadvantage of 1:25, allowing control to within about 80 nm. This latter control could be made more sensitive by increasing the mechanical disadvantage. The third and most fine stage of control, was obtained by setting the voltage across the wall of a piezoelectric tube to give distance resolution of approximately 0.1 nm. PZT4 (a Lead Zirconate Titanate material) was used for the tube because of the relatively small voltage-displacement hysteresis. The outer wall of the piezoelectric tube was split into 4 quadrants to enable translation of the sample in the two dimensions in the plane of the sample. The voltage-displacement response of the tube was calibrated using an interferometer.

Information about the force gradient was derived from measurements of the amplitude of tip vibration as the piezoelectric crystal on which the tip was mounted (the dither piezo) was driven at constant amplitude. The reflection of a 4-mW HeNe laser, from a mirror attached to the cantilever, was directed onto a split diode, each side of which was connected to a differential amplifier. As the lever vibrated, the reflected image oscillated across the split in the diode producing an ac output from the amplifier which

was proportional to the lever deflection. For small deflections the amplitude of this output was proportional to the amplitude of the lever displacement .

The nickel probe was prepared in a four stage operation. A 75 μm-diameter nickel wire was spotwelded to a large (~4mm) stainless-steel stub which could later easily be mounted onto the dither-piezo. The end of the wire was bent into a right angle, with each segment about 0.5 mm long. A small silicon mirror about 250 x 250 x 50 μm^3 was then attached at the bend in the wire using an epoxy resin, and finally, a sharp tip was made at the end of the wire by electrochemical etching in a 25% (by wt) aqueous H_2S0_4 solution. The etching was performed immediately before the experiment. The effective mass of the probe, m, was calculated from the total mass, m_T, using the probe geometry[4]. In this case $m = 0.619\ m_T$. The spring constant was calculated from ω_0^∞ and m. The mica sample was cleaved immediately before the experiment, but no other attempt was made to exclude vapours or contaminants from the tip or mica surface, other than to cover the apparatus with a plastic jar.

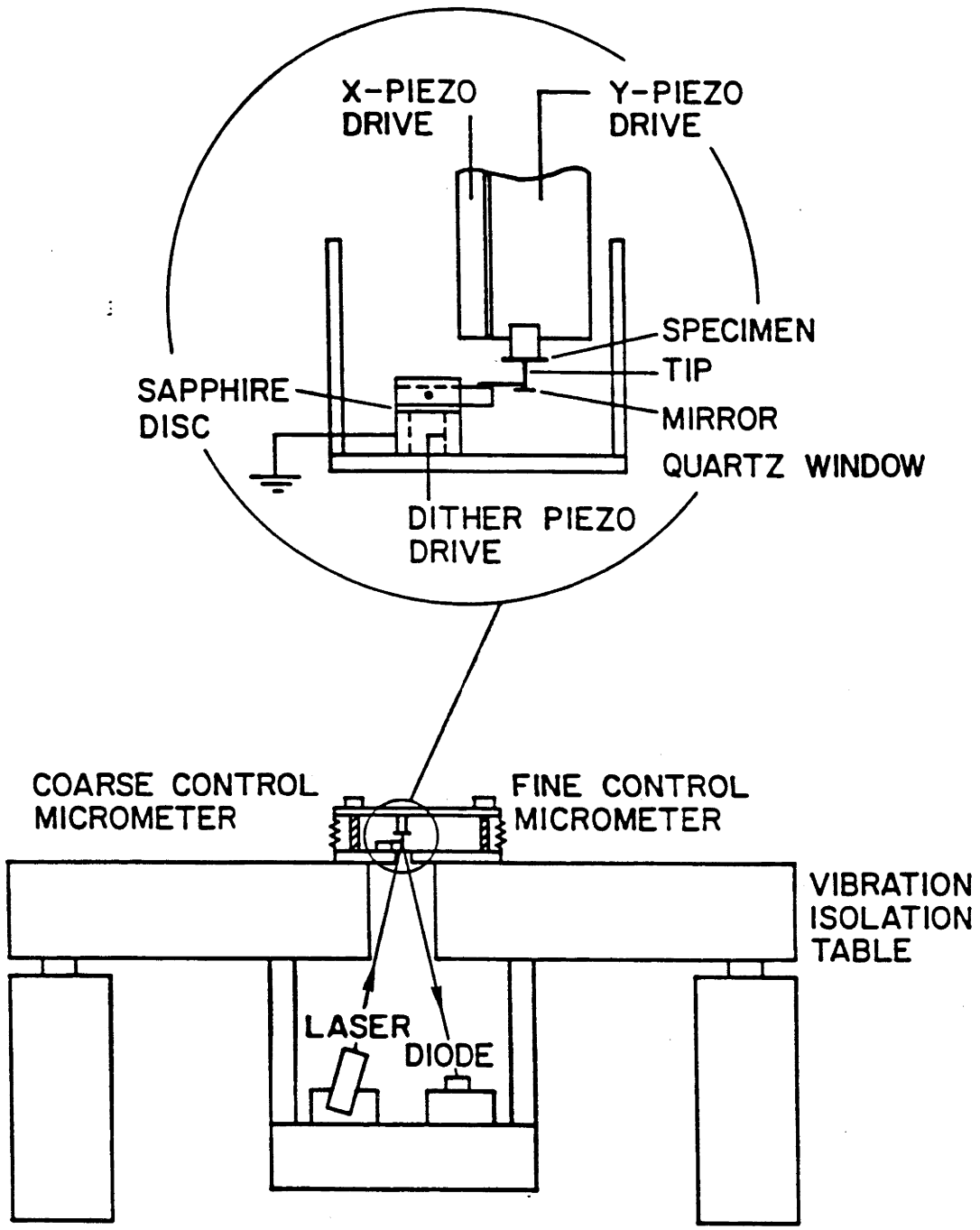

Figure 5.1: Schematic diagram of the force microscope used in this study. The inset shows details of the tip-specimen geometry.

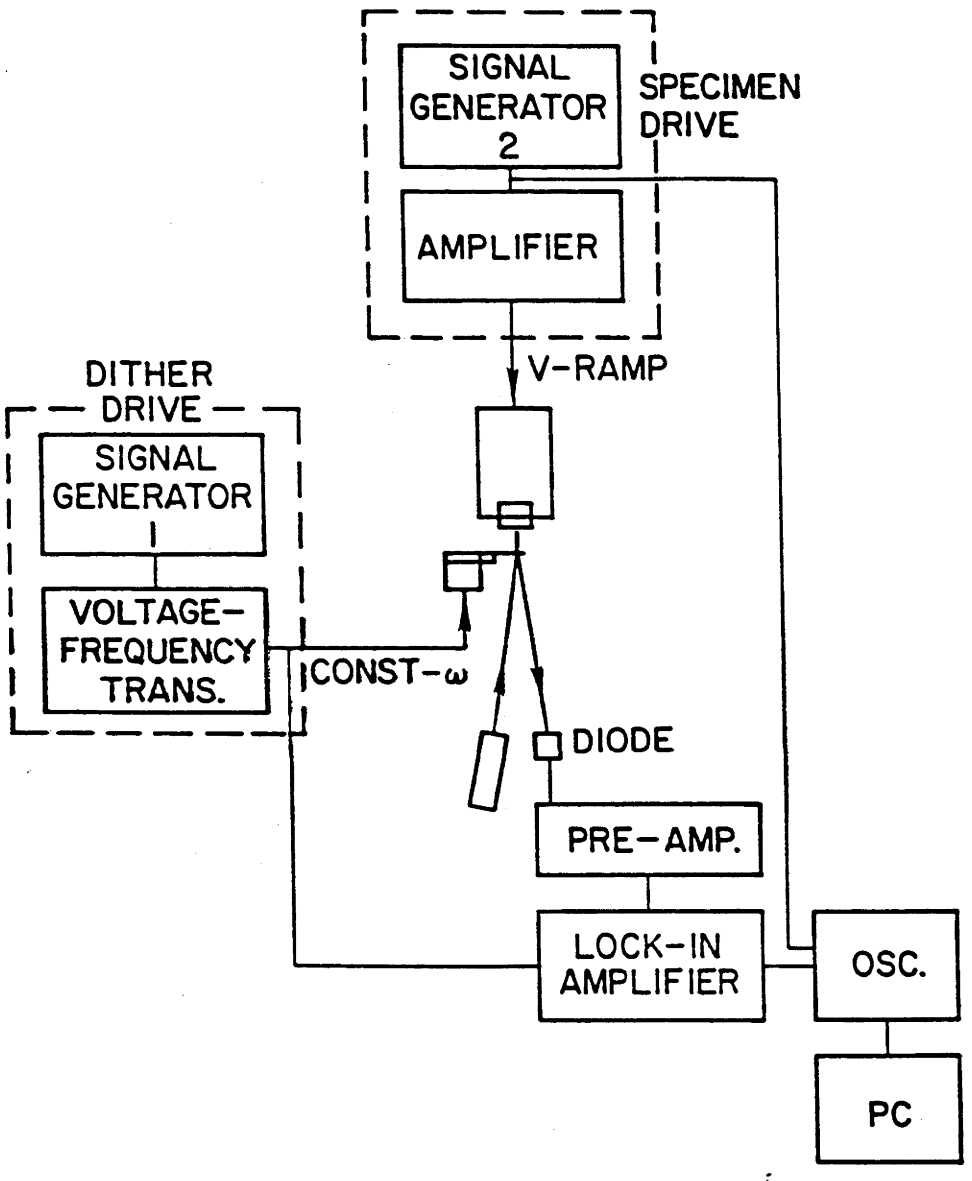

Figure 5.2 Block diagram of the electronic sensing apparatus used in these experiments.

5.4 Results

Examples of forces and velocity coefficients for a grounded nickel tip on approach to mica are shown in figures 5.3 and 5.4 The force was obtained by integration of F', setting the constant of integration such that zero force occurs at the point of zero force gradient closest to the surface. The position of surface contact is not shown because no information on tip movement is obtained after the tip encounters an unstable position (indicated by the vertical dashed lines). In the presence of attractive forces unstable positions occur when $F' > k$, which occurs before surface contact for the usual range of spring constants. It is interesting to note that, within the resolution of this experiment, the force and damping vary over roughly the same distance.

Taken together, Figure 5.3 and 5.4 are significant because they were obtained on the same piece of mica with the same nickel tip at the same time period. After measurement at one point, the tip was retracted 600 nm, moved 600 nm laterally, then again moved toward the surface for measurement. The tip was then moved back and forth between the two regions. The R(Z) and θ(Z) traces measured at each location, reflecting the force and damping coefficient variations, were reproducible within the noise level. Although the two force profiles were measured at the same time, the forces exhibit two very different length scales: the force shown in Figure 5.3 extends over about 40 nm while the force in Figure 5.4 has a range of about 8 nm. The damping coefficient at large separation was the same in both cases but increased monotonically over roughly the same distance as the force in each case.

Figure 5.5 shows a short-ranged force and velocity coefficient measured between a grounded nickel tip and a mica surface in water. Short-range repulsive forces have been measured previously between two mica surfaces in electrolyte solutions[5], and have been attributed to hydration of adsorbed ions. The repulsive force observed here varies as $e^{-Z/\lambda}$, where λ is a decay length of 0.4 nm (as shown in the logarithmic plot

of figure 5.6). The analysis of the measurements in water produced a constant, ω-dependent gradient term, which was removed by setting the constant of integration of F' such that zero force gradient occurred at the point of zero second derivative in the force closest to the surface. The vertical dashed lines in Figures 5.5 and 5.6 indicate the displacement at which R diminished to the level of the noise (10^{-2} nm). This technique can thus be used in a variety of liquids, as well as gaseous environments.

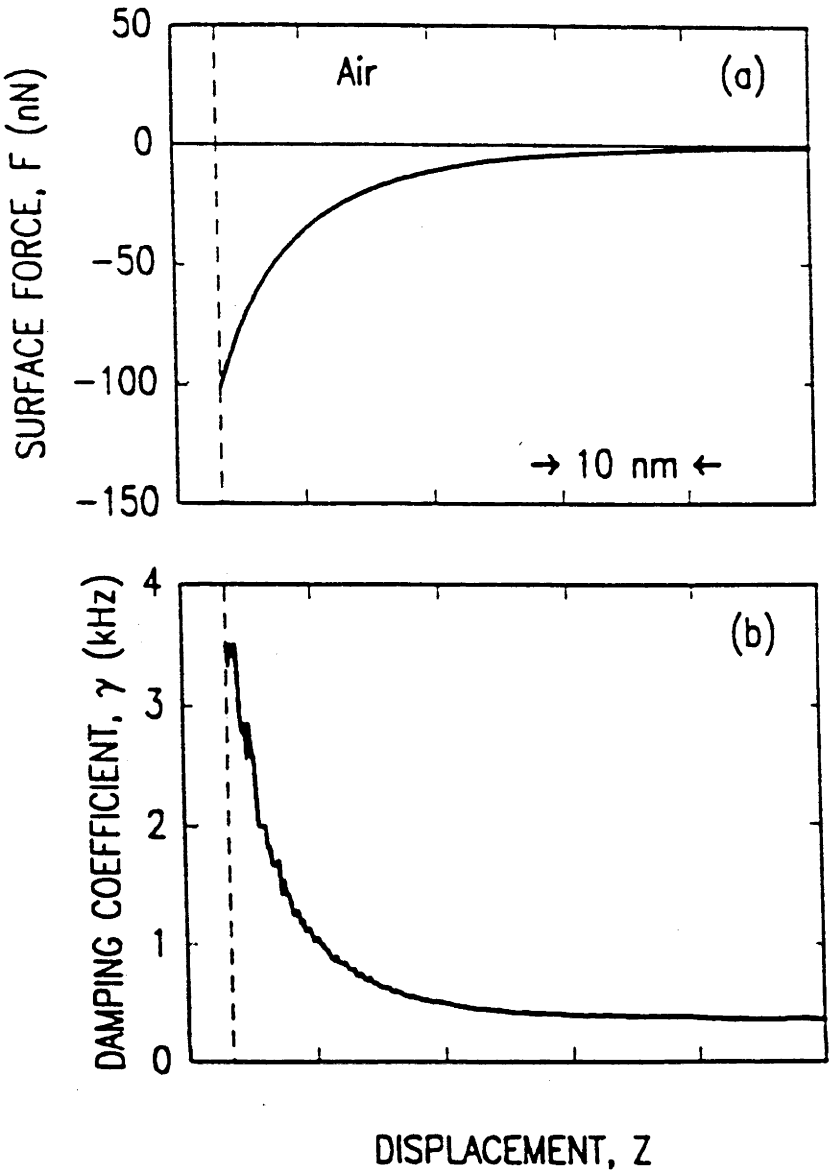

Figure 5.3: (a) Surface force between a grounded nickel tip and a mica surface in air. Note that the horizontal axis shows displacement of the sample, not changes in tip-sample separation. The resonant frequency of the nickel lever at large tip-surface separation was ω_0^∞ = 103.063 kHz with a quality Q = 350. Vibration of the fixed end of the lever at an amplitude A = 7.5 $\times 10^{-4}$ nm at ω_0^∞ resulted in oscillation of the free end (tip) of amplitude R = 0.26 nm. The effective mass of the lever was estimated to be m = 40 μg, yielding a spring constant k = 680 Nm^{-1}. At small tip-surface separations, the amplitude of tip oscillation was less because the system had moved away from resonance and the quality was lower. The time taken for this measurement was 10 s. (b) The damping coefficient measured at the same time as (a).

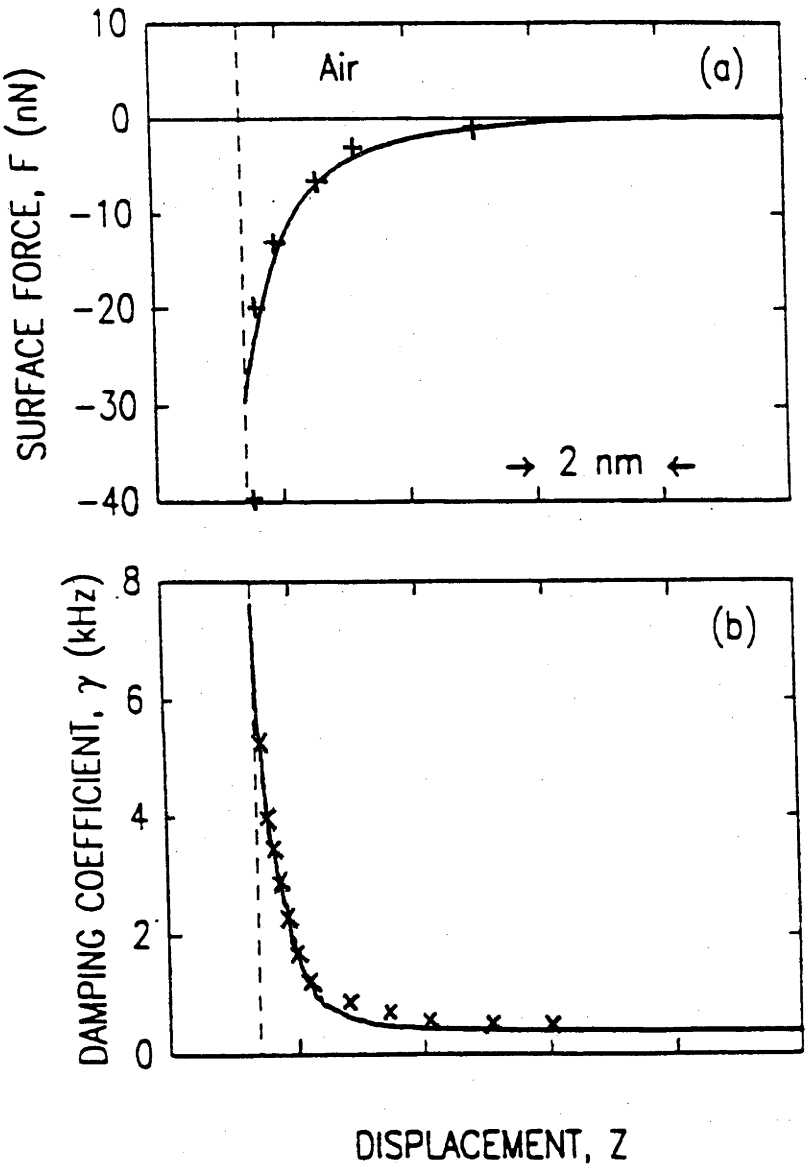

Figure 5.4. (a) Surface force measured after the tip was moved 600 nm laterally from the position measured in figure 5.3. (b) The damping coefficient measured at the same time as the force in (a).

Data from fitted curves (see text) are shown as crosses.

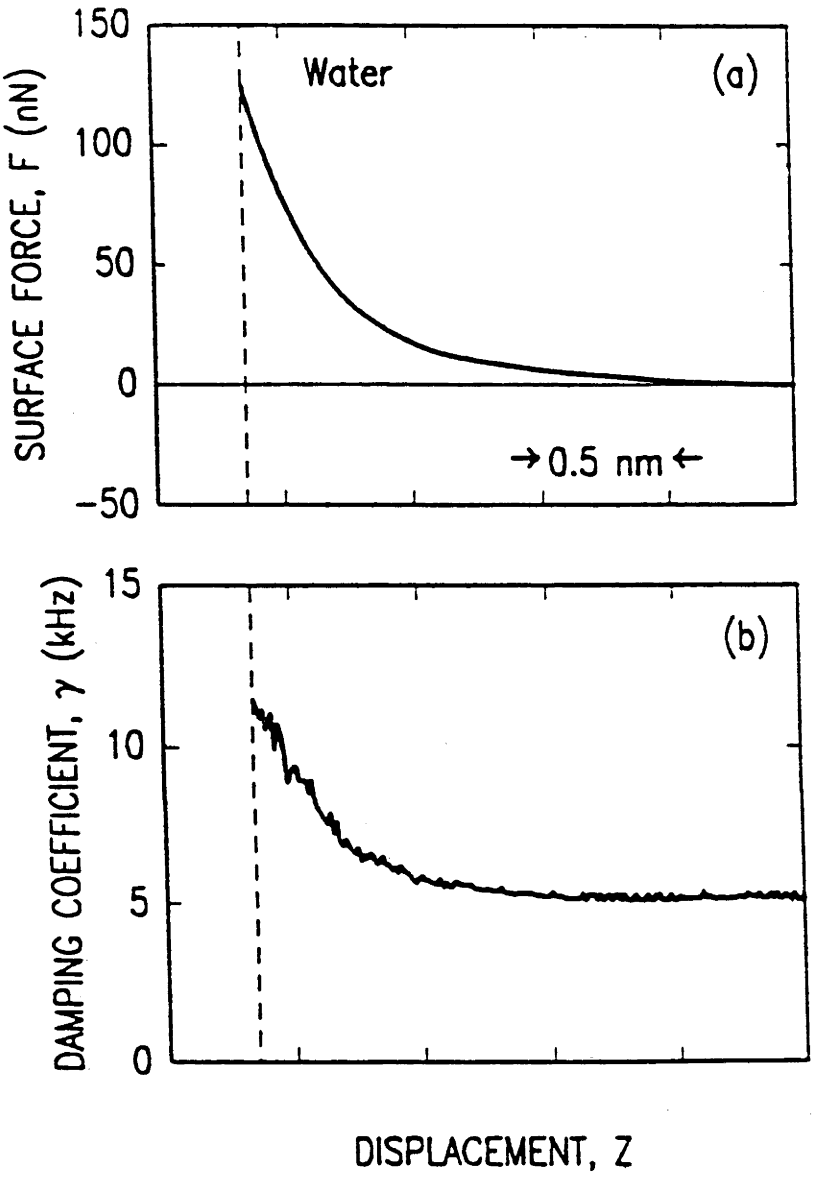

Figure 5.5: (a) Force between a grounded nickel tip and a mica surface in deionized water. Lever characteristics are ω_0^{∞} (air) = 269.2 kHz, Q(water) = 49, k = 5400 Nm^{-1}. Experimental variables are ω = 254.47 kHz, A = 9.5 × 10^{-3} nm. (b) The damping coefficient measured at the same time as the force in (a).

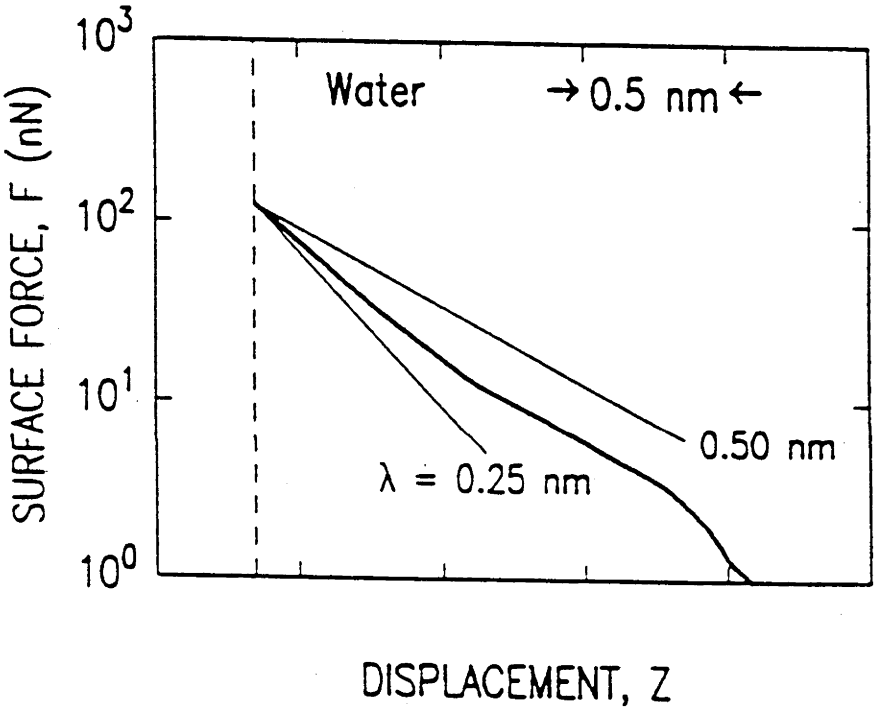

Figure 5.6: Surface force in figure 5.5 plotted on a logarithmic scale. The straight lines show forces with a range of decay lengths.

5.5 Discussion

The measurement of force as a function of distance in air in two locations demonstrates the high lateral resolution of this technique: it is clear from the length-scales that the tip is in different environments in the two positions. Unfortunately, analysis of the curves is made more difficult by the uncertainty in the absolute tip-surface separation, the uncontrolled environment and the lack of knowledge of the tip geometry. The following paragraph will , however, provide some estimates of the expected forces in these circumstances.

Examination of the damping co-efficient provides information about the fluid surrounding the tip. If the tip is modelled as a sphere approaching a flat surface, then the damping force is given by[6]:

$$F = 6\pi r^2 \eta \dot{z} / Z \qquad (5)$$

where r is the radius of the sphere and η is the viscosity of the surrounding medium. Thus,

$$\gamma = 6\pi r^2 \eta / mZ \qquad (6)$$

Now, even for a very large radius, the measured values of γ are much larger than would be expected for an interaction in air. To obtain a reasonable fit to the data in figure 5.4 b it is necessary to use a viscosity of about 4 centipoise, the viscosity of a liquid. This suggests that there is a liquid film between the tip and surface.

Because the values of both γ and F depend critically on the absolute separation of the tip and surface, it is necessary to obtain an estimate of the separation at which the instability occurred. This can be obtained by comparing the gradient of the surface force with the spring constant. For a van der Waals interaction with a Hamaker constant of 2×10^{-19} J, the instability should be 2Å from zero separation. However, to obtain a good fit to the data in figure 5.3(a), it is necessary to use a larger value of the

radius than that estimated by SEM. A radius of 500 nm gives a reasonable fit to both γ and Force curves. Fitted curves are shown in figure 5.4, but it should be noted that these fits are dependent on the assumed radius, geometry and surface separation. Examination of the distance dependence of the curves indicates that both the force and distance decay roughly as one over the distance raised to 1.5, rather than to 2 and 1 respectively. The force may be made to have distance squared dependence by increasing to 1 nm the separation at which instability occurred, but this would require an unreasonably large viscosity.

The above discussion highlights the need for controlled geometry and chemistry for simple interpretation of force measurements using Atomic Force Microscopes. The next chapter describes measurements using an alternative method which facilitates comparison of experiment and theory.

These results have important implications for the measurement of topography using any force microscope that scans away from surface contact. Because the force as a function of displacement normal to the surface may not be constant with respect to lateral displacement, a scan at constant force (or force gradient) is not necessarily a scan at constant surface separation. Instead, a scan at constant force is a convolution of topographical and chemical information. For example, if a tip were scanning across a surface, interacting via a long-ranged force and then moved into a region exhibiting a short-ranged force, this could be interpreted as a depression in the surface - the equivalent topographical feature. In contrast, a technique that measures on the repulsive "hard wall" should be less sensitive to such effects.

Considering now the potential force resolution of this technique, it will be assumed that there is some minimum change in amplitude and phase angle that can be detected by the microscope. Under these conditions, high resolution in static force occurs when the transfer function from amplitude and phase to static force has a large

derivative. Thus, high resolution is attained when the driving frequency is close to the resonant frequency of the lever. For example, if the signal is obscured by noise beyond $2\omega_0^\infty/Q$ from resonance, static force gradients can only be resolved if they are smaller than 16k/Q. (The quality factor of the system is given by $Q = 2\omega_0^\infty/\gamma$.) Thus a high Q provides high resolution in a narrow range of F', and a low Q provides lower resolution but over a larger range. Some compensation for this dilemma arises because Q is a function of displacement. At large displacements Q is large, providing high-force gradient resolution where gradients are changing gradually. At small displacements Q is smaller, which increases the range of accessible gradients but decreases resolution. This is ideal because force gradients are usually large and have large spatial derivatives near a surface.

The best lateral discrimination of changes in the force-distance dependence (leading to resolution in the position of areas of different chemistry) can only be on about the same scale as the range of the force. Thus, if the chemistry of the surface varies on a length scale smaller than the range of the resulting surface force, the spatial variation of chemistry cannot be resolved. For any real tip, the finite tip width will further limit resolution because the sides of the tip will interact with regions of the surface which are "out of range" of the end of the tip and thus the force on the tip will be affected by a larger region of the surface.

It is clear that it is necessary to have resonance behaviour in order to perform a static force measurement with reasonable resolution. This requirement places some limitation on the fluid or other dissipative environments in which forces can be measured. Measurement in water was possible because Q values of 30-50 were obtained for the levers under water, but the viscosity of a liquid such as glycerol is so high that the lever would be over-damped and resolution would be very poor. Additional limitations of this technique are that all interpretation of results is dependent

on the model for the equations of motion, and that distance resolution is limited to the range of vibration of the lever.

5.6 Conclusions

(1) Simultaneous measurement of the amplitude and phase angle of vibration of a cantilever allows both static and dynamic surface forces to be independently measured. Forces in air and water were measured using this technique.

(2) Two types of forces between a Ni tip and a mica surface in air were distinguished. The first was a short-range (~5 nm) attractive force acting between freshly etched Ni and freshly cleaved mica. The spatial extent suggests that this was a van der Waals interaction between the tip and the surface. The second was a long-range (~40 nm) attractive force acting between the materials after exposure to the atmosphere for some hours. The spatial extent here suggests a capillary interaction.

(3)The force between a nickel tip and mica surface in water was measured. The force in the last few nm was found to be exponential with a decay-length of about 3.5 nm.

(4) The damping coefficient in the tip-surface interaction increased as the tip-surface separation decreased. This implies that there is a non-conservative interaction between the tip and surface, and prevents force-separation determination by measuring the amplitude of lever vibration alone

(5) The force measurement technique described in this chapter can be used on a variety of surfaces and in a range of fluid environments.

5.7 References for chapter 5

1. Meyer, G. & Amer, N.M. *Appl. Phys. Lett.* **53**, 1045 (1988).
2. Martin, Y., Williams, C. & Wickramasinghe, H. *J. Appl. Phys.* **61**, 4723 (1987).
3. Pain, H.J. *The Physics of Vibrations and Waves* (Wiley, Chichester, 1983).
4. Nowick, A.S. & Berry, B.S. *Anelastic Relaxation Processes in Solids* (Academic Press, New York, 1972).
5. Pashley, R.M. *J.Col.Int.Sci.* **83**, 531 (1981).
6. Chan, D.Y.C. & Horn, R.G. *J. Chem. Phys.* **83**, 5311 (1985)

Chapter 6

Measurement of the force between silica surfaces using a commercial dc force microscope

6.1 Introduction

This section describes measurements of surface forces on a colloid particle. In the previous section (as in work by other authors) forces were measured on tips designed for force microscopy with little regard for control or measurement of tip geometry and chemistry. The motivation for the work in this section was to perform AFM force measurements with well characterized surfaces, and to measure the forces acting on a colloid particle. Because of the difficulty in working with such small particles, most previous investigations of colloid forces have either used model macroscopic substrates (e.g. the experiments using the surface forces apparatus) and related their findings to colloid systems or have used indirect methods such as sedimentation studies[1, 2] or light or neutron scattering[3] although some force measurements have been performed on lamellar[18] or platelet systems[19]. The disadvantage of using macroscopic substrates is that it is often difficult to find large substrates which are smooth, homogeneous and clean over a large area, and it is sometimes difficult to create large areas of surface which are similar to a particular colloid. In addition, the relative importance of forces such as van der Waals, double-layer and viscous forces changes with the radius of the substrate. The examination of particulate forces by sedimentation or light and neutron scattering is more direct in so far as colloid particles may be used, but in the case of sedimentation studies, only part of the force-distance law may be obtained, and for scattering experiments, the results are model dependent. The most successful attempt to directly measure the forces on colloid particles has been with Total Internal Reflectance Microscopy[4, 5]. Recently, this method has used to measure forces between a particle and a flat plate, but the results agree poorly with

DLVO theory and this technique is limited to the study of interactions between particles and transparent flat plates.

This section presents a technique for force measurement on a colloid particle together with results from some model systems. Silica has been chosen as a model colloid, both because of its common occurrence and because extensive previous investigation using other techniques provides a comparison for results. Spherical geometry was chosen both to facilitate interpretation of results, and to provide a large area of interaction. Results are presented for the silica-silica interaction as a function of NaCl concentration and pH. The utility of the technique is demonstrated by results from force measurements on a gold-coated silica particle.

6.2 Method

Force measurements

All surface force measurements were performed using a commercial AFM, the Nanoscope II atomic force microscope (Nanoscope, Santa Barbara, CA, USA). In this device, forces are measured using the same light-lever technique described in section 5.3. However, in the Nanoscope, the cantilever is not made to oscillate, and the force is measured simply by measuring the cantilever deflection. The sample is mounted on a piezoelectric crystal which allows the tip-sample spacing to be altered. In the experiments reported here, the sample was moved towards the probe at a rate of 0.2-2 $\mu m\ s^{-1}$.

The software provided with the Nanoscope produces a screen file which records the change in output from a photo-diode (receiving reflected light from the cantilever) as a function of sample displacement (see figure 6.1). A program written by Tim Senden

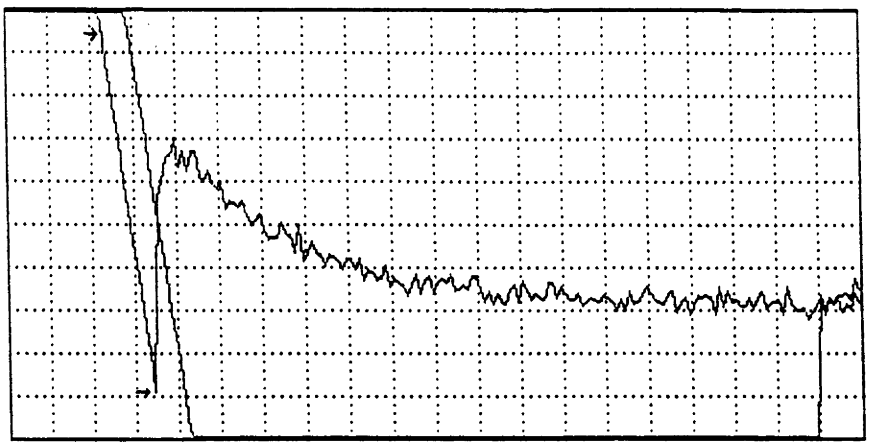

Figure 6.1: An example of the data produced by the Nanoscope software. The horizontal axis shows the distance over which the piezoelectric driver has been moved, and the vertical axis records the corresponding output from the diode. The region of constant compliance is indicated by the arrows. The interaction recorded here is between a pyramidal Si_3N_4 tip (4 μm high and 4 μm along the base) and a mm size piece of Si_3N_4 in aqueous solution. The solution contained $2x10^{-4}$ M NaCl and was at pH 10.

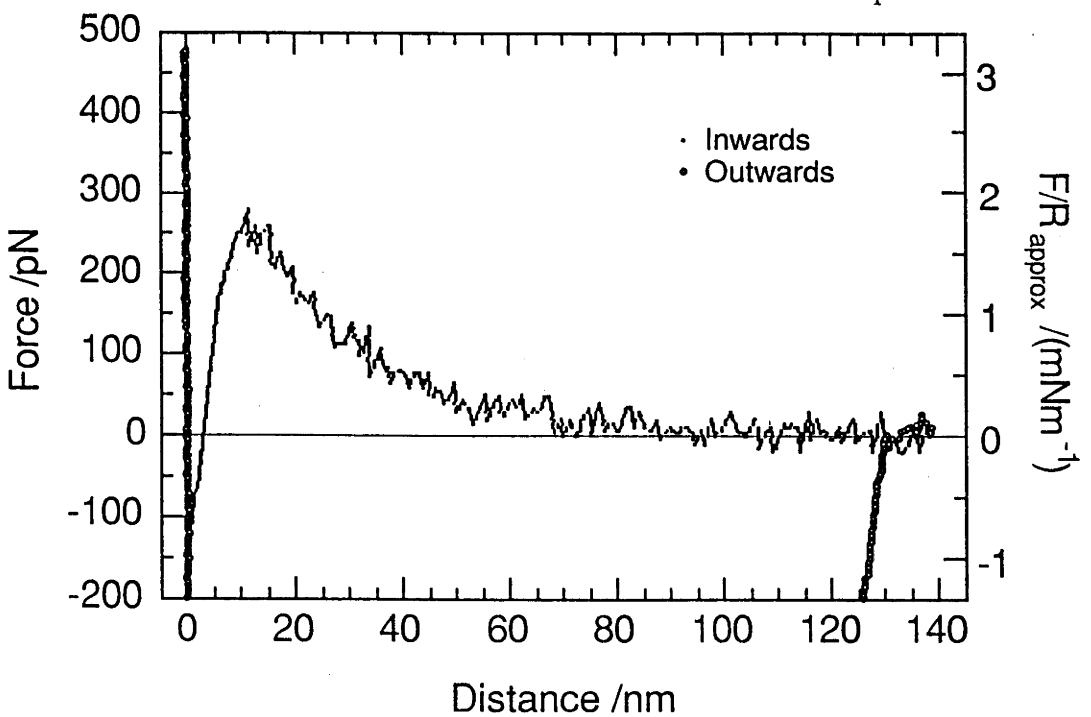

Figure 6.2: The data from figure 6.1 converted to force (in pN) as a function of tip-sample displacement (in nm).

was used to convert the pixel coordinates to a text file which could then be numerically manipulated. In future studies, it would be better to capture the data directly, avoiding this unnecessary transfer and the digitization error incurred.

To convert the deflection versus piezo displacement information (for a probe of any geometry) to a curve of the force as a function of tip-sample displacement it was necessary to define zeros of both force and distance, and to convert the diode signal to force. The zero of deflection was chosen where the deflection was constant (with the particle and flat far apart) but the zero of distance is a more difficult choice. As the sample is driven toward the sphere, the cantilever deflects, and this is registered by the photodiode. At some point, the output of the diode becomes a linear function of displacement of the sample, indicating that the motion of the tip and sample are coupled. In this regime of constant compliance, the particle is "in contact" with the surface, and this separation is defined as the zero of separation. In the experiments presented here, the relationship between displacement and diode response in this region was independent of the surface force, and was used to convert the diode response into the effective displacement of the cantilever. This relationship was also used to determine changes in the sphere-flat separation when the two were not in contact, and to calculate the surface force. An overestimate of surface force will be obtained if the cantilever is not significantly more compliant than the sphere, the flat surface, and the components connecting them. For compliant substrates this problem can be surmounted by an independent calibration of cantilever deflection. In contrast, determination of the sphere-flat separation is not affected by elastic deformation of the substrates or connections.* It should also be noted that for any material it is difficult to measure surface forces which have a gradient much greater than the spring constant of the cantilever. Figure 6.2 shows an example of a force-displacement curve.

Errors in Nanoscope force measurements

Figure 6.1 shows that the Nanoscope II can measure forces with a noise level of ±0.02 nN. (This error is dependent on the value of the spring constant, and in general, the technique is capable of greater resolution with other displacement measuring devices.) The sample may be displaced in increments as small as 10^{-3} nm, which is more than adequate for current force measurements. However, there are systematic errors and errors in the data analysis presented here which limit resolution.

Calculation of normalized surface forces requires knowledge of the spring constant and the probe radius, so measurement of these introduces systematic errors into the surface force. The radius of the silica particles was measured to within 2% after each experiment using a Scanning Electron Microscope. The spring constant was not measured, but the manufacturer's specifications were quoted to two significant figures so an error of 5% has been assumed. (In order to obtain a direct voltage-force calibration a microscopic crystal of galena was attached to the end of the cantilever and a change in force was applied by inverting the microscope. This provided the calibration, but rendered the probe useless for experiments.) There is also some error in calculating the deflection of the cantilever from the region of constant compliance. The least squares fit has an error of about 5% giving a cumulative error of about 12%. Figure 6.3 shows the reproducibility of measurements between experiments using different probes and suggests that perhaps the systematic error has been overestimated.

Relative surface separation was calculated by adding the displacement of the sample to the deflection of the cantilever. The measured deflection of the cantilever contains the 5% error mentioned above and the total error in surface separation depends on the control of the piezo-electric crystal. The crystal response was calibrated by measuring the height of the tracks on a CD stamper which had been measured to within 5% by ellipsometry (by Brett Sexton, CSIRO). The total error in calibrating our piezo

expansion is about 10%. Since measurements of decay-lengths of double-layer forces using force microscopy agree well with those measured by other techniques, measurement of the decay of surface forces may in future be a simple way for AFM users to calibrate crystals.

There is also some error due to the non-linearity of the piezo voltage-distance response and the diode-voltage cantilever-deflection response. These were not measured independently, but in the constant compliance regime, the diode voltage-output to piezo voltage-input response is linear to within 2%.

Finally, some error is introduced into the measurements by the data collection procedure. Because data is read from a screen file which is only 200 by 400 pixels, a digitization error of 1/200 th of the maximum force and 1/400 th of the maximum displacement is incurred. Although this error can be reduced by measuring the force curve in a series of segments of smaller range or by averaging pixel values, this is the limiting error in the low force and small displacement regimes.

Colloid probe preparation

The colloid probes were prepared by attaching a silica sphere to a microfabricated AFM cantilever. The spheres were purchased from Polysciences Inc.(Warrington, PA, USA) and are composed of silica-glass. SEM was used to measure particle geometry. Several radii were measured, and the particles were found to be spherical to within to 1% resolution of the SEM. AFM was used to show that the maximum peak-to-peak roughness on the sphere was 3 nm over $(700\ nm)^2$, but by scanning with the probe it was possible to make the surface more smooth as shown by the rapid loss of lateral resolution while imaging. The cantilevers were standard V-shaped AFM single cantilever springs manufactured by Park Scientific (Mountain View, CA, USA).

Cantilevers with integrated tips could be used provided that the diameter of the particle was greater than the height of the tip.

The colloid particles were attached to the cantilevers with an epoxy resin, epikote 1004, the same resin used in experiments with the Surface Forces Apparatus. The cantilever was placed on a heating stage at a temperature above the melting point of the glue. A thin copper wire (~ 40 μm diameter) attached to a three dimensional translation stage was then used to position about 1 fL of molten resin near the apex of the cantilever. It is important that the glue wets the wire better than it does the cantilever, and care must be taken to avoid coating the underside of the cantilever. A fresh wire was then used to position a colloid particle on the cantilever and the glue was solidified by removal of the cantilever from the heating stage. If more than one particle became attached, the excess could be removed after the glue had solidified.

This method could be used for a wide variety of solid colloid particles, with the main limitation being that the particles must be large enough to view with an optical microscope.

Immediately prior to each experiment, the colloid probe was cleaned by exposure to a water plasma. This also ensured that the silica surface contained a high density of silanol groups. The plasma was created by a 25 W, 18 MHz RF source in 0.03 torr of Argon and 0.02 torr water and the probe was exposed for 3 minutes. This plasma treatment significantly diminished the adhesion of the reflective gold layer on the back of the cantilever. In fact, after longer treatment times the gold film became completely detached after immersion in water.

A SEM image of the probe is shown in figure 6.4. It can be seen that gross quantities of the resin have not crept around the sphere, and this was confirmed by the absence of hydrophobic forces in our experiments. When the surface was deliberately coated

in resin, a characteristic hydrophobic force was observed in water, and this was not seen in our silica experiments.

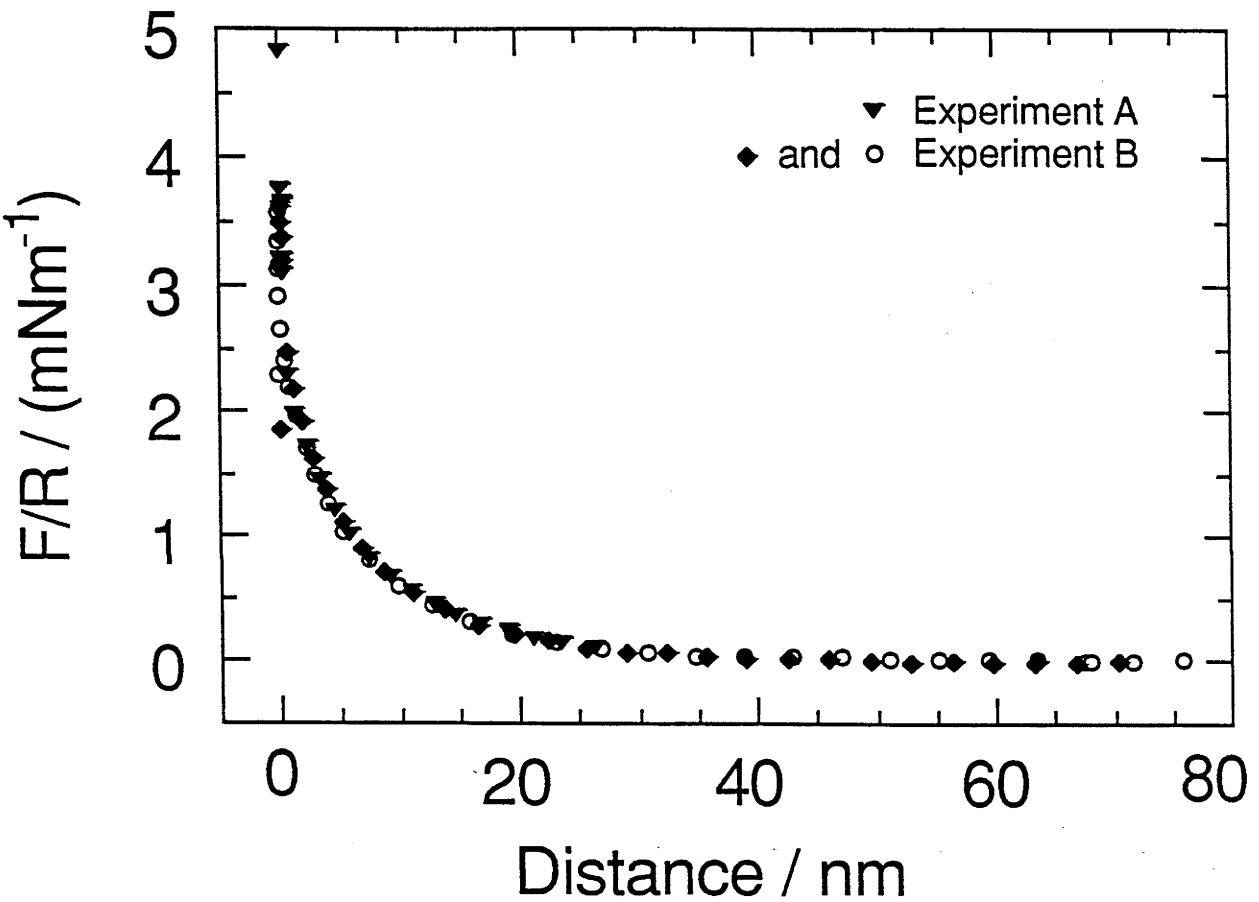

Figure 6.3: The reproducibility of force measurements. Two of the curves were measured in the same experiment, and the third was measured with a different cantilever, particle and silicon wafer.

Figure 6.4: (next page) A SEM image of a colloid probe.

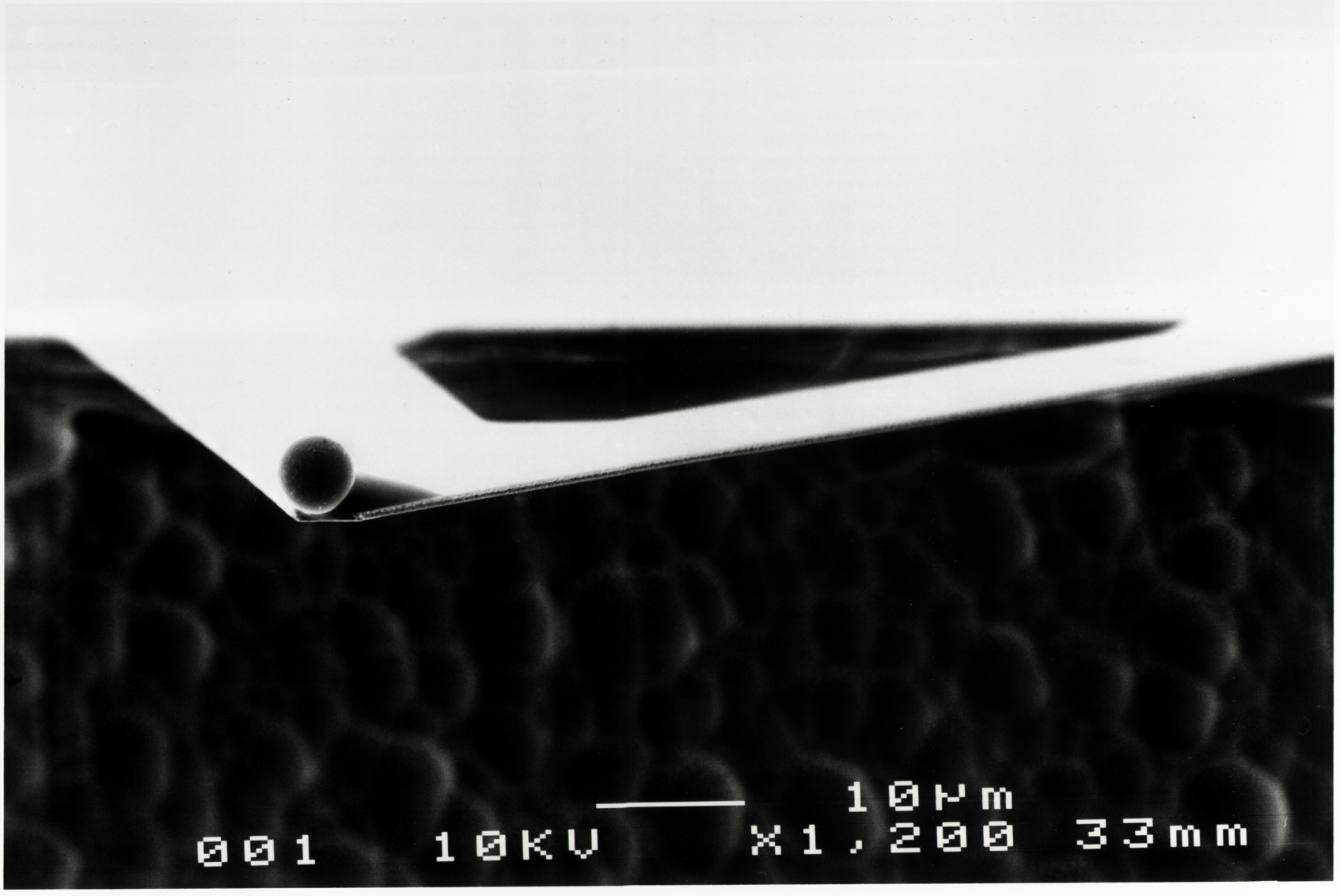
10μm
001 10KV X1,200 33mm

Sample preparation

The silica surfaces were made from a polished silicon wafer. This wafer was oxidized to a depth of 30 nm by heating to 920 °C in purified oxygen. This procedure was performed by Dr Tommy Nylander. AFM images of the oxidized surface revealed that in $(700\ nm)^2$ areas the highest asperity was typically 0.7 nm above mean height and the standard deviation from mean was 0.2 nm. In $(7\ nm)^2$ scans the highest asperity was 0.3 nm above mean height and the standard deviation was 0.1 nm. The hydrophobic surfaces were prepared by exposing some of these wafers to a 1% (w/w) solution of dichlorodimethylsilane in trichloroethane at room temperature for 2 min. This procedure was also performed by Dr Nylander. The roughness was unchanged by this procedure. Gold surfaces were freshly sputter-coated onto freshly cleaved mica, to a thickness of approximately 50 nm. AFM measurement showed that this surface was very rough: the peak to peak roughness was about 20 nm.

To avoid particulate contamination, surfaces were handled and loaded into the AFM in a laminar flow cabinet . All equipment which came into contact with solutions was washed in distilled ethanol and blown dry with nitrogen and rinsed with purified water.

Deionized, particle-free water was purchased from Noble's Pureau (Sydney, Australia) then distilled once inside a laminar flow cabinet before use. When equilibrated with the atmosphere the conductivity of this water was about 1 μScm^{-1} and the pH equal to about 5.7 because of dissolved CO_2. In some experiments, the AFM fluid cell was connected to a 100 ml flask containing a pH meter , a liquid injection port, and nitrogen input and vent lines. In these experiments, CO_2 was displaced by nitrogen, and the pH could be continuously monitored. A peristaltic pump ensured exchange between the flask and cell.

Analytical grade NaCl, NaOH and HCl were used without further treatment.

6.3 Results and Analysis

Force measurements between silica surfaces in aqueous in NaCl solutions

The forces between a silica-glass sphere and an oxidized silicon wafer in NaCl solutions are shown in figure 6.5. The forces at each concentration were independent of both the order in which concentrations were measured, and of whether the measurements were performed on approach or separation of the surfaces. The measured forces decay exponentially with distance, and both the decay length and potential decrease with concentration, as expected. The data is similar to previous measurements between macroscopic silica sheets by Horn *et al* [6] and Peschel *et al* [7] and between quartz fibres by Rabinovich *et al*[8]. The solid lines show the theoretical force/radius calculated from DLVO theory using an exact numerical solution of the Poisson-Boltzmann equation and a Hamaker constant of 0.8 $x10^{-20}$ J[9]. For the particle radius of 3.5 μm used in this experiment, $r/\kappa^{-1} > 35$ so use of the Derjaguin approximation introduces an error of less than 2%. The value of the effective surface-potential-at-infinite-separation was obtained from the best fit of the model to the data with the plane of charge at the onset of the regime of constant compliance. However, because the surface is not smooth, the surface charge is most likely not situated in a single plane, but distributed over a layer equal in thickness to the roughness of each substrate. This means that the potentials fitted from our data are likely to be an underestimate of the surface potential, particularly for short Debye-lengths. A more realistic model may be to make the origin of charge at a negative surface separation equal to half the maximum roughness. In present case, this places the origin of charge at -1.5 nm. Figure 6.6 shows the fitted surface potentials as a function of NaCl concentration calculated for each origin of charge as well as values calculated by other workers. (Note that a residual layer of hydration water on the silica surface would have a similar qualitative effect of moving the origin of charge to negative values.)

Figure 6.7 shows the fitted potentials plotted together with a curve calculated using the simple mass-action model descibed in section 3.3. In this case, the dissociation equation is:

$$\equiv Si\text{-}OH \Leftrightarrow Si\text{-}O^- + H^+$$

with the corresponding equilibrium constant:

$$K_a = \frac{[\equiv Si\text{-}O^-][H^+]}{[\equiv Si\text{-}OH]}$$

Iler's[10] figure of pKa = 6.8±0.2, has been used to calculate the potential in the shaded region of figure 6.7. It was not to be necessary to assume ion sizes larger than the area of an individual silanol site, 0.25 nm^2 (the silica is only sparsely charged) and, there was no need to invoke any binding of the Na^+ ion to the silanol sites.

Returning again to figure 6.5, it can be seen that the force lies between the limits of constant charge and constant potential for all but the last 2-3 nm before the regime of constant compliance. At smaller separations, the force is greater than that predicted by DLVO theory. This effect has been measured previously[6-8], and was attributed to the hydration of the silica, but unfortunately, analysis of this component of the force is complicated by the roughness of the substrates. The surface roughness causes uncertainty in the magnitude of the DLVO contribution as described above, and there may also be a force due to the compression of the asperities on the surface. For example, the force required to elastically compress an asperity of area 1nm x 1nm from a height of 3 nm to nm is about 20 nN (the Youngs Modulus for glass is about $70x10^9$ Nm^{-2})[11]. The force derived from this very simple model corresponds to an F/R of 6 mNm^{-1} in the current experiments - about the magnitude of the force at small separation. However, the force at small separation varies with NaCl concentration (and pH - see next section). Thus, to attribute the short-range force to elastic compression of the silica, the compressibility of the silica must be a function of electrolyte concentration, which seems unlikely.

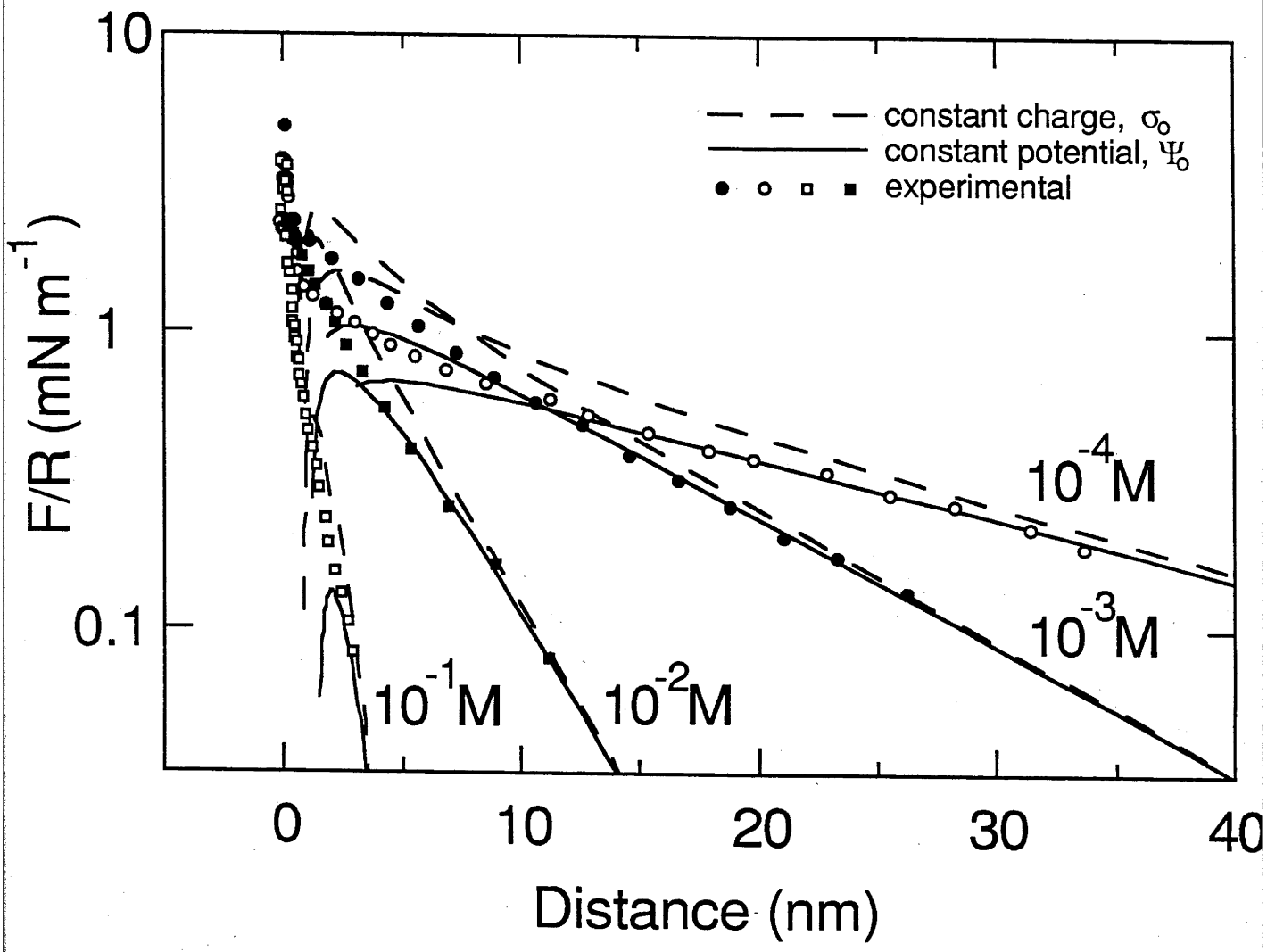

Figure 6.5 The force on a silica-glass particle in aqueous solution in a variety of NaCl solutions at 30 °C. For each concentration, an analog signal was digitized to 400 points, and this data was condensed by averaging sets of ten points to produce the filled circles presented in this figure. The lines were calculated from DLVO theory using an exact numerical solution to the Poisson-Boltzmann equation and a Hamaker constant of 0.8 x 10^{-20} J. At each concentration, the upper line represents the interaction at constant surface charge, and the lower line at constant surface potential. The relevant parameters are 10^{-4} M: $1/\sigma_0$=–56 nm^2/q, ψ_0=–61 mV, κ^{-1} =21 nm; 10^{-3} M: $1/\sigma_0$=–36 nm^2/q, ψ_0=–53 mV, κ^{-1}=9.5 nm; 10^{-2} M: $1/\sigma_0$=–21 nm/q, ψ_0=–34 mV, κ^{-1}=3.2 nm; 10^{-1} M: $1/\sigma_0$=–12 nm^2/q,ψ_0=–21 mV, κ^{-1}=1.1 nm.

	Measured values of the surface potential of silica / mV					
	this work					
	a	b	Horn[c]	Peschel[d]	Rabinovich[e]	Weiss[f]
10^{-1} M	-21	-35	-23			-22
10^{-2} M	-34	-43	-28			-40
10^{-3} M	-53	-58	-32	-50	-45	-67
10^{-4} M	-61	-65	-40	-57		-83

a. calculated with the plane of charge situated at the plane of closest approach.

b. calculated with the plane of charge shifted -1.5 nm relative to the onset of constant compliance. For measurements a. and b., the systematic error arising from the radius and spring constant measurements corresponds to about 2 mV for the measurements at 10^{-1} M and 10^{-2} M and to 4 mV for the measurements at 10^{-3} M and 10^{-4} M.

c. From Horn et al: Force measurements on silica[6]

d.From Peschel et al: Force measurements on silica[7]

e. Rabinovich et al: Force measurements on silica in KCl solution.[8]

f. Weiss et al : Streaming potential on silica in KCl solutions.[12]

Figure 6.6 Comparison of surface potential measurements on silica obtained by various workers.

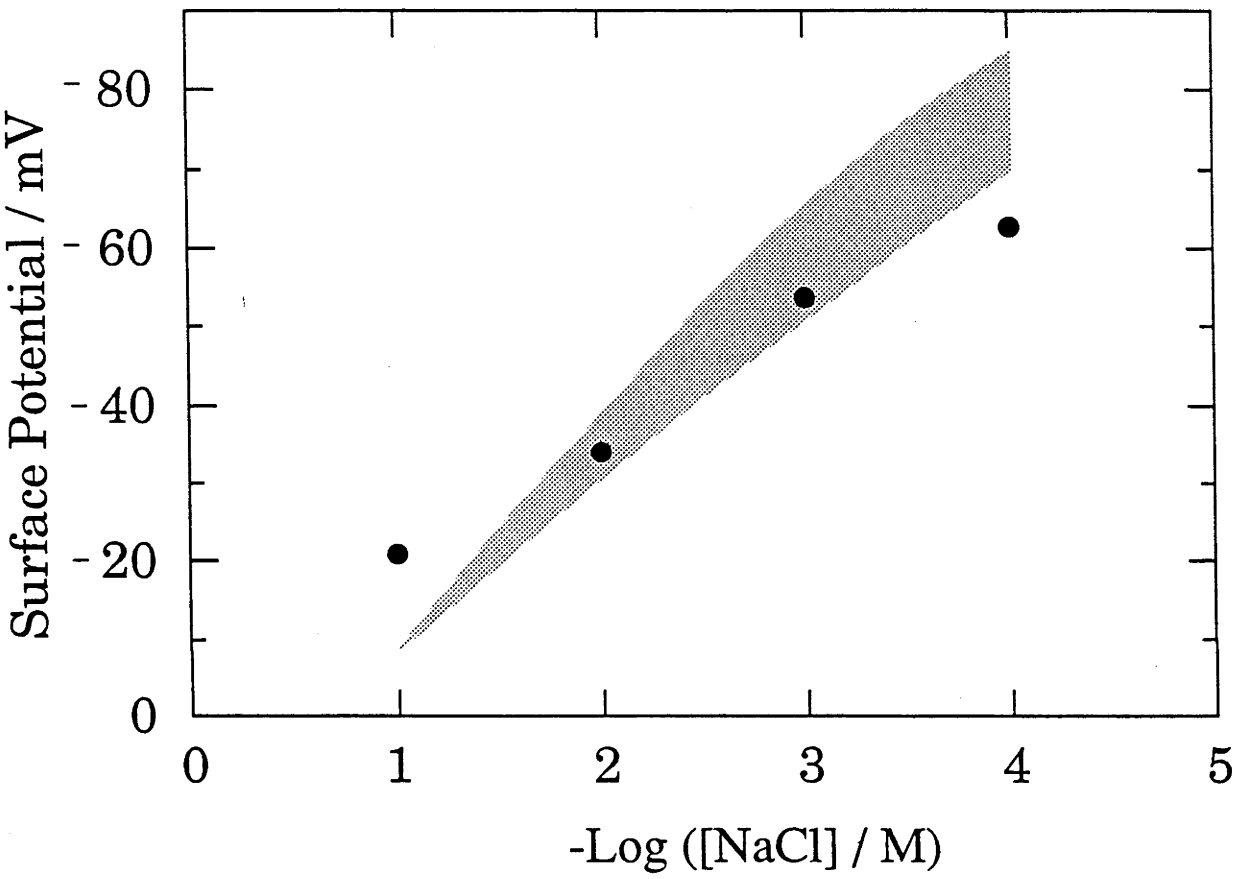

Figure 6.7: The fitted surface potential at infinite separation as a function of NaCl concentration. The circles represent data from the previous figure, and the shaded region is the potential calculated from a simple mass action model assuming no binding of the Na^+ ion. The range of the shaded region is due to the uncertainty in the H^+ binding-constant, $pK_a = 6.8 \pm 0.2$[10].

The force between silica surfaces as a function of pH

Figure 6.8 shows the measured force between a silica-glass sphere and an oxidized silicon wafer as a function of pH. These measurements were performed in a background of 10^{-3} M NaCl. As the pH is reduced, the magnitude of the force decreases and the fitted surface charge diminishes. The force was found to be monotonic increasing over the entire pH range, suggesting that for silica, a hydration force prevents coagulation by van der Waals forces over this pH range. This is in contrast to previous work on *mica*, where it has been shown that the presence of a hydration force is critically dependent on the pH[13](see also section 2.2.1). It is also apparent from comparison of figures 6.5 and 6.8 that the force in the last few nm before contact is much smaller at pH 2 than the force in 10^{-2} M NaCl. It is thus tempting to suggest that the magnitude of a hydration force is greater in the presence of charged surface groups.

The surface potentials of best fit to the data in figure 6.8 are shown in figure 6.9. As in the previous section there is uncertainty in positioning the origin for the plane of charge. The values presented were fitted with the origin at the point of closest approach. The dashed line shows the potentials predicted by the mass-action model with the same pK (H^+) as in figure 6.7, but is a poor fit to the data. However, the fit at high pH can be improved by introducing a finite binding constant for the Na^+, which is 10^7 times more abundant than H^+ at pH 10. In fact, a binding constant, pK(Na^+)=4 produces a good fit to the data. In a similar fashion, the poor fit at low pH can be improved by invoking a pK(H^+) which is a function of surface charge. Iler[10] points out that the pK on silica falls to about 6.3 for a neutralized surface.

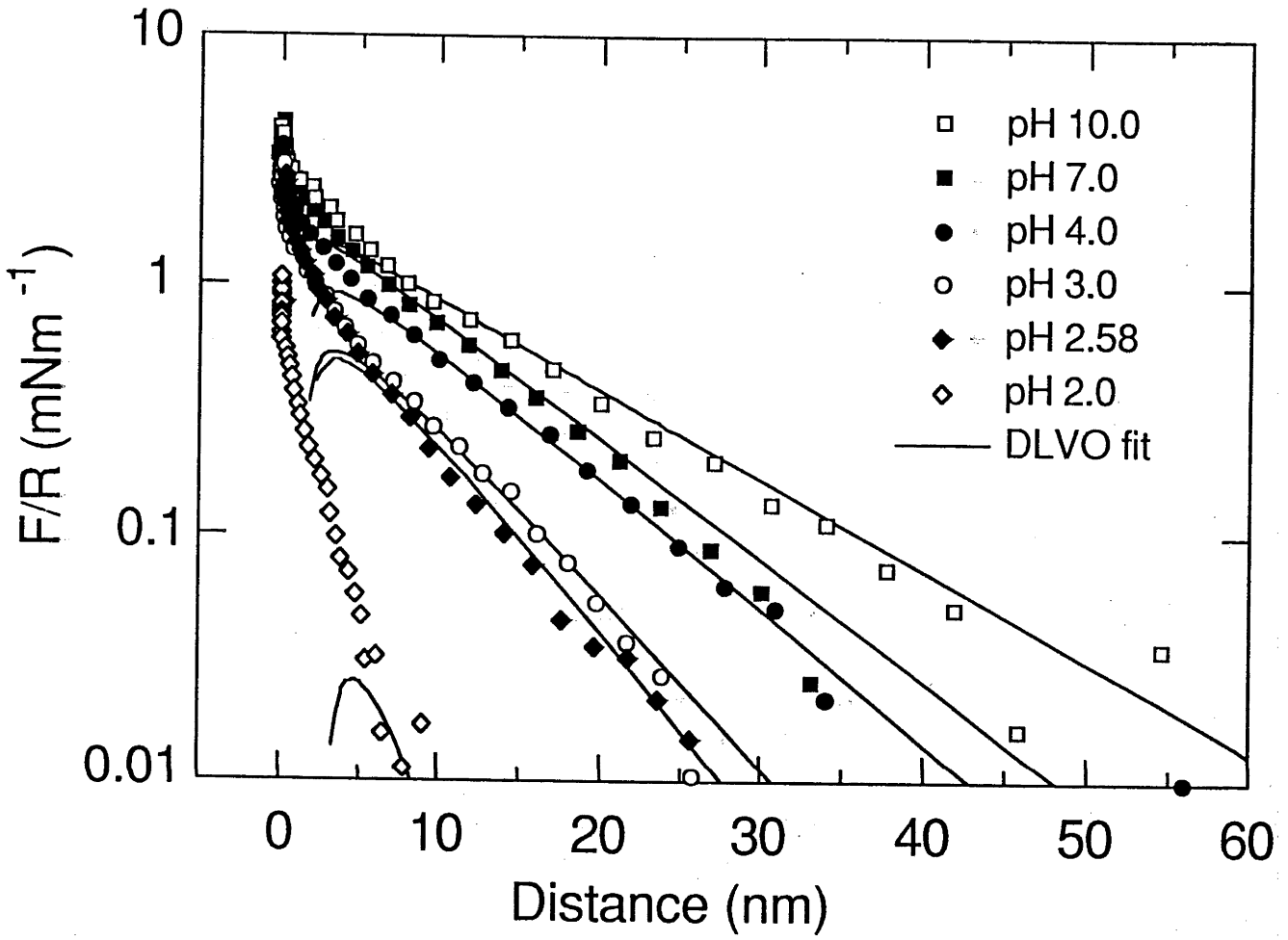

Figure 6.8 The forces between a silica-glass sphere and a flat silica plate as a function of pH at 20 °C. The measurements were performed in a background of 10^{-3} M NaCl. The data points represent measurements of the surface force, and the solid lines are the best fit to DLVO theory at constant surface potential, as in figure 6.3. The following parameters were used: pH 10: $1/\sigma_0 = -27$ nm^2/q, $\Psi_0 = -67$ mV, $\kappa^{-1} = 10.7$ nm; pH 7: $1/\sigma_0 = -26$ nm^2/q, $\Psi_0 = -60$ mV, $\kappa^{-1} = 86$ nm; pH 4: $1/\sigma_0 = -34$ nm^2/q, $\Psi_0 = -48$ mV, $\kappa^{-1} = 80$ nm; pH 3: $1/\sigma_0 = -37$ nm^2/q, $\Psi_0 = -35$mV, $\kappa^{-1} = 62$ nm; pH 2.6: $1/\sigma_0 = -36$ nm^2/q, $\Psi_0 = -35$ mV, $\kappa^{-1} = 56$ nm; pH 2: $1/\sigma_0 = -52$ nm^2/q, $\Psi_0 = -13$ mV, $\kappa^{-1} = 30$ nm.

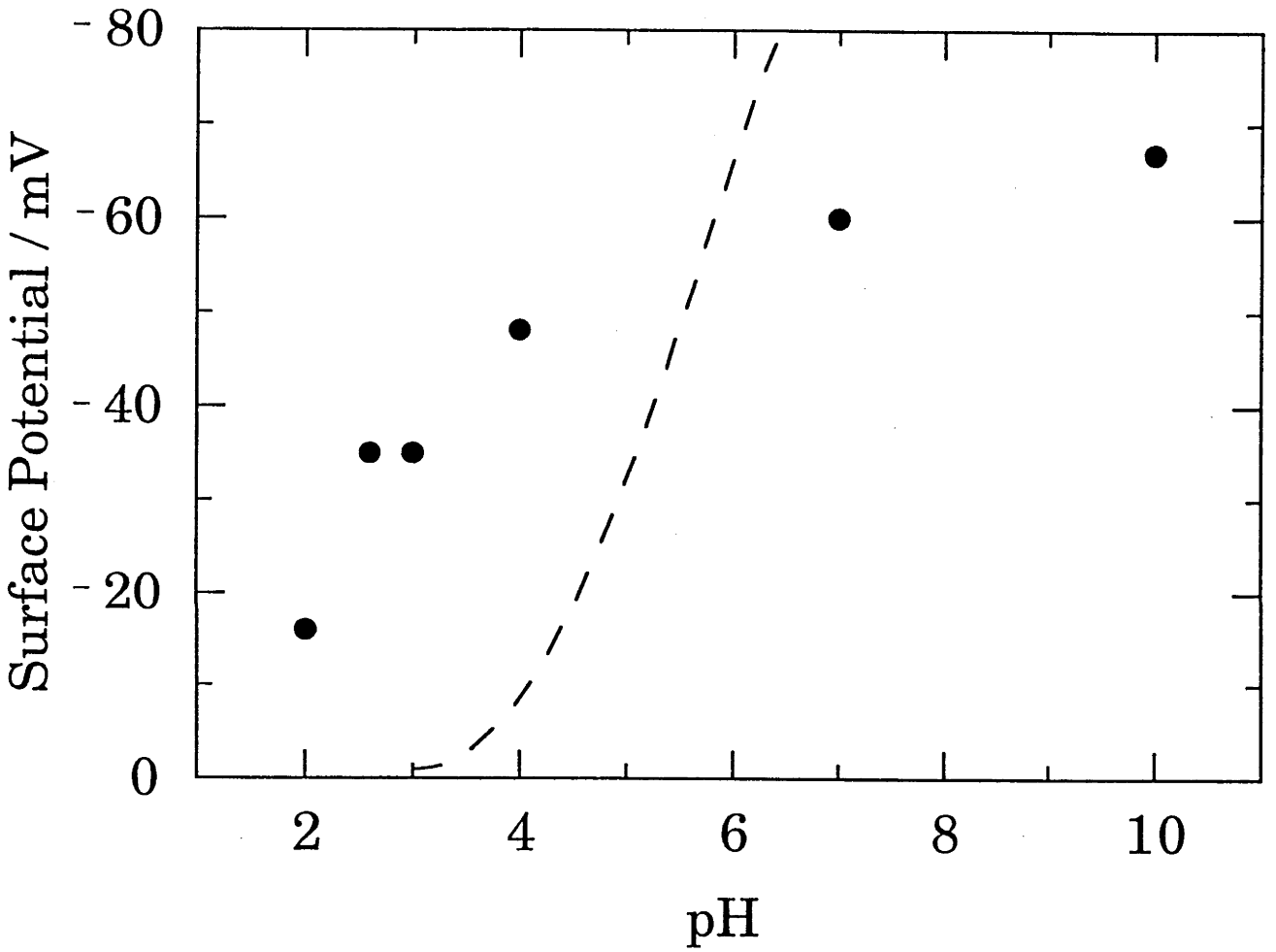

Figure 6.9: The surface potential of silica as a function of pH. The circles were obtained from fits to the data in figure 6.8. The solid line is the potential predicted using a mass action model with $pK(H^+) = 6.8$ and $pK(Na^+) =$ infinite

The force between hydrophobic silica surfaces

A silica sphere was made hydrophobic by exposure to trimethylchlorosilane vapour, and the force was measured as the sphere approached a hydrophobized plate. Unfortunately, the adhesion was too large for the force to be measured on approach, but a pull-off force, F/R = 0.4 Nm^{-1} was obtained. This is in the range of results obtained by Pashley *et al* [14] (F/R = 0.35 Nm^{-1}) and Claesson[15] (0.44 Nm^{-1}).

The force between gold surfaces

The measured forces between a gold-coated particle and a gold surface are shown in figure 6.10. As in the silica-silica interaction, the force decays exponentially with distance at large separation, but in this case the force decreases in the last 2-3 nm. Once the probe comes into contact with the surface, a repulsive force is required from the cantilever to separate the surfaces, indicating adhesion. When a large enough force is applied, the probe cantilever moves to the next stable position which in this case is about 50 nm from the position where the surfaces are touching. This pull-off force was extremely variable, with the unstable region extending up to 300 nm from the surface in some measurements. It was not possible to fit the measured force to a calculated DLVO force using a Hamaker constant of 35 $X10^{-20}$ J[16] when the origin of the plane of charge was placed at the onset of the regime of constant compliance. This was probably because the surfaces were so rough. The effective radius may be smaller the the radius of 3.5 μm obtained from SEM, and it may be more reasonable to assume that the charge on each surface originates from a zone extending up to 20 nm in from the onset of constant compliance (2/3 of the Debye-length). If the interaction is modelled with the plane of charge at minus 10 nm but with no account for the change in van der Waals force, then a reasonable fit is obtained with an effective surface charge at infinite separation of -65 mV. No reasonable fit can be obtained by lowering the Hamaker constant alone.

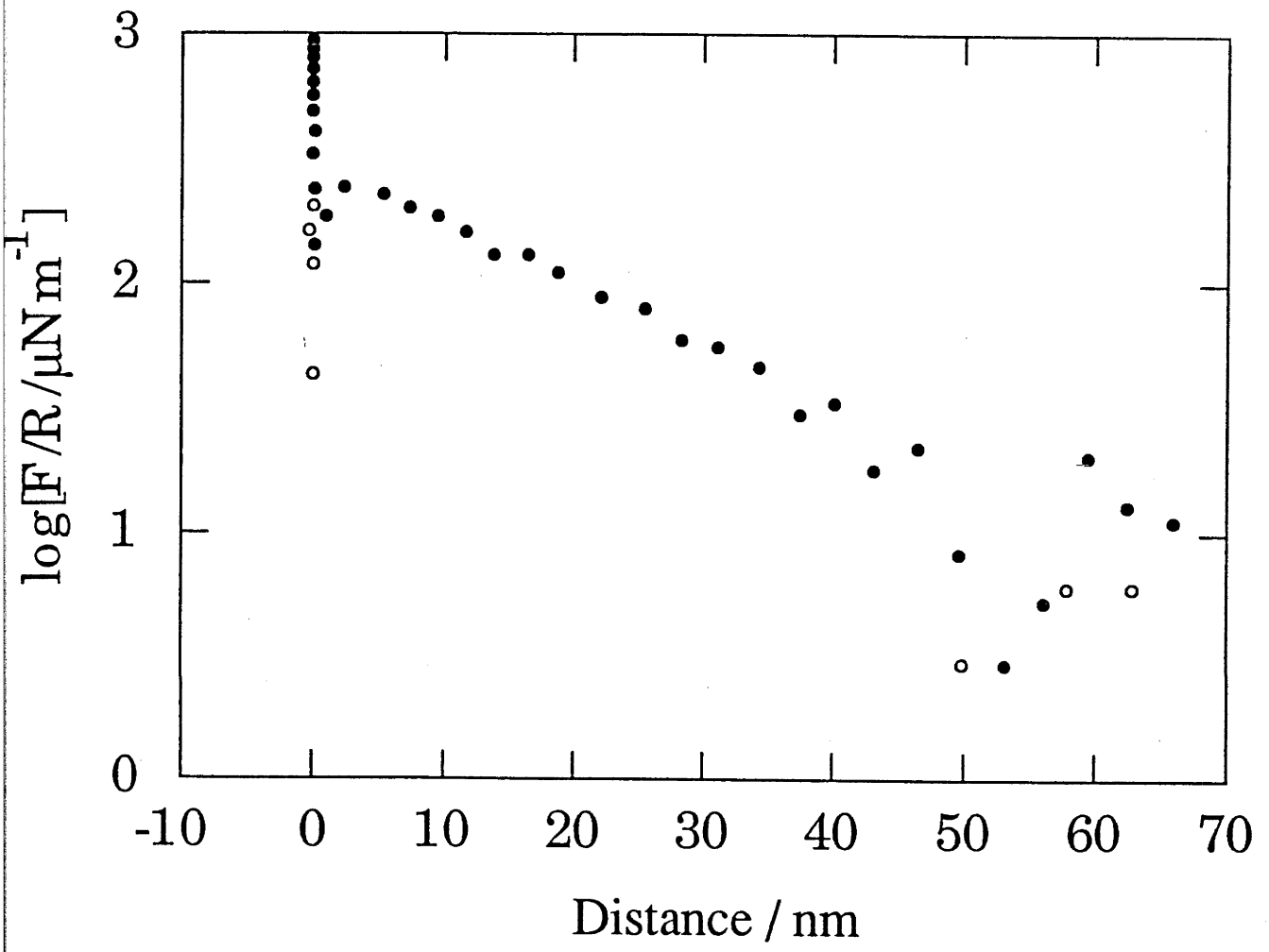

Figure 6.10: The Forces between a gold coated silica sphere and a gold coated mica surface. The filled circles represent measurements taken on approach of the two surfaces and the open ones on separation. The forces have been scaled by the radius of the gold sphere (3.5 μm).

6.4 Discussion

Comparison of ac and dc techniques for surface force measurements

The principal advantages of an ac instrument for measuring static forces are the increased signal to noise ratio and the ability to independently optimize resolution and stability of the cantilever in the force field. For DLVO and hydration measurements on micrometer scale particles, the dc microscope has been shown to provide adequate resolution, but greater resolution would be required for measurement of weaker forces or smaller radii. AC techniques would be useful for these cases, although development of detection methods continues to bring improved resolution for dc instruments. Furthermore, the new force microscope balances no longer require a stiff cantilever to ensure stability in high force gradients so the need for stiff cantilevers has diminished.

In the ac technique resolution is limited by dynamic effects associated with viscous (or other dissipative) processes in the medium and is dependent on modelling of the tip vibration whereas in a dc technique, a signal output directly proportional to F(z) is available. The ac technique, however, remains a useful tool for determining non-conservative forces.

Comparison of the force microscope and surface forces apparatus

The primary difference between force measurements using the SFA and the AFM is the scale of the substrates. The radius of the silica colloid used in the experiments reported in this chapter was about 3 μm, and the radius of the microfabricated tip is of the order of 10-100 nm, so the AFM uses substrates which have radius 10^4 -10^6 times smaller than the SFA. Since most surface forces depend on the radius of the particle, surface forces are most often manifest when the substrate dimensions are in the μm to nm range of the AFM. Thus, the AFM can be used to measure forces on particles of the size for which these forces are usually dominant, whereas the SFA measures forces on macroscopic substrates. Of course, studies on these macroscopic surfaces can still be related to the forces on smaller particles, and can be used for measurements on thin films, adhesion, lubrication and wetting problems. Workers using the the SFA has already been successful in performing these measurements. Until recently, the SFA was also restricted to measurement of forces between transparent substrates, but this limitation has been removed by the adoption of new force measuring techniques such as the piezoelectric-bimorph technology of Parker[17]. In fact, any technique which is used to measure forces in an AFM may also be used in a modified version of the SFA, so the ultimate F/R resolution of the SFA is about 10^4 times higher than for the AFM. However, to utilize this higher F/R resolution, substrates must be found which are homogeneous (and smooth) on a much larger scale. To date this has severely limited the variety of substrates used in the SFA. In comparison, an AFM can measure forces between a wide variety of substrates, and with very high lateral resolution.

The hydrodynamic force on a spherical colloid particle scales with the square of the particle radius. Thus if one wishes to examine viscous forces, the Surface Forces Apparatus provides higher resolution. However, if an experimenter wishes to measure quickly (e.g. to measure relaxation effects), measurement may be performed

at speeds 10^4 times greater in the AFM while maintaining the same viscous force to surface force ratio as in the SFA. In a SFA measurement, the surface separation is typically changed at about 1-10 nm / min but higher speeds of approach more realistically reflect collision speeds in most colloidal systems. Higher measuring speeds also minimize the effects of thermal or other drifts.

One of the major hazards in surface force measurement is contamination with particles. Since the probability of trapping a contaminating particle in the zone between the substrates is proportional to the radius of the substrate, the AFM is less subject to such contamination, and this has been borne out in experiments. However, in the surface forces apparatus, a number of contact regions may be investigated on the one both surface, which raises the probability of locating a "clean" region.

Other differences between the techniques depend more on the manner in which forces and distances are measured. Because the drift in the optical distance measuring technique utilized in the SFA is negligible, the SFA is well suited for measurement of the thicknesses of adsorbed films, and is better suited for measurements in which a constant surface separation must be maintained(although the rapid advance of AFM technology may change this). However, the same optical system is cumbersome, difficult to automate and it is necessary to use substrates which are transparent. Data analysis for the AFM is greatly simplified because the outputs are analogue electrical signals. Finally, the smaller size of the AFM reduces the effect of thermal drifts and mechanical vibrations.

6.4 Conclusions

(1) A method has been presented for measurement of the forces on large colloid particles. This technique has been shown to be simple, quick and reproducible, and could be used on a variety of colloid particles and fibres.

(2) This method has been demonstrated by measurement of the forces between a silica-glass particle and a flat silica surface as a function of separation, NaCl concentration and pH. Results of these experiments are consistent with previous measurements of the forces between silica surfaces. At large separation, (>3 nm) the measured forces agree well with classical DLVO theory, with the interaction occuring between constant charge and constant potential. An additional repulsive force at small separation prevents adhesion in a van der Waals minimum.

(3) The forces on a gold-coated sphere and a Si_3N_4 pyramid have been measured. This demonstrates the utility of the technique for measurements on a variety of materials and substrates.

6.5 References for Chapter 6

1. Zhenge, X. & Yoon, R. *J.Col.Int.Sci.* **134**, 427 (1990).
2. Ellmelech, M. *J. Chem. Soc. Faraday Trans.* **86**, 1623 (1990).
3. Ottewill, R.H. Chapter 9: Concentrated Dispersions in *Colloid Dispersions* Goodwin, J.W. Ed (Royal Society of Chemistry, London, 1982).
4. Brown, M.A. & Staples, E.J. *Langmuir* **6**, 1260 (1990).
5. Prieve, D.C. & Frej, N.A. *Langmuir* **6**, 396 (1990).
6. Horn, R.G., Smith, D.T. & Haller, W. *Chemical Physics Letters* **162**, 404 (1989).
7. Peschel, G., Belouschek, P., Muller, M.M., Muller, M.R. & Konig, R. *Colloid and Polymer Science* **260**, 444 (1982).
8. Rabinovich, Y.I., Derjaguin, B.V. & Churaev, N. *Adv. Coll. Interface Sci.* **16**, 63 (1982).
9. Hunter, R.J. *Foundations of Colloid Science Volume 1* (Oxford University Press, N.Y.1987) Page 222 .
10. Iler, R.K. *The Chemistry of Silica*1 (Wiley, New York, 1979) Page 182.
11. Condon, E.U. *Handbook of Physics* 1 (McGraw-Hill, New York, 1967) Page 3.
12. Wiese, G.R., James, R.O. & Healy, T.W. *Disc. Faraday Soc.* **52**, 302 (1975).
13. Pashley, R.M. *J.Col.Int.Sci.* **83**, 531 (1981).
14. Pashley, R.M., McGuiggan, P.M., Ninham, B.W. & Evans, D.F. *Science* **229**, 1088 (1985).
15. Claesson, P.M. & Christenson, H.K. *J. Phys. Chem.* **92**, 1650 (1988).
16. Derjaguin, B.V., Rabinovich, Y.I. & Churaev, N.V. **272**, 313 (1978).
17. Parker, J.L. *Langmuir* Submitted
18. LeNevea, D.M.,Rand, R.P. and Parsegian, V.A. *Nature* **259** *601 (1976)*
19. Lubetkin, S.D., Middleton, S.R. and Ottewill, R.H. *Phil. Trans. Roy. Soc. Lond. A* **311** 353 (1984)

Chapter 7
Conclusions

Surface forces have been studied using both a Surface Force Apparatus and a Force Microscope. Two new Force Microscope techniques are presented. A new resonance technique allows measurement of forces in dissipative media, including measurement of non-conservative forces. A new static technique allows direct measurement of the forces on individual colloid particles for the first time. A study of the forces on a silica-glass particle in NaCl solutions and over a range of pH values successfully demonstrates this technique. In NaCl solutions, the measured force agrees well with results obtained from other techniques.

Surface forces have also been investigated using the Surface Forces Apparatus, with established techniques. The interaction between mica crystals in an aqueous solution of diammonium salt was found to be attractive at separations greater than about 1 nm, suggesting that the surface is neutralized by the salt. The mica surfaces adhere at a separation of 0.8 nm (equal to the length of the diammine), probably because the salt bridges between the two sheets. This suggests that aqueous dispersions of similar clay particles should be unstable in the presence of the diammine. This was borne out by experiments where the diammine was found to cause more rapid precipitation of a montmorillonite suspension than an equivalent solution containing Ca^{2+}.

The interaction between mica sheets in a range of ammonium chloride solutions was found to be similar to that measured previously in solutions of alkali-metal ions, even though the ammonium ion can hydrogen-bond to the solvent, and is a polyatomic, acidic ion. The forces were well described by classical DLVO theory at low salt concentration, but an additional repulsive force was measured at short range in concentrated solutions.

The development of a method for measuring interparticlulate forces on individual particles allows a new range of experiments. For example, the effects of particle collision speed and particle adhesion can be examined, and surface forces can now be measured on a variety of metal, metal oxide, covalent and ionic particles. The behavior of particular particles in an industrial product or process can be examined directly, instead of using model systems.

Appendix

Force measurement using an atomic force microscope

A1 Introduction

Previous force measurements using an ac force microscope determined the magnitude of a surface force from measurement of the amplitude of vibration of the free end of a cantilever. The "fixed" end of the cantilever was attached to a piezoelectric crystal to force oscillations and a fine tip was situated on the free end to obtain high lateral resolution. This Appendix describes experiments in which it is shown that the damping coefficient of a cantilever is a function of tip-sample displacement. Thus, measurement of the amplitude of vibration of a cantilever at one frequency is not sufficient to measure the surface force: it is necessary to measure complete amplitude-displacement-frequency spectra. Results of measurements are presented in which (1) the tip surface separation was varied at a fixed driving frequency and (2) the driving frequency was scanned at a fixed tip-surface separation. The second set of results is analysed to determine the surface force.

A strong short-range force was observed for freshly prepared surfaces, implying a van der Waals interaction. A weak, long-range force was observed after exposure of the surfaces for a number of hours, suggesting that a capillary force is dominating the interaction. The long-ranged force contained a non-conservative element which increased on approach to the surface.

A2 Measurement of surface forces

Two types of measurement were performed, involving variations in tip-surface separation and tip vibration frequency, respectively. A block diagram of the sensing equipment used for the displacement scans is shown in figure A1. A constant amplitude and frequency signal was input to the dither piezo from signal generator 1 via a voltage-to-frequency transducer, and the sample-tip separation was scanned via the sample piezo, using signal generator 2 and a voltage amplifier. A lock-in amplifier measured the rms amplitude of the signal from the differential amplifier attached to the diode, and this was plotted against the output from signal generator 2 to yield an amplitude versus displacement trace, shown in the inset in figure A1. This measurement was repeated for a range of frequencies around resonance.

The sensing equipment used in the frequency scans is shown in the block diagram of figure A2. In this measurement, tip-sample displacement was held constant and the driving frequency of the dither piezo was varied continuously. This frequency was controlled by signal generator 1, via the voltage-to-frequency transducer. The output from the differential amplifier was plotted against the output from signal generator 1, and the frequency was scanned at a rate slow enough to allow 15-16 periods in each 1-Hz interval of the frequency spectrum. This process was repeated 16 times, and an envelope of the maximum amplitude was obtained to yield a plot of the amplitude of the sinusoidal output versus driving frequency, shown in the inset in figure A2. The tip-sample separation was then changed using signal generator 2 and a new spectrum recorded.

Referring to the schematic diagram of figure A3, the experimental variables were the dither-piezo surface separation, Z, controlled by the specimen piezo, and the tip driving frequency ω_d controlled by the dither piezo (Z will be refered to as the lever-surface separation) . The rms amplitude, A, of the ac cantilever motion (sensed by the

diode through changes in l) was measured as a function of ω_d and Z, thereby permitting the surface force variation F(z) to be determined.

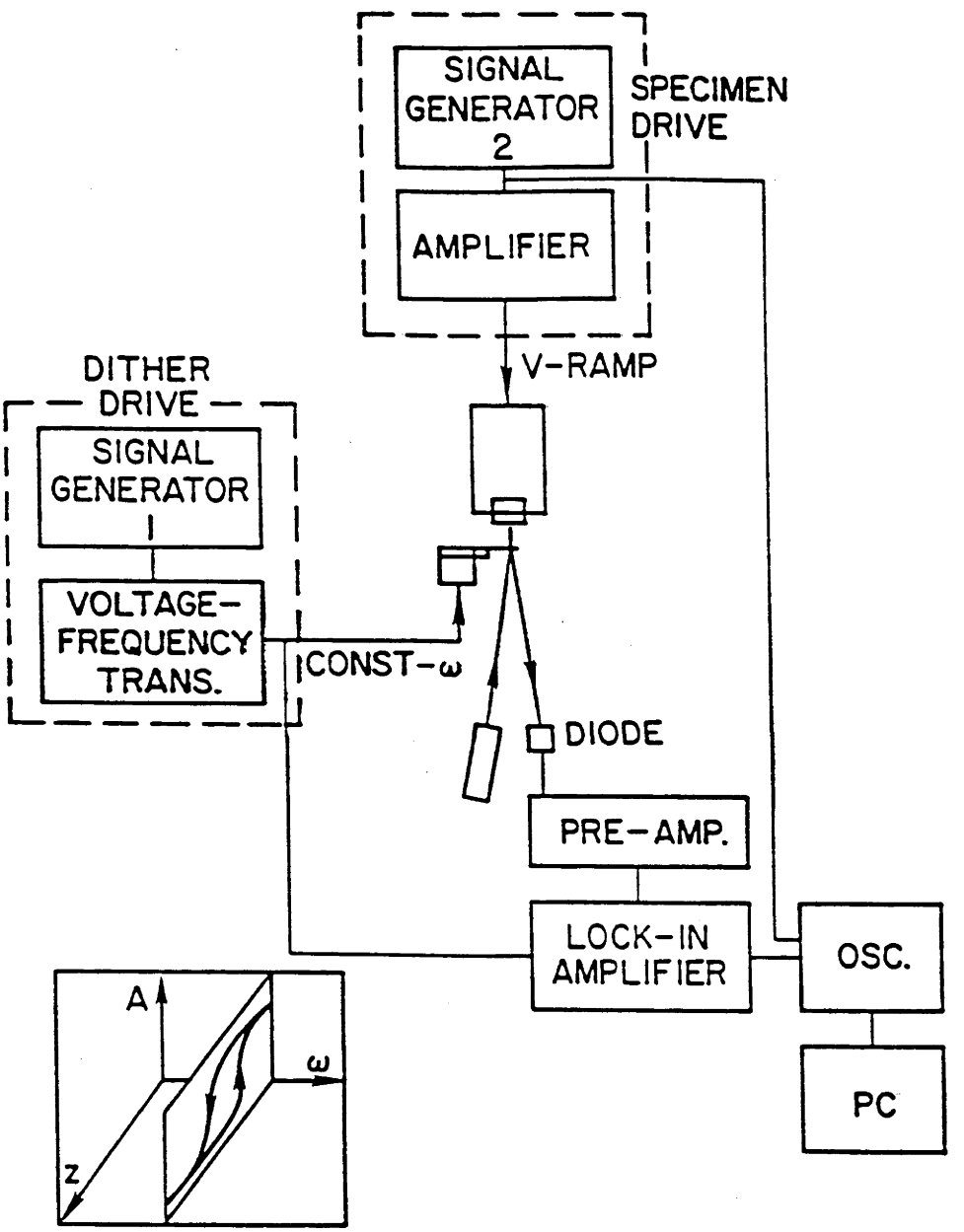

Figure A1: Block diagram of the electronic sensing apparatus used in the displacement scans. The inset shows the form of the data in (ω,Z,A) space.

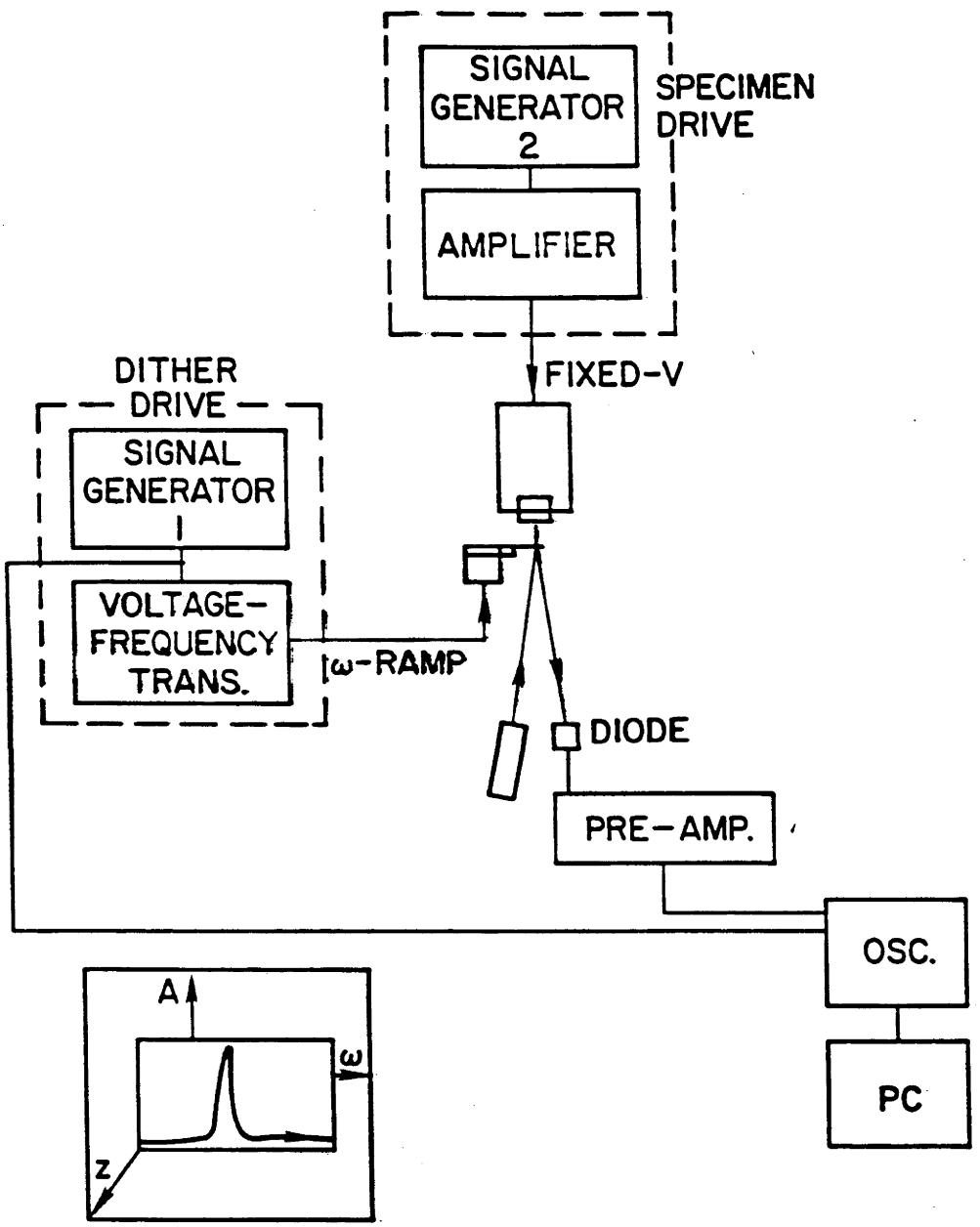

Figure A2: Block diagram of the electronic sensing apparatus used in the frequency scans.

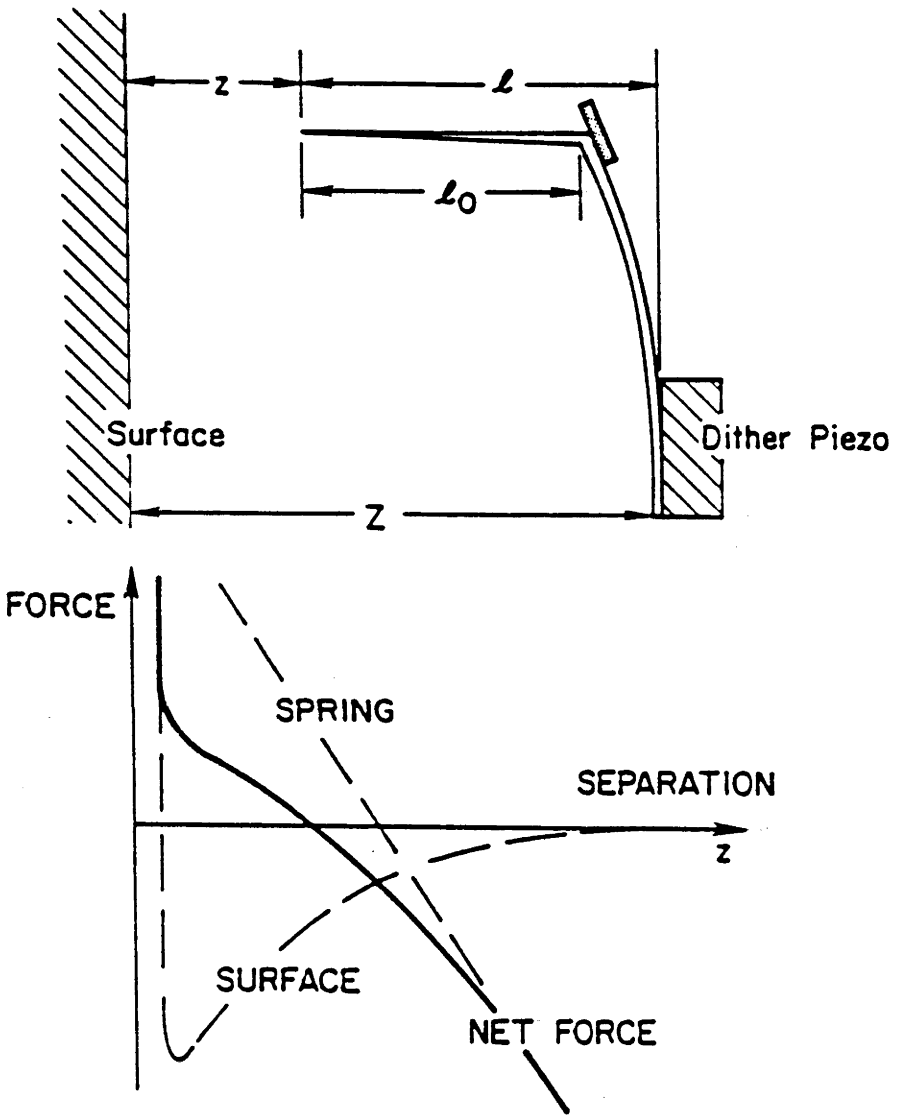

Figure A3: Schematic diagram showing the parameters of the tip-surface geometry (upper), and the forces on the tip as a function of tip-surface separation and cantilever deflection (lower). The solid line represents the net force acting on the tip, for a given value of the lever-surface separation Z.

A3 Results

Measurement of lever vibration amplitude as a function of sample displacement.

Figure A4 shows an oscilloscope trace of the output of the lock-in amplifier (using a 1-kHz low-pass filter) during a displacement scan. The upper trace was recorded on the tip approach to the surface, and the lower trace in the opposite direction. The distance scale shows changes in Z. The tip was driven at a frequency slightly greater than the resonant frequency measured at large separations (10.76 kHz).

The decrease in amplitude indicates a force with positive gradient with respect to displacements from the surface (*i.e.* an attractive force). The discontinuity indicates an unstable equilibrium point, at which incremental motion of the specimen piezo leads to rapid, non-equilibrium motion of the tip towards a stable equilibrium position on the specimen surface. The discontinuity in the amplitude occurs at a tip-surface separation at which the gradient of the surface force equals the spring constant of the lever, see figure A3. There is no absolute measure of the distance between the two equilibrium points, but, by extrapolation of the oscilloscope trace, it appears that the surface is about 1 nm beyond the onset of instability.

When the direction of specimen motion was reversed, the amplitude of tip vibration remained small for about 5 nm beyond the original point of instability, indicating that there was some surface adhesion. For a spring constant of 125±6 Nm^{-1} this corresponds to a pull-off force of about 625 nN, which for a tip radius of 100 nm is equivalent to an energy of 550 mJm^{-2} to separate mica and Ni in air. This measured value is higher than expected, suggesting that either the radius has been underestimated or that some of the Ni remained attached to the surface. The pull-off force varied with time, as might be expected in an uncontrolled environment. The measured value of the

pull-off force was also found to depend on the driving amplitude. For larger amplitudes the force was found to be smaller, presumably because of the extra kinetic energy of the tip. It is interesting to note that the outwards portion of the hysteresis loop is not flat, indicating that the lever is stiff enough to measure the force gradient beyond the first equilibrium position established on the surface during the approach.

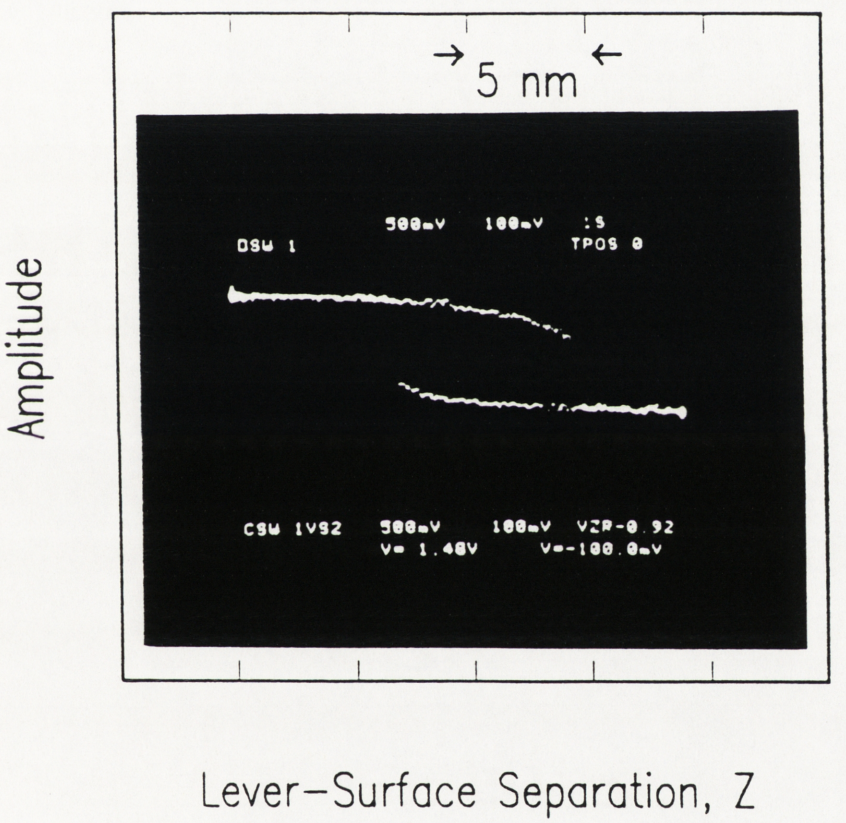

Figure A4: Oscilloscope plot of lever vibration amplitude vs specimen displacement for a freshly prepared Ni-mica system. Note the change in amplitude over a small displacement range, and the hysteresis associated with tip-surface adhesion. The arrows indicate the points of instability.

The small spatial range of the change in force gradient in figure A4 suggests that the dominant force on the tip is in this case due to van der Waals forces. Although such forces were reproducible over the first 30 min, exposing the Ni and mica to air for some hours generated a much longer range attractive force between the tip and the surface, probably due to capillary condensation of atmospheric water. Figure A5 plots the rms amplitude, A, versus lever-surface separation, Z for an exposed Ni-mica system at the resonant frequency measured at large lever-surface separations. Compared with the trace of figure A4 the trace of figure A5 indicates a force of much greater range. There is also no hysteresis due to adhesion in this plot, and the small degree of hysteresis evident is thought to be due to drift or hysteresis in the specimen piezo.

Figure A6 shows displacement scans, each measured at a different frequency, layered on the same diagram. As in figure A5, the vertical axis represents rms amplitude, but each trace now represents a continuous variation in distance at constant frequency. (The trace from figure 6 is arrowed at the center of the diagram.) At low frequencies the tip-surface separation for resonance (given by the point of maximum amplitude) decreases. For the traces in which a maximum was evident, the displacement and amplitude at resonance were determined. The amplitude at identical displacements was then determined from the remaining traces, generating a plot of amplitude versus frequency, figure A7. (The amplitude in figure A7 has been squared to permit comparison with data acquired during frequency scans.)

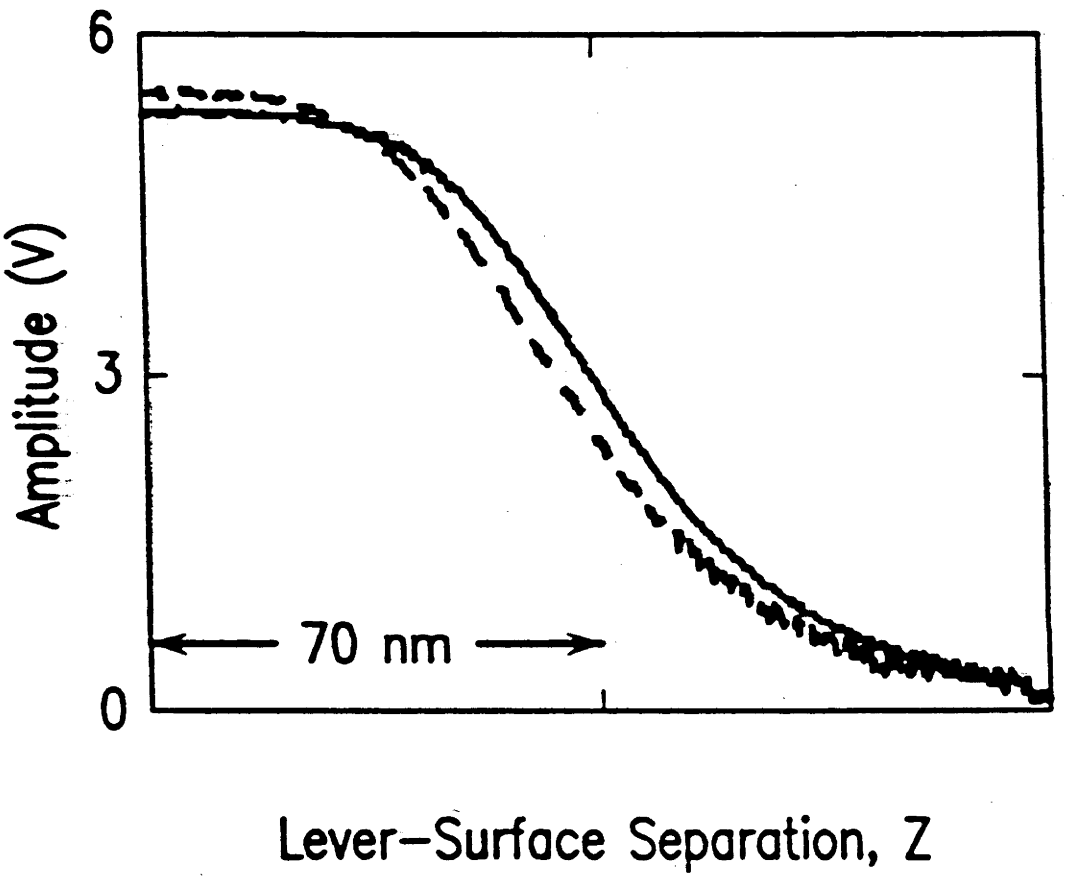

Figure A5: Plot of lever vibration amplitude vs specimen displacement for a Ni-mica system exposed to air for several hours. The larger range of the change in force gradient suggests capillary forces between the tip and surface. The solid line represents measurements on approach to the surface, and the dashed line on retreat.

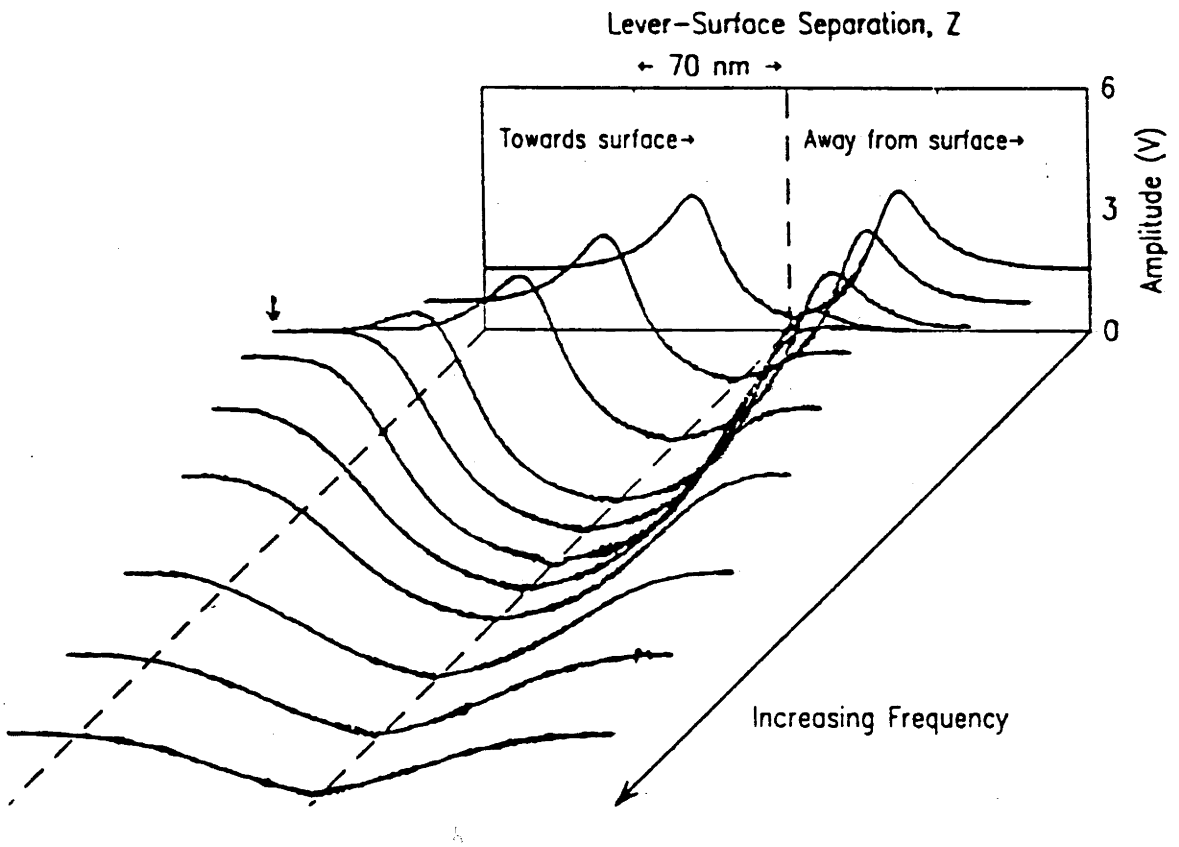

Figure A6: Overlaid traces of cantilever vibration amplitude vs specimen displacement for a range of frequencies around the resonant frequency determined at large separations (center arrow).

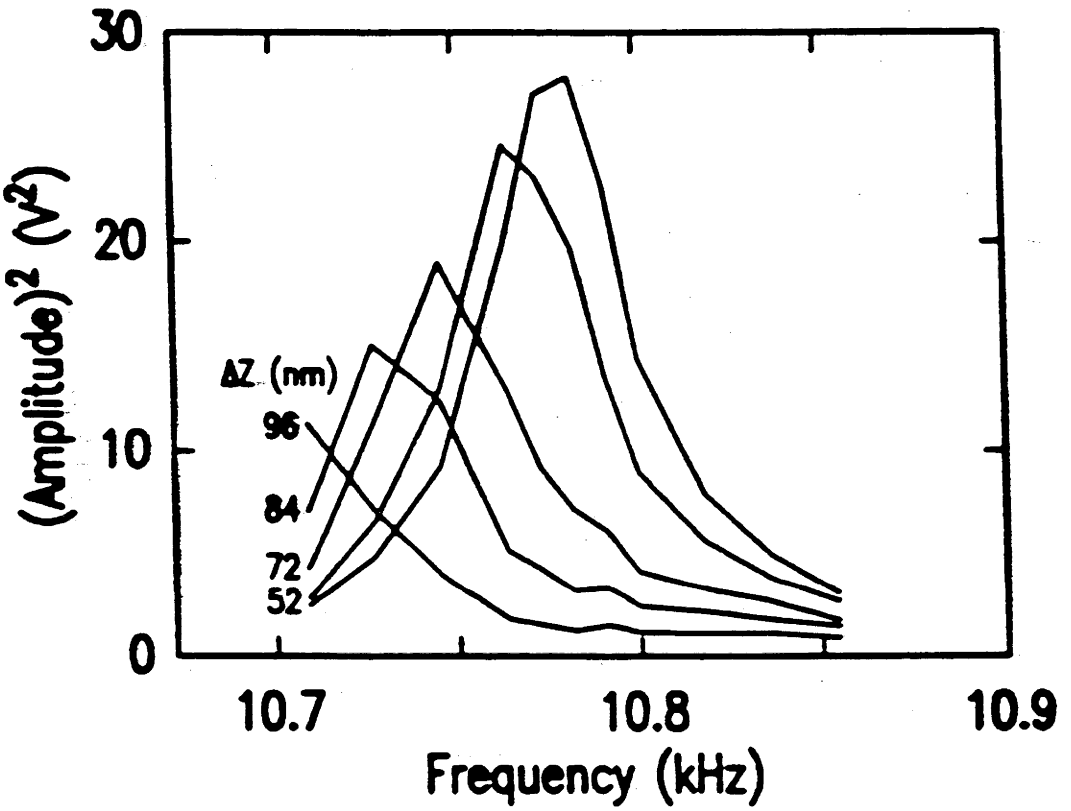

Figure A7. Squared amplitude of cantilever vibration vs frequency at various lever-surface separations. ΔZ is the separation from the curve of maximum amplitude. These data were derived from Figure A6.

Measurement of lever vibration-amplitude as a function of frequency.

Knowledge of the amplitude-frequency response of the cantilever provides information about the gradient of the force and the magnitude of the damping in the region of the tip. The amplified diode output for a frequency scan at a constant, large, lever-surface separation is shown in figure A8 (a). Figure A8 (b) shows the same information after squaring and smoothing (the data was averaged over 1% of the range for noise reduction). When a fresh tip was placed in the microscope, an attempt was made to measure frequency spectra at a variety of distances, but it was found that the range of the force was so short that it was impossible to hold the tip in the force field in the presence of thermal drift and vibrations (*i.e.*, the instability evident in figure A4 prevented maintenance of a stable tip position). However, in the presence of a longer range force (figure A5) it was possible to measure frequency spectra.

Figure A9 shows a number of frequency spectra, like that in figure A8 (b), taken over a range of 30 nm and superimposed to give a full plot of amplitude versus frequency as a function of lever-surface separation. As the tip approaches the surface the amplitude of the vibration decreases, and the resonant frequency also decreases. These two effects are quantified in figure A10, which plots the resonant frequency, ω_0 and the Quality ($2\omega_0/\gamma$), Q as a function of separation. The resonant frequency at each separation was the frequency of maximum amplitude. The Q factor was determined from the ratio of the resonant frequency to the width at half-maximum amplitude. Figure A10 (b) shows that there is greater energy dissipation in the system as the tip approaches the surface. The measurements of figure A10 (a) allow an estimation of the surface force variation as a function of lever-surface separation, and this is considered in the following section. The data in Figure A7, although less complete, could also be analyzed in this manner.

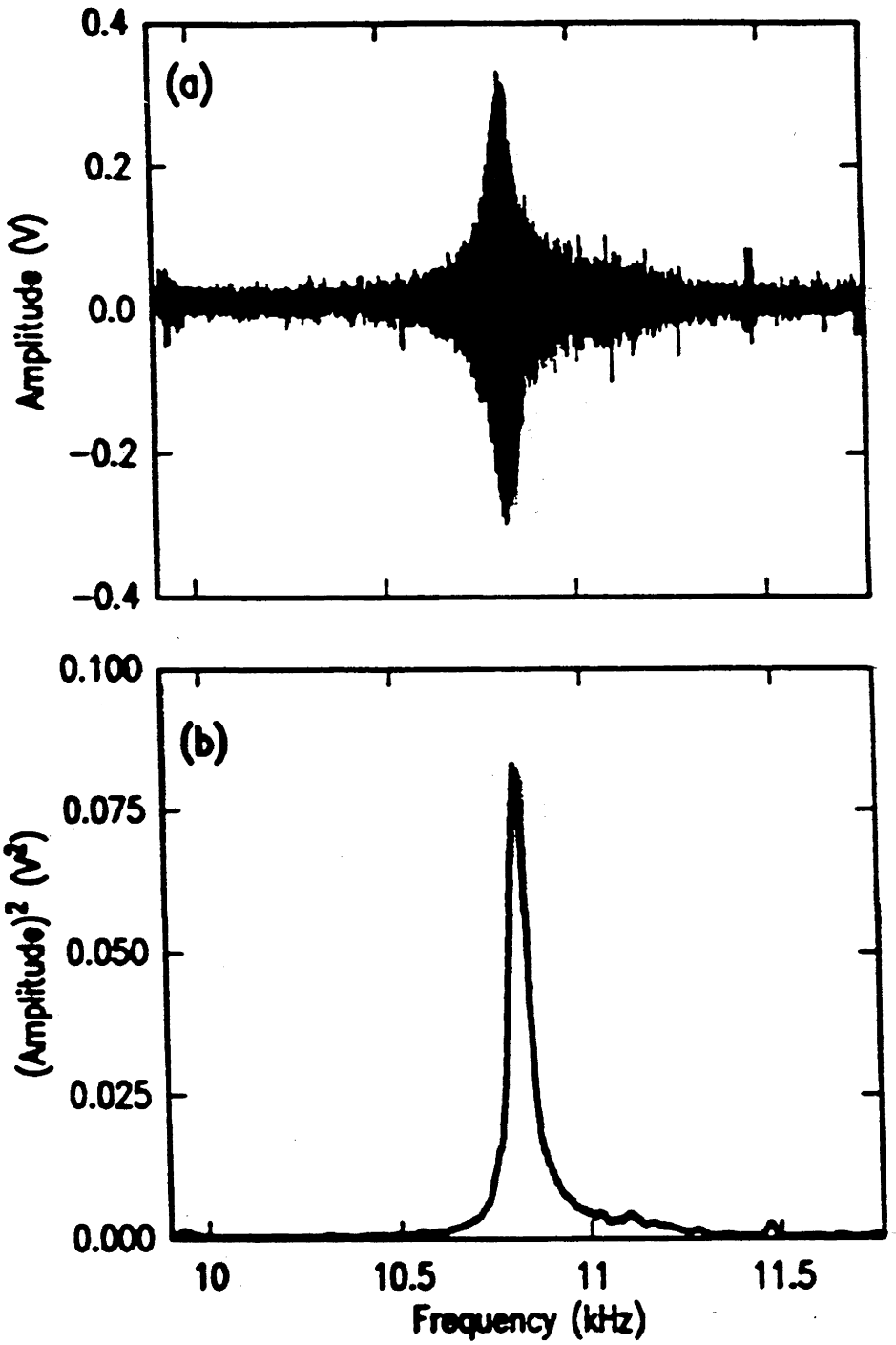

Figure A8: (a) Amplitude of lever vibration vs. frequency at a large lever-surface separation. (b) Data from (a) squared and smoothed to reveal the resonance at 10.8 kHz.

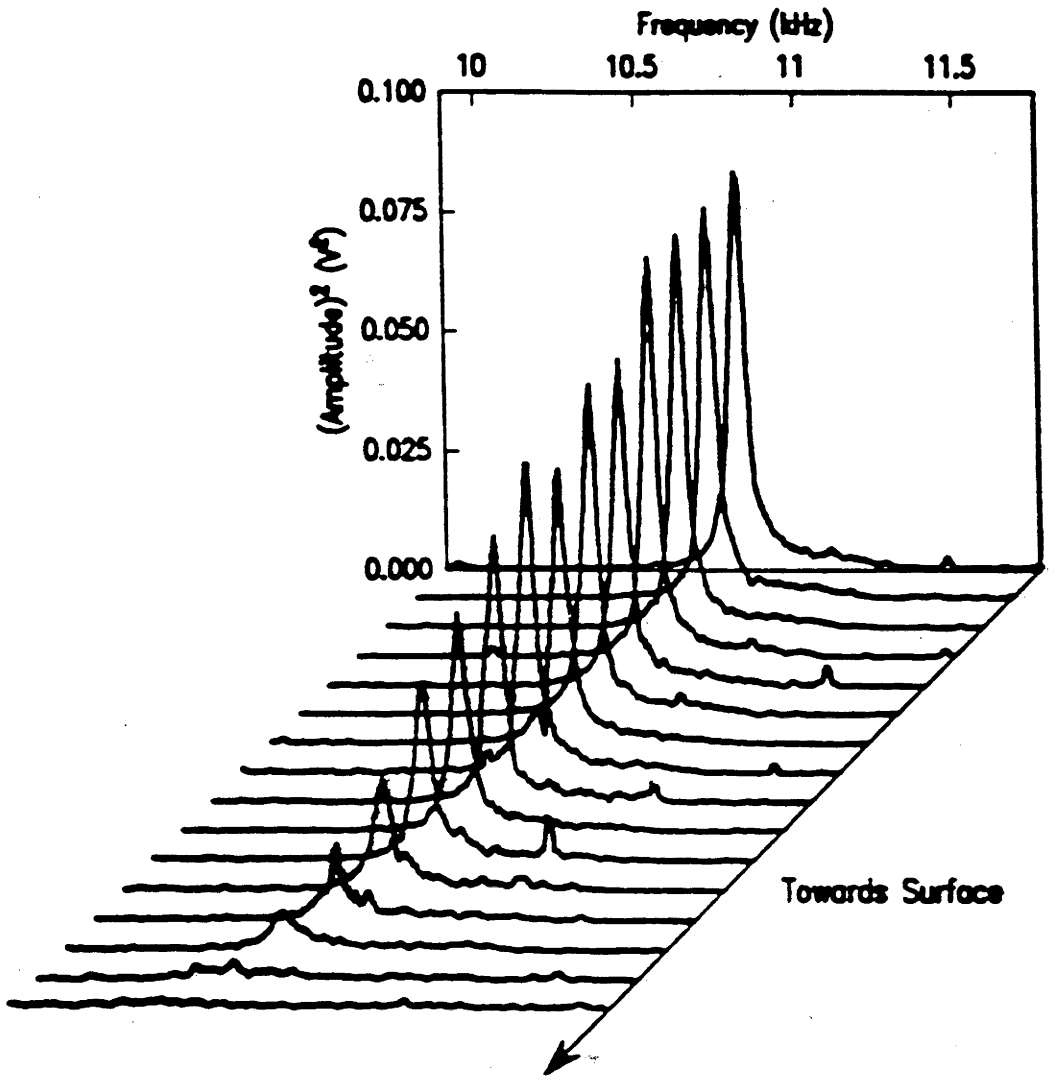

Figure A9: Overlaid traces of amplitude of cantilever vibration vs frequency for a range of lever-surface separations. Note the decrease in amplitude and decrease in resonant frequency as the tip approaches the surface.

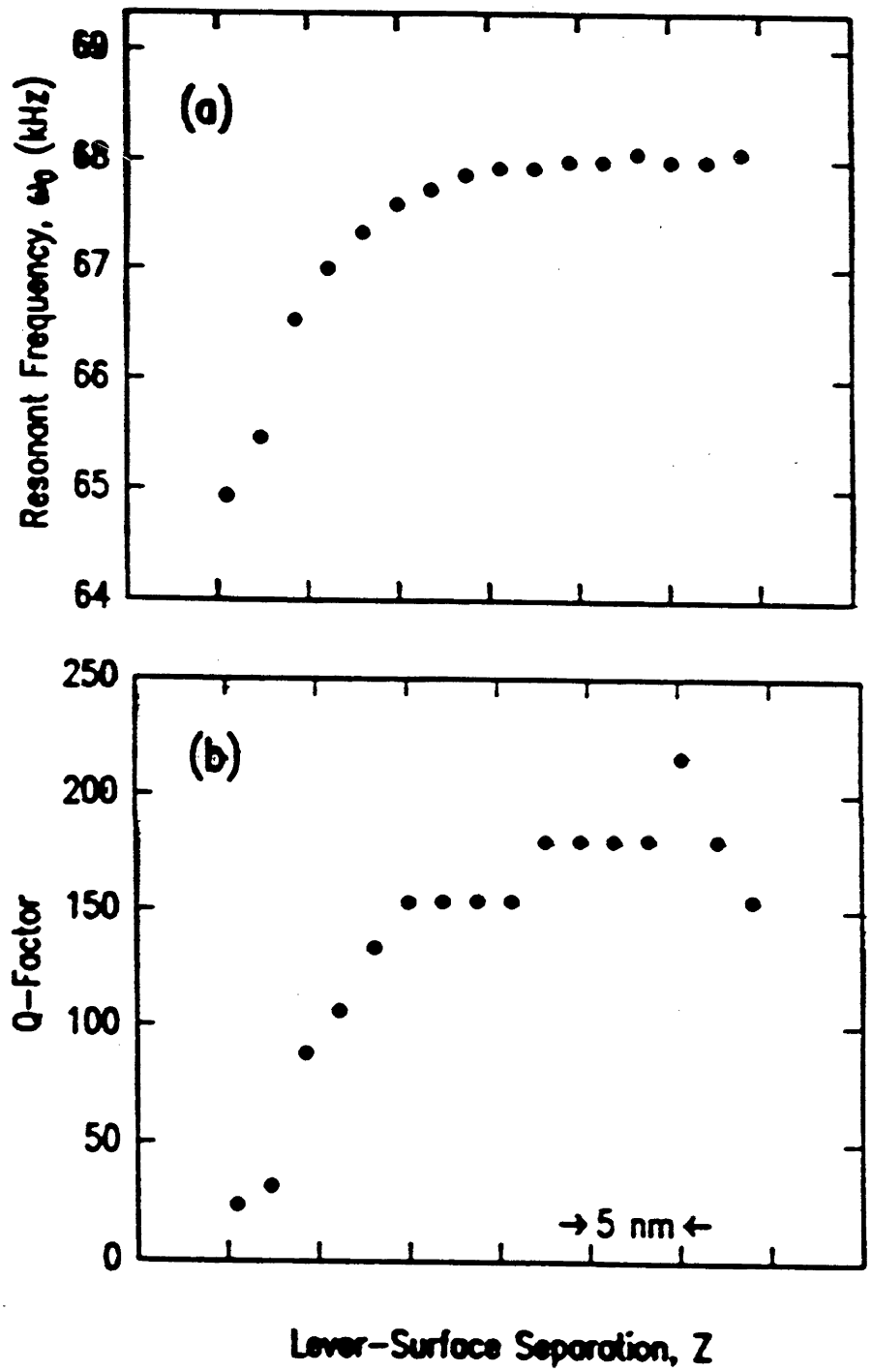

Figure A10: (a) Resonant frequency vs lever-surface separation taken from the data in figure A9. (b) Q factor vs lever-surface separation.

Analysis of frequency scan data

In order to interpret the data in Figure A10 (a), it is necessary to consider the forces on the tip. The lever-surface separation Z (see Figure A3) is given by

$$Z = z+l = z_0+l_0 = z_e+l_e \quad (1)$$

where z is the distance between the end of the tip and the surface, l_0 is the tip length, and z_0 is the tip-surface separation in the absence of any force on the tip or perturbation of the dither piezo, and thus the cantilever is undeflected. (note that z_e is equivalent to Z in Chapter 5) In the presence of a surface force F(z) the cantilever deflects to an equilibrium position, denoted by the subscript e, such that

$$F(z_e) = -k\,(z_0-z_e) = -k\,(l_e-l_0) \quad (2)$$

For an arbitrary tip position the equation of motion is thus

$$m_{eff}\,\ddot{z} = F(z) - k(z-z_0) - m_{eff}\,\gamma\,\dot{z} \quad (3)$$

where m_{eff} is the effective mass of the tip-cantilever system, k is the spring constant, γ quantifies the damping and $\dot{}$ represents differentiation with respect to time, t. If the amplitude of vibration of the tip about the equilibrium position is small, a linear approximation to F(z) is reasonable,

$$F(z) = F(z_e) + (z- z_e)\,F'(z_e) \quad (4)$$

where ' referes to differentiation with respect to distance.

Combining Eqs. (1), (2), and (4) into Eq. (3) leads to a new equation of motion,

$$m_{eff}\,\ddot{z}+m_{eff}\,\gamma\,\dot{z} + [k - F'(z_e)]\,z = [k - F(z_e)]z_e(t) \quad (5)$$

which is the equation of a driven, damped harmonic oscillator. The driving force originates in the sum of the dither piezo oscillation,

$$Z = Z_0 + A_0 \sin(\omega_0 t) \quad (6a)$$

and the concomitant oscillation in the equilibrium cantilever position about l_e, has amplitude:

$$A_0F'(z_0) / [\,k - F'(z_e)\,] \quad (6b)$$

using equations (2) and (4). Hence combining equations (1) and (6), the driving force on the tip may be expressed in terms of the experimental variables.

$$[\, k\text{-}F'(z_e)\,]\; z_e(t) = kA_0 \sin(\omega_d t) + [k - F'(z_e)\,]\,(Z_0 - l_e) \qquad (7)$$

where Z_0 is controlled by the specimen piezo (and thus sets l_e and z_e), and A_0 and ω_d are controlled by the dither piezo. (In this work A_0 was typically 0.04 nm and ω_d was typically 50-100 kHz.)

The solution to Eqs. (5) and (7) for the vibration of the tip about z, and hence the lever about l_e is given by

$$z - z_e = l_e - l = A \sin(\omega_d t + \alpha) \qquad (8)$$

where

$$A = \omega_0^2 A_0 / [\,(\omega_0^2 - \omega_d^2)^2 + \gamma^2 \omega_d^2]^{1/2} \qquad (9a)$$

and

$$\tan\alpha = \frac{\omega_d \gamma}{\{[k\text{-}F'(z_e)] / m_{eff}\} - \omega_d^2} \qquad (9b)$$

and the resonant frequency is given by:

$$\omega_0(z) = \left(\frac{k - F'(z)}{m_{eff}}\right)^{1/2} \qquad (10)$$

Thus, rearranging,

$$F'(z_e) = k\left(1 - \frac{\omega_0(z_e)^2}{\omega_0(\infty)^2}\right). \qquad (11)$$

Figure A11 plots $F'(z_e) / k$ as a function of Z_0 using the data from Figure A10 (a) and Equation 11. It is clear that for the data in the figure, F' is always much smaller than k, and thus it is a reasonable approximation to equate the changes in Z to changes in Z_e.

Hence, the force gradient data in figure A11 may be integrated to obtain the force and potential between the tip and the surface as a function of the tip-surface separation (note that an exact relationship between Z_0 and Z_e could be used for larger force gradients). These quantities are plotted in Figures A12a and A12b, respectively, in appropriately normalized units. Interferometric calibration of the specimen piezo yields the length scale on the horizontal axis, and determination of the spring constant k yields the force and energy scales on the vertical axes. Note that the force is

approximately 60 nN in this case, about an order of magnitude less than that measured on a "fresh" surface in figure A4. (This compares with an estimated capillary force of 2-50 nN for a capillary of radius 100 nm.)

If one ignores many-body effects, the force in Figure A12 (a) can be considered to be the sum of the forces between each small element in the tip, and each small element in the surface. If the surface acts like an infinite half-space,

$$F(z) = \int_{tip}^{\infty} \sigma(z^{el}) dA_{tip} \qquad (12a)$$

where $\sigma(z^{el})$ is the force per unit area between an elemental area of the tip dA_{tip} (at a distance z^{el} from the surface) and the entire surface, and is related to the energy per unit area, E by

$$E(z^{el}) = \int_{z^{el}}^{\infty} \sigma(s)\, ds \qquad (12b)$$

Equation 12 (a) can only be solved if the geometry of the tip, and thus the relationship between z and z^{el}, is known. In the surface forces apparatus, the crossed cylinder geometry makes this integral trivial[1], and allows σ, and hence E, between two equivalent flat surfaces to be calculated. However, with the force microscope, there is usually uncertainty about the shape of the tip, and irregularities in shape make calculation of $\sigma(z)$ difficult. This problem has been addressed in section Chapter 6 of this thesis.

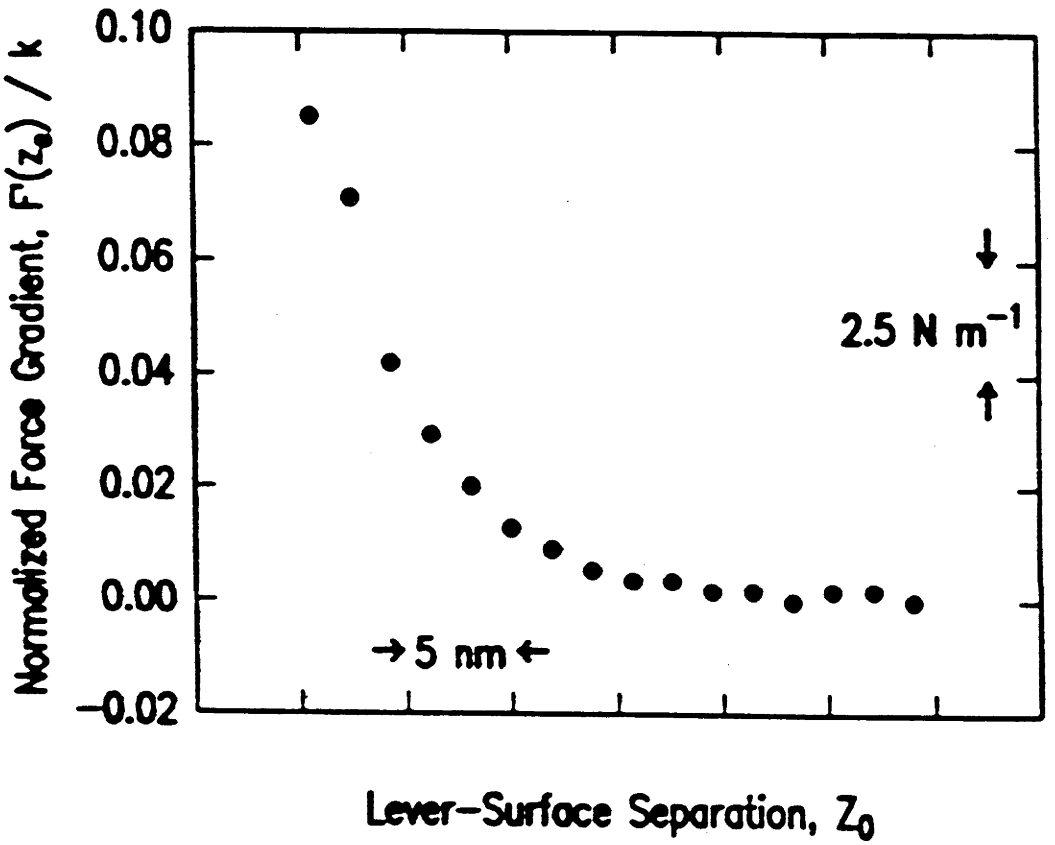

Figure A11: Force gradient vs lever-surface separation taken from the data in figure A10 (a).

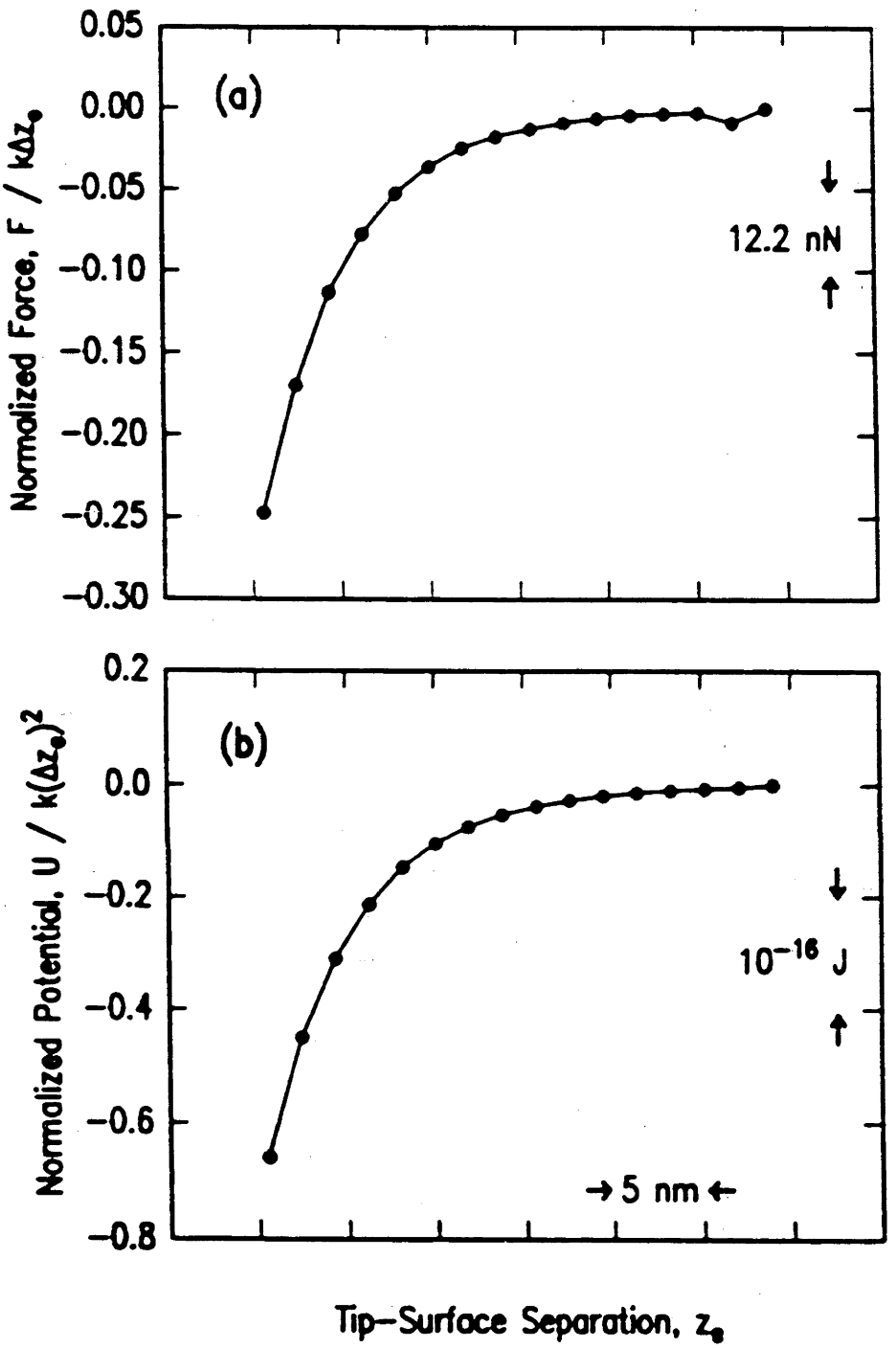

Figure A12:(a) Force vs tip-surface separation taken from the data in Figure 12. Δz_e is the distance between successive data points. (b) Potential vs tip-surface separation. The potential varies from a z^{-1} dependence to a z^{-3} dependence over the range of the data as the tip approaches the surface.

A4 Discussion

Two procedures for force determination were demonstrated. The first identified the shift in the resonant frequency of the vibrating tip by scanning the lever-surface separation, at discrete vibration frequencies. Individual scans may be performed rapidly in this procedure, but analysis of the data to derive the shift in resonant frequency as a function of separation is somewhat tedious. In the second procedure the vibration frequencies were scanned, at a variety of fixed lever-surface separations. Although the shift in the resonant frequency was immediately identified here, the rate of data acquisition, and hence scanning, was limited by the need to allow the amplitude of vibration within each scanned frequency interval to be properly measured. Both procedures were used here on a long-range force (figures A7 and A9) and gave consistent results. The displacement-scan procedure was used for a short-range force (figure A4), as tip instabilities prevented frequency scans from being performed at small separations. When there is a large force gradient, the displacement-scan procedure is superior because the tip is driven through the instability.

For the long-range force the Q factor of the system changes with lever-surface separation, implying that F(z) includes a varying, non-conservative element. This is consistent with results from the surface forces apparatus[2, 3] which show that although the viscosity of thin films of liquids is constant for thicknesses greater than a few molecular diameters, the viscous force between crossed cylinders increases linearly as separation decreases. Furthermore, it is likely that in our experiments more of the tip became immersed into the surface film as the tip approached the surface, further increasing the viscous force.

A force gradient may be obtained from a single amplitude-displacement measurement, provided that no variation in Q with displacement occurs. In this work it was found that full measurement of the $A(z,\omega_d)$ response (A9) is required to determine the force

gradient unambiguously because of the large variation in the Q factor with distance (figure A10 b). A constant Q factor cannot be assumed in all ac AFM experiments.

This result has implications for imaging with an ac force microscope. To obtain topographic images, it is usual to scan in both X and Y dimensions at a constant tip-surface separation. This separation is controlled by a feedback circuit set to maintain constant phase or amplitude of an output signal derived from the lever position. The topographic signal is given by the changes in Z position of the tip or sample necessary to maintain constant output signal. The highest vertical resolution is obtained at a distance and frequency where this signal varies maximally. Thus, because in some cases Q decreases as the tip approaches the surface, resolution is not necessarily enhanced by scanning close to the surface. However, it must be noted that any attempt to maximize Q will result in a decrease in the rate at which data can be acquired.

In addition, examination of Figure A6 reveals that before scanning it is important to ascertain the sign of F"(z) . The feedback loop will be unstable (i.e. positive feedback) at some set points if there is a turning point in the signal. Scanning microscopy will thus only be metastable at some set points when the driving frequency is less than the frequency at resonance for attractive forces, and when the driving frequency is greater than the frequency at resonance for repulsive forces.

A5 References for Appendix

1. Derjaguin, B. *Kholloid Zh.* **69**, 155 (1934).

2. Chan, D.Y.C. & Horn, R.G. *J. Chem. Phys.* **83**, 5311 (1985).

3. Israelachvili, J.N. *J. Coll. Int. Sci.*. **110**, 263 (1985).

Appendix B

Additional Notes on the Text

These notes are applicable to places marked * in the text.

Page 55.

The potential data shown in figure 3.7 has been compared to an ion-binding model by using a fitted pH and a previously obtained value of K_H. Because the addition of the weakly acidic ammonium ion does cause a small variation on pH, it is perhaps more reasonable to use a fitted binding constant, and use the theoretical pH of the solutions. Figure B1 shows the the data together with 3 curves calculated with a fitted binding constant, K_H=5.5 and the following values of pH:10^{-4} M: 5.7, 10^{-3} M: 5.6, 3 X 10^{-3} M: 5.6, 10^{-2} M: 5.5 and 10^{-1} M: 5.0. Note that as in the main text, only the model which treats the ammonium ion as larger than the site size on the mica provides a good fit to the data.

Page 59.

K_{diss} (mica) = $[S^-]$ $[X^+]$ / [SX]

X = NH_4, K or Cs

Page 65.

The forces have also been examined in detail in 0.1 M and 1M NaCl (Chapter 2 Reference 117). At these concentrations, the force was found to be stepped, with a period of 0.3 ± 0.05 nm.

Page 67.

The layering at 0.2 nm and 0.8 nm is suggested by the steeply increasing force and the presence of adhesive minima. The force also increased rapidly with no measurable change in separation at about 0.6 nm suggesting the presence of another layer at this separation. Thus 3 layers at 0.2, 0.6 and 0.8 nm are indicated, compared to values of 0.27, 0.54 and 0.81 nm expected when considering the diameter of a water molecule.

Note that there is no overlap between the points in figures 4.3 and 4.4.

A comparison of the force in the absence and presence of the diammonium salt at pH 6 and in the presence of the salt at pH 11.6 is shown in figure B2.

Page 71

Comparisons of the experiments on clays to those on mica are limited by differences in both the chemistry and shape of the two substrates; specifically, the clay platelets are small (with dimensions of approximately 10 x 10 x 1 nm) and flexible, and have ends which carry positive charge. Although these differences should be noted, the stability of the clay can be explained as follows. When a sample of Na-montmorillonite is placed in water, the clay will swell, causing the platelets to separate and these fine particles will take a long time to settle. If there is a deep minimum in the force between platelets then the clay will remain clumped and settle rapidly after dispersion. Such a minimum has been measured previously in the short-ranged force between mica surfaces in Ca^{2+} solutions (reference 2, Chapter 4), and is shown in figure 4.4 for diammine solutions. The rapid settling in the equivalent clay systems is shown in figure 4.5.

The diammine also has the effect of adsorbing to the mica surface to neutralize the charge so that the long-range force is attractive. This removes an additional driving force for swelling, and means that on approach, two widely separated plates will be attracted, and a larger number of collisions will result in coagulation. This should

result in more rapid sedimentation and in less ordering of the sediment leading to a larger sediment volume as shown in figure 4.5.

Page 94

This section describes the effects of the finite stiffness of the mechanical components in the Nanoscope AFM force measurements. Consider the following schematic diagram of the measurement system:

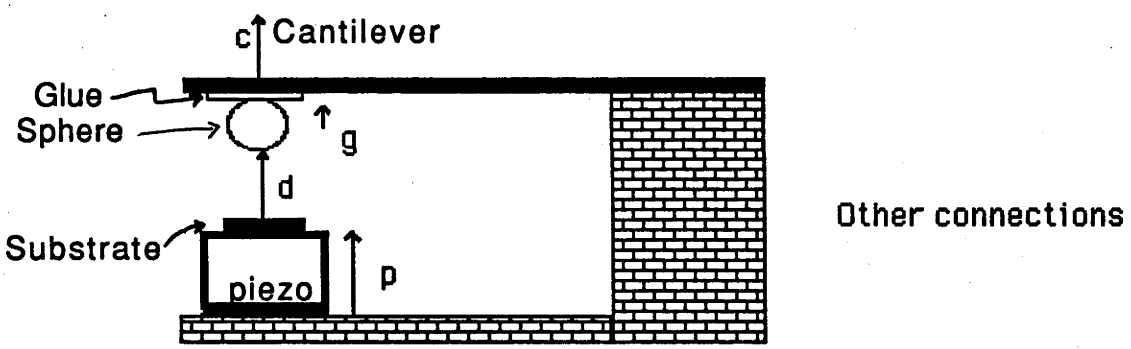

We will consider just two deformations, deformation of the cantilever spring, c and deformation of an arbitrary component g. Because the glue is the most deformable material, this will be considered, but the analysis is true for other components. From the above diagram:

$$d = -p + c + g \tag{1}$$

It is assumed that all materials are perfectly elastic, and so obey Hooke's Law. For the very small loads and deformations considered in these experiments this is likely to be a very good approximation.

If the spring is in mechanical equilibrium:

$$k_c c = k_g g \tag{2}$$

where k_c is the Young's Modulus of the cantilever and k_g is the Young's Modulus of the glue.

Combining (1) and (2):

$$d = -p + c\,(1 + k_c / k_g) \tag{3}$$

If c is measured directly (eg by interferometry), the force and d can be obtained directly from 2 and 3.

In these experiments, the measured variable, s is proportional to the endslope of the cantilever. For small deflections, this is proportional to the cantilever deflection, ie $c = a\,s$. The constant, a, is obtained by measuring a as a function of p where $d = 0$ (in the region of constant compliance):

$$p = a\,s\,(1 + k_c / k_g)$$

ie

$$a = (p_{d=0} / s_{d=0}) / (1 + \{k_c / k_g\}) \tag{4}$$

The force and distance can now be obtained by substitution of 4 into 3 and 2:

$$d = -p + (p_{d=0} / s_{d=0})\,s$$

This is the same result as obtained if the deformations are not considered.

$$\text{Force} = [k_c \, (p_{d=0} / s_{d=0}) / (1 + \{k_c / k_g\}] \, s.$$

which for $k_g >> k_c$ reduces to the result used in the thesis, and for $k_g \sim k_c$, results in a reduced force. i.e. the force calculated without considering deformations is an over-estimate.

Notes:

1) All the materials in this apparatus have much greater stiffness than the spring, except possibly the glue layer. Although the Young's Modulus of the glue is smaller than that of Si_3N_4, the spring is the most compliant component because the layer of glue is thin (see electron micrograph) and the spring has cantilever geometry.

2) Deformations of the substrates under applied load may lead to changes in the geometry of the interacting surfaces thus resulting in incorrect conclusions about the force law. In the current AFM setup, the substrates are much stiffer than the spring, so these effects do not need to be considered. Note that in contrast to measurements using the SFA, deformation of the glue layer does not affect substrate geometry.

3) This analysis assumes that all forces act, and all deformations occur along the same line.

Page 102

The data in figure 6.5 could also be fitted to a charge regulation model (Reference 11, Chapter 2), where the charge on the each surface is determined by the binding constants of surface dissociable groups and the interaction with the other surface, rather than by the boundary conditions of constant fitted charge or potential used in this thesis. Unfortunately, in this experiment, the position of the plane of charge, the extent of a hydration force and the value of the binding constants are not well known, so the fitting of a charge regulation model is of limited usefulness. However, for comparison, Figure B3 shows the measured force between silica surfaces in 10^{-2} M NaCl together with a fit using the charge regulation model.

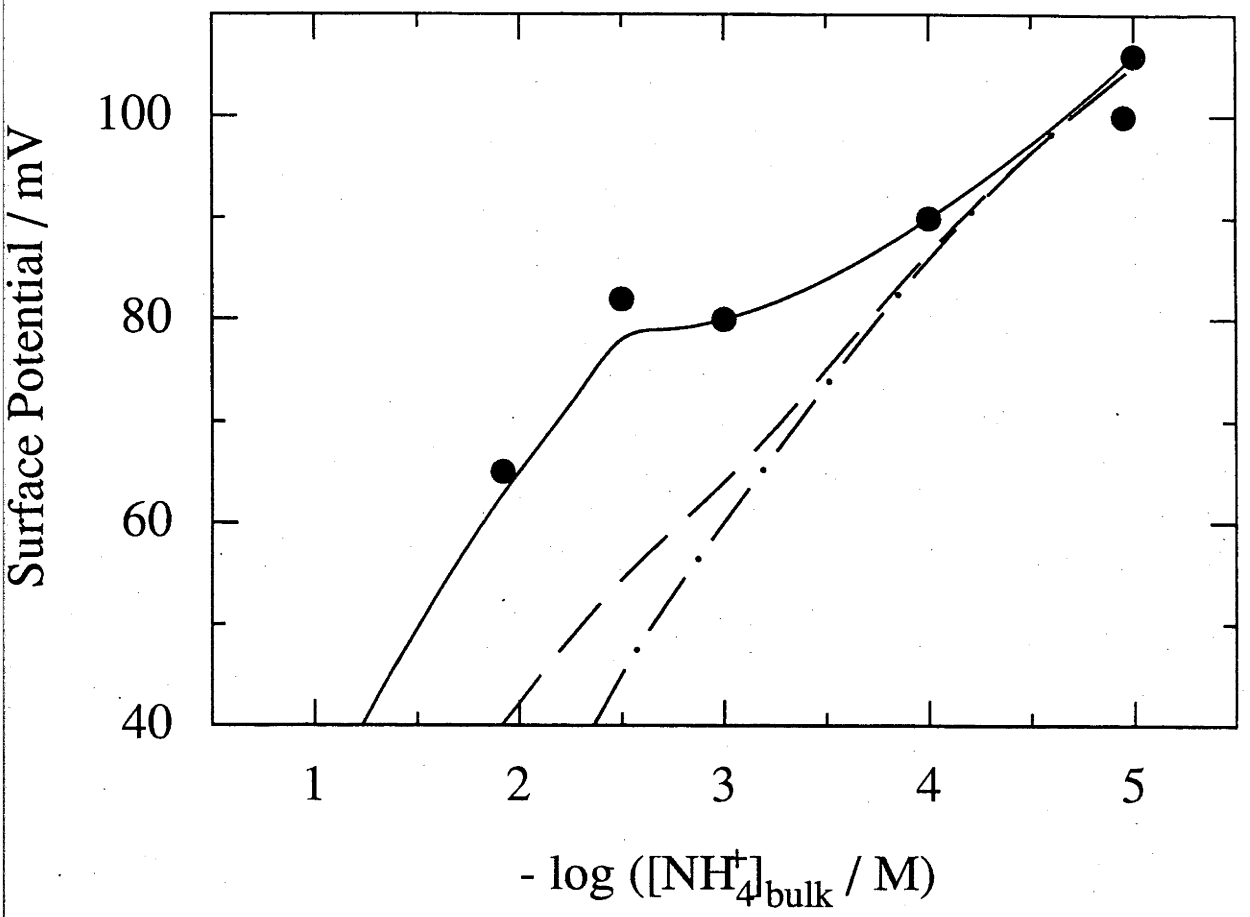

Figure B1 The surface potentials obtained in figures 3.3 to 3.4 are plotted here as a function of concentration. The solid line was calculated using the model described in the text with the following parameters: $A_N = 0.52$ nm^2 ; $A_H = 0.48$ nm^2; $pK_N = 3.12$ and with the pH varying according to the ammonium concentration. The dashed/dotted line was calculated with the same binding constant, but with $A_N = A_H = 0.48$ nm^2. The dashed line was calculated by assuming there is no binding of NH_4^+ (K_N infinite), only electrolyte screening.

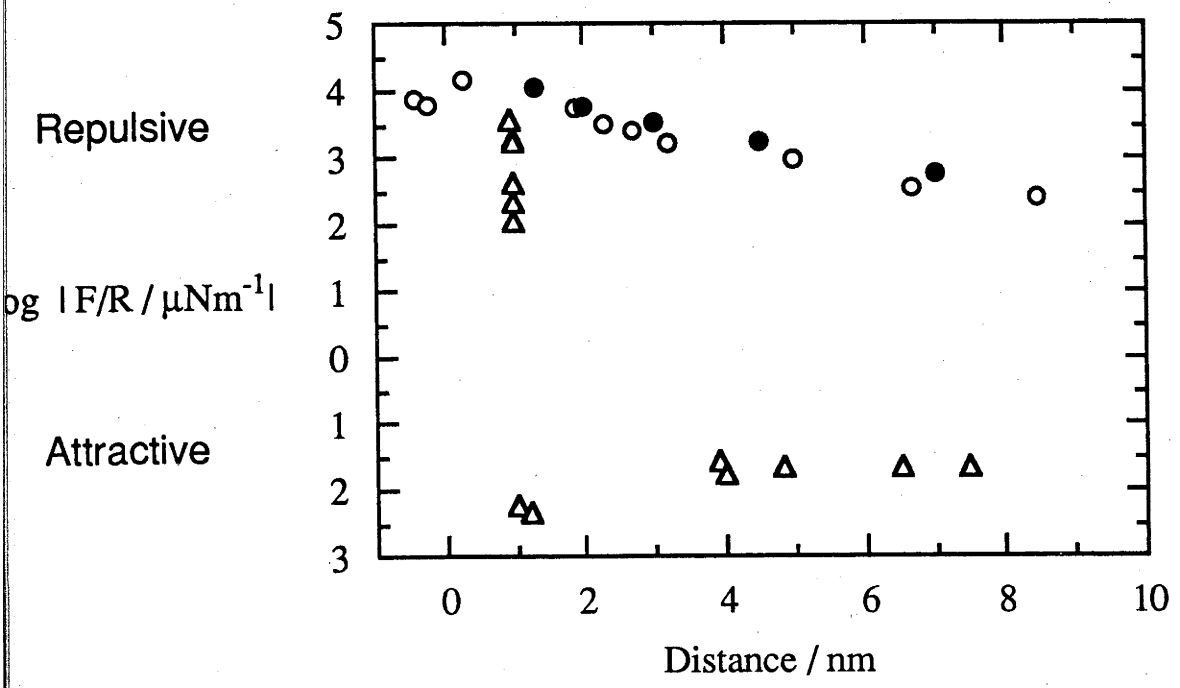

Figure B2: The force between two mica sheets in aqueous solution. The measurements represented are: 1.4 x 10^{-2} M NaCl: filled circles; addition of 3mM diammonium salt: triangles; addition of 6 mM NaOH: open circles. Note that the original double-layer force was restored after the diammonium salt was neutralized.

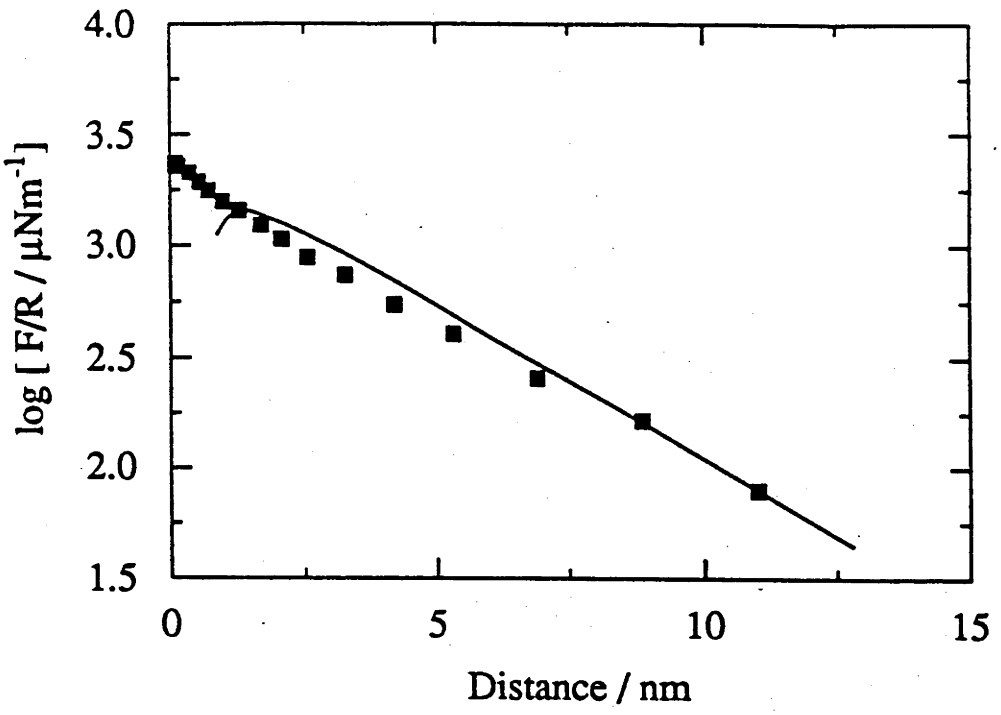

Figure B3: The interaction between a silica-glass sphere and a silica flat in 10^{-2} M NaCl. The data points are the same as those in figure 6.5, but here the solid curve has been calculated using an exact numerical solution to the Poisson-Boltzmann equation using a charge regulation model (Reference11, Chapter 2). The curve has been calculated using pK_H = 6.9 and a fitted value of pK_{Na} = 2.8 to obtain Ψ_0 = 35 mV. Note that there is still uncertainty in the calculated curve because of the unknown binding constants, the surface roughness and/ or hydration effects.